

Master's thesis

Thomas Røbekk Krogstad

# Attitude Control of Satellites in Clusters

Trondheim June 2005

NTNU  
Norwegian University of Science and Technology  
Department of Engineering Cybernetics  
IME







## MASTEROPPGAVE

Kandidatens navn: Thomas Krogstad

Fag: Teknisk Kybernetikk

Oppgavens tittel (norsk): Koordinert styring av orientering for satellitter.

Oppgavens tittel (engelsk): *Attitude control of satellites in clusters.*

Oppgavens tekst:

The work consists of two parts: I) A study of formation flight of satellites, and II) Refinement and publication of results on magnetic attitude control achieved during project work, autumn 2004.

*I) A study of formation flight of satellites*

In the framework of synchronization of mechanical systems, synchronized attitude control of satellites is to be studied.

- Perform a literature study on coordinated attitude control for formations of satellites.
- Derive a mathematical model of a satellite with four reaction wheels
- Design controllers and observers for attitude control of the leader-satellite, and synchronization for the formation using techniques from the nonlinear control literature.
- Derive an adaptive controller for synchronization of attitude.
- Derive a momentum dumping scheme for the reaction wheels.
- Write and submit a paper for the 56th International Astronautical Congress, Fukuoka, Japan, based on the main results of the Thesis.

*II) Magnetic attitude control*

Write papers based on the results on the project work Krogstad, T.R, "Attitude control and stability analysis of satellites in earth and moon orbit", Dept. of Eng. Cybernetics, 2004. Submit papers to

- The 13th Mediterranean Conference on Control and Automation, Limassol, Cyprus
- Space Technology Education Conference, STEC2005, Aalborg, Denmark
- The 56th International Astronautical Congress, Fukuoka, Japan

Oppgaven gitt: 18/1-05

Besvarelsen leveres: 13/6-05

Besvarelsen levert:

Utført ved Institutt for teknisk kybernetikk

Veileder: Raymond Kristiansen, Høgskolen i Narvik

Trondheim, den

  
Jan Tommy Gravidahl  
Faglærer



# Preface

This thesis is submitted in partial fulfillment of the requirements for the degree of Master of Science (Master i Teknologi/Siv. Ing.) in Engineering Cybernetics, and has been carried out at the Norwegian University of Science and Technology, Department of Engineering Cybernetics.

I would like to thank my supervisor and advisor Associate Professor Jan Tommy Gravdahl for his input and advice during the course of this work. I would also like to thank PhD student Raymond Kristiansen for being my co-advisor and PhD Student Anne Karin Bondhus for her input on Lyapunov analysis. Finally a great thanks to my fellow students in office G-238, for a fun and interesting final year.

Trondheim, June 13, 2005

Thomas R. Krogstad



# Contents

<b>List of Figures</b>	<b>vii</b>
<b>List of Tables</b>	<b>ix</b>
<b>Abstract</b>	<b>xi</b>
<b>1 Introduction</b>	<b>1</b>
1.1 Purpose . . . . .	1
1.2 Background information . . . . .	1
1.2.1 The satellite cluster . . . . .	1
1.3 Previous work . . . . .	1
1.4 Outline of the report . . . . .	2
1.5 Related work . . . . .	2
<b>2 Satellite Kinematics and Dynamics</b>	<b>5</b>
2.1 Preliminaries . . . . .	5
2.1.1 Coordinate frames . . . . .	5
2.1.2 Vectors . . . . .	6
2.1.3 Vector cross product . . . . .	6
2.1.4 Time derivative of vectors . . . . .	6
2.1.5 Rotation matrices . . . . .	7
2.1.6 Transformations between frames . . . . .	7
2.2 Kinematic equations . . . . .	8
2.2.1 Translational kinematics . . . . .	8
2.2.2 Rotational kinematics . . . . .	8
2.3 Attitude parametrization . . . . .	9
2.3.1 Angle axis . . . . .	9
2.3.2 Euler angles . . . . .	9
2.3.3 Euler parameters . . . . .	10
2.4 Dynamic model . . . . .	11
2.4.1 Inertial coordinate model . . . . .	13
2.5 External forces and torques . . . . .	14
2.5.1 Gravitational forces and torques . . . . .	14
2.5.2 Aerodynamical forces and torques . . . . .	15
2.5.3 Magnetic torques . . . . .	15
2.5.4 Solar radiation and solar wind . . . . .	16
2.5.5 Thruster forces and torques . . . . .	17
2.6 Internal torques . . . . .	17
2.6.1 Reaction wheels . . . . .	17

<b>3</b>	<b>Stability Theory</b>	<b>19</b>
3.1	Introduction to nonautonomous systems . . . . .	19
3.2	Stability definitions . . . . .	20
3.3	Stability theorems and lemmas . . . . .	20
3.3.1	Autonomous systems . . . . .	20
3.3.2	Nonautonomous system . . . . .	20
<b>4</b>	<b>Formation Flying</b>	<b>23</b>
4.1	Introduction . . . . .	23
4.2	Application of formation flying . . . . .	23
4.2.1	Earth observation . . . . .	23
4.2.2	Space-based interferometry . . . . .	24
4.2.3	Current projects . . . . .	24
4.3	Literature review . . . . .	24
4.3.1	Leader-follower . . . . .	25
4.3.2	Behavioral . . . . .	25
4.3.3	Virtual structure . . . . .	25
<b>5</b>	<b>Synchronization of mechanical systems</b>	<b>27</b>
5.1	Introduction . . . . .	27
5.2	The problem formulation . . . . .	27
5.2.1	External synchronization . . . . .	27
5.2.2	Mutual synchronization . . . . .	28
5.3	Synchronization of robot manipulators . . . . .	28
5.3.1	External synchronization . . . . .	28
5.3.2	Mutual synchronization . . . . .	29
<b>6</b>	<b>Controller Design and Analysis</b>	<b>33</b>
6.1	Preliminaries . . . . .	33
6.1.1	System variables . . . . .	33
6.1.2	Control deviation . . . . .	33
6.1.3	The attitude reference . . . . .	33
6.2	External synchronization . . . . .	34
6.2.1	Leader controller . . . . .	34
6.2.2	Synchronizing controller . . . . .	37
6.2.3	Observer design . . . . .	40
6.3	Mutual synchronization . . . . .	43
6.3.1	Synchronizing controller . . . . .	43
6.3.2	Observer design . . . . .	46
6.3.3	Control using estimated variables . . . . .	46
6.4	Desaturation of reaction wheels . . . . .	47
6.5	Discussion . . . . .	48
6.5.1	Robustness issues . . . . .	48
6.5.2	Control using estimated states . . . . .	48
6.5.3	Acceleration feedback . . . . .	49
6.5.4	Adaptive controller . . . . .	49
6.5.5	Unstable equilibrium point $\eta = -1$ . . . . .	49
<b>7</b>	<b>Simulations</b>	<b>51</b>
7.1	Observer simulation . . . . .	51
7.2	Leader controller simulation . . . . .	54
7.3	Lyapunov-based external synchronization controller . . . . .	56
7.3.1	With actual variables and no noise . . . . .	56
7.3.2	With estimated state variables, no noise . . . . .	59

7.3.3	With estimated state variables, measurement noise . . . . .	61
7.4	Adaptive synchronizing controller . . . . .	63
7.4.1	With actual state variables, no measurement noise . . . . .	63
7.4.2	With estimated state variables, measurement noise and environmental noise . . . . .	66
7.5	Mutual synchronization . . . . .	68
7.6	Momentum dumping scheme . . . . .	70
7.7	Summary . . . . .	70
<b>8</b>	<b>Concluding Remarks</b>	<b>73</b>
8.1	Conclusions . . . . .	73
8.2	Recommendations . . . . .	73
	<b>Bibliography</b>	<b>78</b>
<b>A</b>	<b>Model Parameters</b>	<b>79</b>
A.1	Robot manipulator parameters . . . . .	79
A.2	Satellite data . . . . .	79
<b>B</b>	<b>CD contents</b>	<b>81</b>
B.1	Other . . . . .	81
B.2	Matlab source files and Simulink diagrams . . . . .	81
B.2.1	Robotic-manipulator example files . . . . .	81
B.2.2	Mutual matlab files . . . . .	82
B.2.3	Simulink simulation files . . . . .	82
B.2.4	Mutual synchronization files . . . . .	82
<b>C</b>	<b>Accepted Papers, Posters and Presentation</b>	<b>83</b>
C.1	Paper accepted for the proceedings of 13th Mediterranean Conference on Control and Automation . . . . .	83
C.2	Abstract of 2 papers accepted for IAC 2005, and ESA Outreach sponsorship . . . . .	90
C.3	Powerpoint presentation . . . . .	93



# List of Figures

2.1	Gyrostat illustration . . . . .	12
2.2	Illustration of the Earth's magnetic field . . . . .	16
2.3	4 reaction wheel assemblies in tetrahedron composition . . . . .	18
5.1	Simulation of the robot manipulator external synchronization scheme . . . . .	30
5.2	Simulation of the robot manipulator using the mutual synchronization scheme . . . . .	32
7.1	Observer simulation, no measurement noise . . . . .	52
7.2	Observer simulation, measurement noise and environmental forces . . . . .	53
7.3	Simulation of leader controllers, no measurement noise, no process noise . . . . .	55
7.4	Simulation of external synchronization control, Lyapunov-base, synchronization errors . . . . .	56
7.5	Simulation of external synchronization control, Lyapunov-based, tracking errors . . . . .	57
7.6	Simulation of external synchronization control, Lyapunov-based, trajectories . . . . .	57
7.7	Simulation of external synchronization control, Lyapunov-based, wheel torque and velocity . . . . .	58
7.8	Simulation of external synchronization control, Lyapunov-base, synchronization errors . . . . .	59
7.9	Simulation of external synchronization control, Lyapunov-based, trajectories . . . . .	59
7.10	Simulation of external synchronization control, Lyapunov-based, tracking errors . . . . .	60
7.11	Simulation of external synchronization control, Lyapunov-based, wheel torque and velocity . . . . .	60
7.12	Simulation of external synchronization control, Lyapunov-base, synchronization errors . . . . .	61
7.13	Simulation of external synchronization control, Lyapunov-based, trajectories . . . . .	61
7.14	Simulation of external synchronization control, Lyapunov-based, tracking errors . . . . .	62
7.15	Simulation of external synchronization control, Lyapunov-based, wheel torque and velocity . . . . .	62
7.16	Simulation of external synchronization control, adaptive, synchronization errors and parameter estimate . . . . .	63
7.17	Simulation of external synchronization control, adaptive, tracking errors . . . . .	64
7.18	Simulation of external synchronization control, adaptive, trajectories . . . . .	64
7.19	Simulation of external synchronization control, adaptive, wheel torque and velocity . . . . .	65
7.20	Simulation of external synchronization control, adaptive, synchronization errors and parameter estimate . . . . .	66
7.21	Simulation of external synchronization control, adaptive, trajectories . . . . .	66
7.22	Simulation of external synchronization control, adaptive, tracking errors . . . . .	67
7.23	Simulation of external synchronization control, adaptive, wheel torque and velocity . . . . .	67
7.24	Simulation of mutual synchronization control . . . . .	69
7.25	Simulation of momentum dumping scheme . . . . .	70



# List of Tables

4.1	Current projects on formation flying . . . . .	24
6.1	Suggestion for the $H(\tilde{\eta})$ -function used in output injection, and controller feedback. . .	43
7.2	Simulation initial conditions and desired state for the $\mathcal{F}_i$ set-point controller . . . . .	54
7.3	Simulation initial conditions and desired state for the $\mathcal{F}_o$ set-point controller . . . . .	54
7.4	Simulation initial conditions and desired state for tracking controller in $\mathcal{F}_i$ . . . . .	54
7.5	Simulation initial conditions and desired states, Lyapunov-based synchronizing controller. . .	56
7.6	Simulation initial conditions and desired states, adaptive synchronizing controller. . .	63
7.7	Simulation initial conditions and desired states, adaptive synchronizing controller. . .	68
A.1	Parameters for the robot manipulators . . . . .	79
A.2	Relevant data for the reaction wheel assembly DRALLRAD by TELDIX-Bosch Telecom . . . . .	79
A.3	Relevant data for the simulated satellite . . . . .	80
B.1	Matlab files for the robotic-manipulator example . . . . .	81



# Abstract

The topic of this thesis is the coordinated attitude control of satellites in formations. Applying methods from synchronization of mechanical systems and nonlinear control theory, nonlinear observer-controller structures are developed for a leader-follower satellite formation. A nonlinear mathematical model of the satellites is derived, using rigid body dynamics, assuming actuation by means of reaction wheels. The attitude is parameterized in Euler parameters and Euler angles.

Two control schemes are designed, referred to as external synchronization and mutual synchronization. In the external synchronization scheme, the formation leader is assumed separately controlled and the objective is to design feedback interconnections *from* the leader *to* the follower, which enables synchronization of the relative attitude. In this work three controllers are proposed for leader control, and proved stable using nonlinear systems' analysis. Two feedback interconnections are suggested, based on state feedback and adaptive backstepping. Due to unavailable angular velocity measurements, a nonlinear Luenberger observer is proposed and proved uniformly globally asymptotically stable using an extension of Matrosov's theorem.

The mutual synchronization scheme is designed with the objective of creating interconnections between satellites in the formation in such a way that both tracking and synchronization errors of all satellites converge. Based on work presented on robot manipulators, a control algorithm is derived by designing a virtual reference which combines the two objectives. Uniform global asymptotic stability is proved. In addition an observer is proposed, and uniform local asymptotic stability is suggested.

A momentum dumping scheme is proposed, to deal with wheel speed saturation. The scheme enables tracking during momentum dumping.

The various systems are simulated in Matlab/Simulink to evaluate transient, steady-state and tracking performance. To determine robustness, measurement noise and environmental disturbances are added. The results demonstrate the required performance of  $\pm 0.1^\circ$  about all axis, which was achieved also in the presence of bounded environmental forces and with feedback from estimated states.



# Chapter 1

## Introduction

### 1.1 Purpose

The purpose of this thesis is to develop coordinated attitude control schemes for formation flying of micro-satellites, enabling the formation to keep its relative attitude in the presence of environmental disturbances and measurement noise. The method proposed is based on the theory of synchronization of mechanical systems, and is a nonlinear observer-controller structure. Stability is proved using methods from nonlinear systems' analysis. To evaluate performance and substantiate the stability proofs, the closed-loop systems are simulated in MATLAB<sup>TM</sup>/Simulink<sup>TM</sup>. The final part is the refinement and publication of results obtained through this work and the work presented in Krogstad (2004).

### 1.2 Background information

The work has been carried out at the Department of Engineering Cybernetics at the Norwegian University of Science and Technology.

#### 1.2.1 The satellite cluster

The exact composition of the cluster is not defined, but it will be made up of two or more micro-satellites. The individual satellite will be  $70 \times 70 \times 70 \text{cm}^3$  in size and weigh about 150 kg. It is to be controlled about all axes by means of 4 reaction wheels, composed in a tetrahedron structure for redundancy and performance.

The satellites in the cluster will perform ocean surveillance, and possible missions include monitoring ship activity, oil spills, ocean currents, iceberg activity in the arctic waters. The focus area will primarily be the Norwegian waters, but to depending on the orbit it is possible to offer surveillance services to other countries.

The exact mission profile is not decided yet, but either there will be independent synthetic aperture radar (SAR) antennas on all satellites or an interferometric SAR. The interferometric SAR will be most demanding in terms of inter-spacecraft positioning and orientation. The details of interferometric SAR will be given later in the thesis.

### 1.3 Previous work

Attitude control of rigid bodies, and of spacecraft in particular, is a thoroughly researched discipline and numerous results exists on the subject. For the derivation and representation of attitude dynamics the reader is referenced to Hughes (1986) and for an introduction to the control of attitude Chobotov (1991), Bryson (1994) and Wen & Kreutz-Delgado (1991) are excellent references. An extensive

overview of the design of complete attitude determination and control systems is given in Vallado (2001).

Lately there have been an increased effort towards the coordinated attitude control of satellites and spacecraft operating in formation. Though most of the effort within the formation flying community have been focused on the case of relative positioning, several notable results exist on the attitude case. A literature review of some of this work is given in chapter 4 of this thesis.

Observer design has been an active research area for a long time, and several standardized schemes exist for the linear case. Observer design was extended to the nonlinear case in the beginning of the 1980's, and since then several results have been presented. An acknowledged result on spacecraft observers is Salcudean (1991). Great general references are Nijmeijer & Fossen (1999) and Robertsson (1999).

The theory of synchronization of mechanical systems stretches back to Huygens and Rayleigh. Recently it has been applied to robot manipulators in Rodriguez-Angeles (2002), ships in Kyrkjebø & Pettersen (2003) and satellites in Bondhus, Pettersen & Gravdahl (2005).

## 1.4 Outline of the report

- **Chapter 2** - Introduction with theoretical background information; mathematical notation and definitions, attitude dynamics and kinematic equations, and disturbance torques.
- **Chapter 3** - Stability theorems, lemmas and definitions used throughout the thesis, are reviewed for the sake of completeness and ease of reference.
- **Chapter 4** - The results of a literature study on coordinated attitude control for formations of satellites are given.
- **Chapter 5** - An introduction to synchronization of mechanical systems. The theory is presented and illustrated with an example from robot manipulators.
- **Chapter 6** - Contains the main contribution of the thesis. In this chapter set-point and tracking controllers are proposed for the leader satellite, and proved uniformly globally asymptotically stable. A nonlinear attitude observer is designed and proved stable using an extension of Matrosov's Theorem. Two synchronizing control schemes are derived for a leader-follower satellite cluster, and proven stable using nonlinear control theory. In addition a momentum dumping scheme is derived.
- **Chapter 5** - The nonlinear observer, leader satellite controller, synchronizing controllers and the momentum dumping scheme are simulated in MATLAB/Simulink, including relevant environmental disturbances and measurement noise.
- **Appendix A** - Model parameters
- **Appendix B** - Contents of the included CD.
- **Appendix C** - In this appendix is a copy of the paper accepted for presentation at the 13th Mediterranean Conference on Control and Automation, Limassol, Cyprus, based on results derived in the preparing project work, two abstracts of papers accepted for the 56th International Astronautical Congress, Fukuoka, Japan, one of which presents the main contribution of this thesis, and which have received ESA Outreach sponsorship. Finally a presentation which was held during Space Technology Education Conference 2005 in Aalborg, Denmark, and which will be presented in Cyprus and Japan, is included.

## 1.5 Related work

The main results of this thesis and the project report Krogstad (2004) are published in

- Krogstad, T.R., Gravdahl, J.-T. and Kristiansen, R., "Coordinated control of satellites: the attitude case", in *Proceedings of the 56th International Astronautical Congress, Fukuoka, Japan, 2005*
- Krogstad, T.R., Gravdahl, J.-T. and Tøndel, P., "Attitude control and stability analysis of satellites in earth and moon orbit", in *Proceedings of the 56th International Astronautical Congress, Fukuoka, Japan, 2005*, (Accepted for ESA Outreach sponsorship).
- Krogstad, T.R., Gravdahl, J.-T. and Tøndel, P., "Explicit model predictive control of a satellite with magnetic torquers", in *Proceedings of the 13th Mediterranean Conference on Control and Automation, Limassol, Cyprus, June, 2005*

Krogstad, Gravdahl & Tøndel (2005) is included in Appendix D. The above papers will be presented at their respective conferences, and a copy of the presentation is present in Appendix D and on the included CD.

In addition a presentation was held at the *Space Technology Education Conference 2005* in Aalborg, Denmark.



## Chapter 2

# Satellite Kinematics and Dynamics

In this chapter dynamical equations describing satellite attitude are derived using rigid body dynamics. The kinematical equations are parameterized in Euler parameters and Euler angles. Some preliminary background material used throughout the thesis is presented first.

## 2.1 Preliminaries

### 2.1.1 Coordinate frames

To describe position and attitude of a satellite we need coordinate frames or reference frames. Following the derivation by Fjellstad (1994), a rigid-body in  $n$ -dimensional space  $\mathbb{R}^n$  has  $n(n + 1)/2$  degrees-of-freedom (DOF) and  $n(n + 1)/2$  independent coordinates.  $n$  coordinates are used to represent the position, leaving  $n(n - 1)/2$  to represent the attitude. For a satellite in  $\mathbb{R}^3$  this gives 6 DOF, whereof 3 coordinates represent the position and 3 for the minimal attitude representation.

Four different coordinate frames are used to represent attitude and orientation of the satellite. In the following we will use  $\mathcal{F}_a$  to denote the coordinate frame  $a$ .

#### ECI - Earth-centered inertial frame

This reference frame has its origin in the center of the earth, the  $x_i$ -axis is pointing in the vernal equinox direction,  $\Upsilon$ . This is in the direction of the vector from the sun's center through the center of the earth during vernal equinox. The  $y_i$ -axis points 90° east, spanning the equatorial plane together with the  $x_i$ -axis. The  $z_i$ -axis points through the north-pole, completing the right-hand system.

The ECI frame is non-rotating and is assumed fixed in space, i.e. it is an inertial frame in which Newton's laws of motion apply. This is therefore the frame in which the equation of motion is evaluated.

In the following this frame will be denoted by  $\mathcal{F}_i$

#### Orbit-fixed reference frame

This frame, denoted  $\mathcal{F}_o$ , will have its origin in the satellites center of gravity. The  $z_o$ -axis will point in the nadir direction. The  $y_o$ -axis will point in the direction of the negative orbit normal. The  $x_o$ -axis is chosen as to complete a right-hand coordinate system.

#### Body-fixed reference frame

As the  $\mathcal{F}_o$  frame, this reference frame will originate at the satellites center of gravity, with the axes pointing along the satellites principle axes of inertia. The frame is denoted  $\mathcal{F}_b$ .

### 2.1.2 Vectors

To represent forces, velocities, torques, positions and so on, vector notation will be applied. Vectors  $\vec{v}$  are described by their length or magnitude  $|\vec{v}|$  and their direction. We will in the following only consider vectors in 3-dimensional space.

A vector may be expressed in a reference frame  $\mathcal{F}_a$ , by a  $3 \times 1$  array consisting of its components along the reference frame's basis vectors. Such a vector is referred to as a *column vector*, and is denoted  $\mathbf{v}^a$  to distinguish it from the *Gibbsian* or *coordinate free* vector  $\vec{v}$ .

**Definition 2.1.** *The column vector written with respect to the reference frame  $\mathcal{F}_a$  may be defined as follows*

$$\mathbf{v}^a = \begin{bmatrix} v_1 \\ v_2 \\ v_3 \end{bmatrix} \quad (2.1)$$

Here the components are defined as the scalar product between  $\vec{v}$  and the basic vectors of the reference frame  $\mathcal{F}_a$

$$v_i = \vec{v} \cdot \vec{a}_i \quad (2.2)$$

### 2.1.3 Vector cross product

The vector cross product between two coordinate free vectors  $\vec{v}$  and  $\vec{u}$ , is given by

$$\vec{v} \times \vec{u} = \vec{n} |\vec{v}| |\vec{u}| \sin \theta. \quad (2.3)$$

To be able to evaluate the cross product between two column vectors, we define the skew-symmetric matrix operator  $\mathbf{S}(\cdot)$ .

**Definition 2.2.** *Skew-symmetric cross product matrix*

$$\mathbf{S}(\mathbf{v}) = \mathbf{v}^\times \triangleq \begin{bmatrix} 0 & -v_3 & v_2 \\ v_3 & 0 & -v_1 \\ -v_2 & v_1 & 0 \end{bmatrix} \quad (2.4)$$

Where  $v_i$  is given by (2.2).

**Property 1.** *Properties of the skew-symmetric operator*

- $\mathbf{S}(\beta \mathbf{a} + \gamma \mathbf{b}) = \beta \mathbf{S}(\mathbf{a}) + \gamma \mathbf{S}(\mathbf{b})$
- $\mathbf{S}(\mathbf{a})\mathbf{b} = \mathbf{a}^\times \mathbf{b}$
- $\mathbf{S}(\mathbf{a})\mathbf{S}(\mathbf{b}) = \mathbf{b}\mathbf{a}^T - \mathbf{a}^T\mathbf{b}\mathbf{I}_{3 \times 3}$
- $\mathbf{S}[\mathbf{S}(\mathbf{a})\mathbf{b}] = \mathbf{b}\mathbf{a}^T - \mathbf{a}\mathbf{b}^T$
- $\mathbf{a}^T \mathbf{S}(\mathbf{b})\mathbf{a} = 0$
- $\mathbf{S}(\mathbf{a})\mathbf{a} = 0$

### 2.1.4 Time derivative of vectors

The time derivative of a vector  $\vec{v}$  with reference to the frame  $\mathcal{F}_a$  may be written

$$\frac{{}^a d}{dt} \vec{v} \triangleq \dot{v}_1^a \vec{a}_1 + \dot{v}_2^a \vec{a}_2 + \dot{v}_3^a \vec{a}_3. \quad (2.5)$$

Which can be given as the time derivative of the vector in another frame and the cross product of the angular velocity between the coordinate systems and the vector.

$$\frac{{}^a d}{dt} \vec{v} = \frac{{}^b d}{dt} \vec{v} + \vec{\omega}_{ab} \times \vec{v} \quad (2.6)$$

For a column vector this may be written:

$$\dot{\mathbf{v}}^a = \begin{bmatrix} \dot{v}_1^a \\ \dot{v}_2^a \\ \dot{v}_3^a \end{bmatrix} \quad (2.7)$$

### 2.1.5 Rotation matrices

**Definition 2.3.** *The rotation matrix is defined to be any matrix  $\mathbf{R}$  member of the special orthogonal group of order three,  $SO(3)$ , which is defined as*

$$SO(3) \triangleq \{\mathbf{R} | \mathbf{R} \in \mathbb{R}^{3 \times 3}, \mathbf{R}^T \mathbf{R} = I, \det \mathbf{R} = 1\}. \quad (2.8)$$

The rotation matrix has two interpretations:

- 1 *To rotate a vector within a given reference system.*
- 2 *To transform a vector between reference frames.*

The rotation matrix which rotates a vector from frame  $\mathcal{F}_a$  to frame  $\mathcal{F}_b$ , is denoted  $\mathbf{R}_b^a$ . And the column vector  $\mathbf{v}^a$  given in  $\mathcal{F}_a$ , may be transformed into the column vector  $\mathbf{v}^b$  in  $\mathcal{F}_b$  as

$$\mathbf{v}^b = \mathbf{R}_a^b \mathbf{v}^a. \quad (2.9)$$

#### Properties of the rotation matrix

The rotation matrix has some useful properties:

$$\mathbf{R}_a^b \mathbf{R}_b^a = I \quad \text{and} \quad \mathbf{R}^T = \mathbf{R}^{-1} \quad (2.10)$$

$$\Downarrow$$

$$\mathbf{R}_a^b = (\mathbf{R}_b^a)^{-1} = (\mathbf{R}_b^a)^T \quad (2.11)$$

We may also split a rotation into composite rotations,

$$\mathbf{R}_c^a = \mathbf{R}_b^a \mathbf{R}_c^b. \quad (2.12)$$

### 2.1.6 Transformations between frames

In order to represent orientation in different frames, one needs to define the transformations between them. In this section we will define some of the most common transformations, given as rotation matrices.

#### Transformation from $\mathcal{F}_o$ to $\mathcal{F}_i$

When finding the transformation from the orbit frame to the inertial frame, we will use the classical orbit elements (COE) as derived in Vallado (2001). Here, a rotation matrix from ECI to a frame called RSW is given. The RSW frame does not coincide with our orbit frame, but can be made to do so by means of two simple rotations (Hegrenæs 2004). Giving the following:

$$\mathbf{R}_o^i = \mathbf{R}_{RSW}^i \mathbf{R}_o^{RSW} = \mathbf{R}_{RSW}^i \mathbf{R}_z(\frac{\pi}{2}) \mathbf{R}_x(-\frac{\pi}{2}) \quad (2.13)$$

$$= \begin{bmatrix} -c(i)s(\Omega)c(u) - c(\Omega)s(u) & -s(i)s(\Omega) & -c(\Omega)c(u) + c(i)s(\Omega)s(u) \\ c(i)c(\Omega)c(u) - s(\Omega)s(u) & s(i)c(\Omega) & -s(\Omega)c(u) - c(i)c(\Omega)s(u) \\ s(i)c(u) & -c(i) & -s(i)s(u) \end{bmatrix} \quad (2.14)$$

where  $u = \omega + \nu$  and  $c(\cdot)$  and  $s(\cdot)$  denote  $\cos \cdot$  and  $\sin \cdot$  respectively.

### Transformation from $\mathcal{F}_b$ to $\mathcal{F}_o$

The transformation matrix from body frame to the orbit frame, may be given based on the angular parameters chosen. With Euler parameters the transformation is

$$\mathbf{R}_b^o = \mathbf{R}(\eta, \boldsymbol{\epsilon}) = \begin{bmatrix} 1 - 2(\epsilon_2^2 + \epsilon_3^2) & 2(\epsilon_1\epsilon_2 - \eta\epsilon_3) & 2(\epsilon_1\epsilon_3 + \eta\epsilon_2) \\ 2(\epsilon_1\epsilon_2 + \eta\epsilon_3) & 1 - 2(\epsilon_1^2 + \epsilon_3^2) & 2(\epsilon_2\epsilon_3 - \eta\epsilon_1) \\ 2(\epsilon_1\epsilon_2 + \eta\epsilon_2) & 2(\epsilon_2\epsilon_3 + \eta\epsilon_1) & 1 - 2(\epsilon_1^2 + \epsilon_2^2) \end{bmatrix}, \quad (2.15)$$

and in Euler angles

$$\mathbf{R}_b^o = \begin{bmatrix} c(\phi)c(\theta) & c(\phi)s(\theta)s(\psi) - s(\phi)c(\psi) & c(\phi)s(\theta)c(\psi) + s(\phi)s(\psi) \\ s(\phi)c(\theta) & s(\phi)s(\theta)s(\psi) + c(\phi)c(\psi) & s(\phi)s(\theta)c(\psi) - c(\phi)s(\psi) \\ -s(\theta) & c(\theta)s(\psi) & c(\theta)c(\psi) \end{bmatrix}. \quad (2.16)$$

These rotation matrices will be derived in the next section.

## 2.2 Kinematic equations

In this section we present kinematic equations for translation and attitude.

### 2.2.1 Translational kinematics

The translational kinematics represent the relation between position and velocity. As we usually represent velocities in body coordinates, the relation is

$$\dot{\mathbf{x}}^i = \mathbf{v}^i = \mathbf{R}_b^i \mathbf{v}^b, \quad (2.17)$$

where  $\mathbf{x}^i$  is position in the inertial frame,  $\mathbf{R}_b^i$  is a rotation matrix between  $\mathcal{F}_i$  and  $\mathcal{F}_b$  and  $\mathbf{v}^b$  is the body velocities.

### 2.2.2 Rotational kinematics

To derive the equations representing rotational kinematics, we first find the time derivative of a rotating vector which is constant in  $\mathcal{F}_b$ .

$$\frac{{}^a d}{dt} \vec{r} = \frac{{}^b d}{dt} \vec{r} + \vec{\omega}_{ab} \times \vec{r} \quad (2.18)$$

$$= \vec{\omega}_{ab} \times \vec{r} \quad (2.19)$$

Decomposing (2.19) in  $\mathcal{F}_a$  results in

$$\dot{\mathbf{r}}^a = \mathbf{S}(\boldsymbol{\omega}_{ab}^a) \mathbf{r}^a. \quad (2.20)$$

Application of the orthogonal transformation of a vector in  $\mathcal{F}_a$  to  $\mathcal{F}_b$  and the fact that this vector is constant in  $\mathcal{F}_b$ , results in

$$\mathbf{r}^b = \mathbf{R}_a^b \mathbf{r}^a \quad (2.21)$$

$$\dot{\mathbf{r}}^b = \dot{\mathbf{R}}_a^b \mathbf{r}^a + \mathbf{R}_a^b \dot{\mathbf{r}}^a \quad (2.22)$$

$$= \dot{\mathbf{R}}_a^b \mathbf{R}_b^a \mathbf{r}^b + \mathbf{R}_a^b \mathbf{S}(\boldsymbol{\omega}_{ab}^a) \mathbf{R}_b^a \mathbf{r}^b \quad (2.23)$$

$$= \dot{\mathbf{R}}_a^b \mathbf{R}_b^a \mathbf{r}^b + \mathbf{S}(\boldsymbol{\omega}_{ab}^b) \mathbf{r}^b = 0, \quad (2.24)$$

$$(2.25)$$

where the relation

$$\mathbf{R}_a^b \mathbf{S}(\boldsymbol{\omega}_{ab}^a) \mathbf{R}_b^a = \mathbf{S}(\mathbf{R}_a^b \boldsymbol{\omega}_{ab}^a) = \mathbf{S}(\boldsymbol{\omega}_{ab}^b) \quad (2.26)$$

has been used. This leads to the rotational kinematic in terms of the rotation matrix:

$$\dot{\mathbf{R}}_b^a = \mathbf{R}_b^a \mathbf{S}(\boldsymbol{\omega}_{ab}^b) = \mathbf{S}(\boldsymbol{\omega}_{ab}^a) \mathbf{R}_b^a. \quad (2.27)$$

## 2.3 Attitude parametrization

To represent the attitude of a rigid body, we choose a parametrization of the rotation matrix. In this section three different parameterizations are presented; the angle-axis, the Euler angles and the unit quaternion or Euler parameters. We end the section with a discussion.

### 2.3.1 Angle axis

A rotation may be represented as an angle  $\theta$  about an arbitrary axis  $\vec{k}$ . This is usually referred to as angle-axis parametrization. The resulting rotation matrix is written

$$\mathbf{R}_k(\theta) \triangleq \cos \theta \mathbf{I} + \mathbf{S}(\mathbf{k}) \sin \theta + \mathbf{k}\mathbf{k}^T(1 - \cos \theta). \quad (2.28)$$

### 2.3.2 Euler angles

In this description, the attitude is given as a composite rotation of simple rotations about the principal axis. There are many variations of the Euler angles parametrization, but the two most common are the roll-pitch-yaw (ZYX) and the classical Euler angles (ZYZ). The roll-pitch-yaw variation is most often used when describing the attitude of free moving objects, and hence the description suitable for satellites. The rotation matrix between frames a and b, is found by pre-multiplying three composite rotation matrices obtained from simple rotations about the axis of a frame fixed in the the body's center of mass. (Sciavicco & Siciliano 2000)

**Definition 2.4.** *The rotation matrix for roll-pitch-yaw parameters*

$$\mathbf{R}_b^a = \mathbf{R}_z(\psi)\mathbf{R}_y(\theta)\mathbf{R}_x(\phi), \quad (2.29)$$

where the rotation matrices are given by

$$\mathbf{R}_x(\phi) = \begin{bmatrix} 1 & 0 & 0 \\ 0 & \cos \phi & -\sin \phi \\ 0 & \sin \phi & \cos \phi \end{bmatrix} \quad (2.30)$$

$$\mathbf{R}_y(\theta) = \begin{bmatrix} \cos \theta & 0 & \sin \theta \\ 0 & 1 & 0 \\ -\sin \theta & 0 & \cos \theta \end{bmatrix} \quad (2.31)$$

$$\mathbf{R}_z(\psi) = \begin{bmatrix} \cos \psi & -\sin \psi & 0 \\ \sin \psi & \cos \psi & 0 \\ 0 & 0 & 1 \end{bmatrix}. \quad (2.32)$$

The complete rotation may be written:

$$\mathbf{R}_b^a = \begin{bmatrix} c(\phi)c(\theta) & c(\phi)s(\theta)s(\psi) - s(\phi)c(\psi) & c(\phi)s(\theta)c(\psi) + s(\phi)s(\psi) \\ s(\phi)c(\theta) & s(\phi)s(\theta)s(\psi) + c(\phi)c(\psi) & s(\phi)s(\theta)c(\psi) - c(\phi)s(\psi) \\ -s(\theta) & c(\theta)s(\psi) & c(\theta)c(\psi) \end{bmatrix} \quad (2.33)$$

**Remark 2.1.** *The matrix  $\mathbf{R}_b^a$  becomes singular when  $\theta$  is equal to  $\pm\frac{\pi}{2}$  and hence is not invertible in the whole state-space.*

### Kinematic differential equation for Euler angles

One cannot simply integrate the velocities, to obtain the Euler angles, as this integral has no physical interpretation. Instead, we derive kinematic relation between the angular velocities and the time derivative of the Euler angles by noting that

$$\boldsymbol{\omega} = \begin{bmatrix} \dot{\phi} \\ 0 \\ 0 \end{bmatrix} + \mathbf{R}_x(\phi) \begin{bmatrix} 0 \\ \dot{\theta} \\ 0 \end{bmatrix} + \mathbf{R}_x(\phi)\mathbf{R}_y(\theta) \begin{bmatrix} 0 \\ 0 \\ \dot{\psi} \end{bmatrix} = \begin{bmatrix} 1 & 0 & -\sin \theta \\ 0 & \cos \phi & \sin \phi \cos \theta \\ 0 & -\sin \phi & \cos \phi \cos \theta \end{bmatrix} \dot{\boldsymbol{\Phi}} = \mathbf{T}(\boldsymbol{\Phi})^{-1} \dot{\boldsymbol{\Phi}} \quad (2.34)$$

and using this to obtain the kinematic differential equation

$$\dot{\Phi} = \mathbf{T}(\Phi)\boldsymbol{\omega}, \quad (2.35)$$

where

$$\Phi = \frac{1}{\cos \theta} \begin{bmatrix} \cos \theta & \sin \phi \sin \theta & \cos \phi \sin \theta \\ 0 & \cos \phi \cos \theta & \sin \phi \cos \theta \\ 0 & \sin \phi & \cos \phi \end{bmatrix} \quad (2.36)$$

**Remark 2.2.** *As can be seen, (2.36) is not defined for  $\theta = \pm \frac{\pi}{2} + n\pi, n \in \mathbb{N}$ .*

### 2.3.3 Euler parameters

Euler parameters use four variables to represent attitude, compared to the three Euler angles. The advantage of adding an extra variable is that the parametrization is non-singular for all angles. This is an attractive property for satellites, as their movement will reach the singularities of the Euler angles. Euler parameters are also more computational efficient compared to Euler angles, as they do not contain any trigonometric functions.

**Definition 2.5.** *The Euler parameters  $(\eta, \boldsymbol{\epsilon})$  are defined in terms of the angle-axis parameters given in section 2.3.1:*

$$\eta = \cos \frac{\theta}{2} \quad (2.37)$$

$$\boldsymbol{\epsilon} = \mathbf{k} \sin \frac{\theta}{2}, \quad (2.38)$$

Which we usually denote

$$\mathbf{q} = [\eta \quad \boldsymbol{\epsilon}^T]^T \quad (2.39)$$

It follows from 2.5 that the rotation matrix is defined

$$\mathbf{R}_e(\eta, \boldsymbol{\epsilon}) = \mathbf{I} + 2\eta\mathbf{S}(\boldsymbol{\epsilon}) + 2\mathbf{S}(\boldsymbol{\epsilon})^2 \quad (2.40)$$

$$= \begin{bmatrix} 1 - 2(\epsilon_2^2 + \epsilon_3^2) & 2(\epsilon_1\epsilon_2 - \eta\epsilon_3) & 2(\epsilon_1\epsilon_3 + \eta\epsilon_2) \\ 2(\epsilon_1\epsilon_2 + \eta\epsilon_3) & 1 - 2(\epsilon_1^2 + \epsilon_3^2) & 2(\epsilon_2\epsilon_3 - \eta\epsilon_1) \\ 2(\epsilon_1\epsilon_2 + \eta\epsilon_2) & 2(\epsilon_2\epsilon_3 + \eta\epsilon_1) & 1 - 2(\epsilon_1^2 + \epsilon_2^2) \end{bmatrix}. \quad (2.41)$$

**Definition 2.6** (The quaternion product). *The quaternion product of two unit quaternions, is defined as*

$$\mathbf{q}_1 \otimes \mathbf{q}_2 = \begin{bmatrix} \eta_1\eta_2 - \boldsymbol{\epsilon}_1^T \boldsymbol{\epsilon}_2 \\ \eta_1\boldsymbol{\epsilon}_2 + \eta_2\boldsymbol{\epsilon}_1 + \mathbf{S}(\boldsymbol{\epsilon}_1)\boldsymbol{\epsilon}_2 \end{bmatrix} = \mathbf{F}(\mathbf{q}_1)\mathbf{q}_2, \quad (2.42)$$

where the matrix  $\mathbf{F}(\mathbf{q})$  is defined as

$$\mathbf{F}(\mathbf{q}) = \begin{bmatrix} \eta & -\boldsymbol{\epsilon} \\ \boldsymbol{\epsilon} & \eta\mathbf{I}_{3 \times 3} + \mathbf{S}(\boldsymbol{\epsilon}) \end{bmatrix} \quad (2.43)$$

**Definition 2.7** (The unity property). *The quaternion vector is confined to be of unit length, that is*

$$\eta^2 + \boldsymbol{\epsilon}^T \boldsymbol{\epsilon} \equiv 1. \quad (2.44)$$

This results in the state  $\mathbf{q}(t)$  evolving on a unit sphere in  $\mathbb{R}^4$ , i.e.  $\mathbb{S}^4$ .

### Kinematic differential equation for Euler parameters

As shown in Egeland & Gravdahl (2001), the time derivative of the quaternion elements is

$$\dot{\eta} = -\frac{1}{2}\boldsymbol{\epsilon}^T \boldsymbol{\omega}_{ib}^b \quad (2.45a)$$

$$\dot{\boldsymbol{\epsilon}} = \frac{1}{2}[\eta\mathbf{I}_{3 \times 3} + \mathbf{S}(\boldsymbol{\epsilon})]\boldsymbol{\omega}_{ib}^b, \quad (2.45b)$$

Or,

$$\dot{\mathbf{q}} = \frac{1}{2}\mathbf{J}(\mathbf{q})\boldsymbol{\omega}_{ib}^b, \quad (2.46)$$

where  $\mathbf{J}(\mathbf{q})$  is

$$\mathbf{J}(\mathbf{q}) = \begin{bmatrix} -\boldsymbol{\epsilon}^T \\ \eta\mathbf{I}_{3\times 3} + \mathbf{S}(\boldsymbol{\epsilon}) \end{bmatrix}. \quad (2.47)$$

Matrix multiplication verify that

$$\mathbf{J}(\mathbf{q})^T \mathbf{J}(\mathbf{q}) = \mathbf{I}_{3\times 3}, \quad (2.48)$$

leading to the expressions

$$\boldsymbol{\omega}_{ib}^b = 2\mathbf{J}(\mathbf{q})^T \dot{\mathbf{q}} \quad (2.49)$$

$$\boldsymbol{\omega}_{ib}^b = 2\mathbf{J}(\mathbf{q})\ddot{\mathbf{q}}, \quad (2.50)$$

where we have used that  $\dot{\mathbf{J}}(\mathbf{q})^T \dot{\mathbf{q}} = \mathbf{J}(\mathbf{q})^T \dot{\mathbf{q}} = 0$

## 2.4 Dynamic model

Using Newton-Euler equations of motion, a mathematical model for the satellite is developed. The satellite consists of an assumed rigid structure, the internal electronic devices, sensors, etc. and four reaction wheels, which are spinning about a fixed axis of inertial symmetry, such that the total moment of inertia may be assumed constant in the body frame. Such a mechanical structure, consisting of a rigid body combined with several spinning rotors or wheels, is commonly referred to as a gyrost (Hughes 1986).

Looking at figure 2.1, one can see the placement of the mass centra of the body, the  $i$ 'th wheel and the total mass marked  $\oplus_b$ ,  $\oplus_w$  and  $\oplus$  respectively. To derive a general model, it will be developed in the  $O$  coordinate system displaced from the center of mass. The total mass  $m$  is equal to the sum of the mass of the wheels and the rigid body:

$$m = m_b + \sum_{i=1}^4 m_{w,i} \quad (2.51)$$

We also define the first and second moment of inertia about the point  $O$  as

$$\vec{c} = \vec{c}_b + \sum_{i=1}^4 m_{w,i} \vec{b}_i \quad (2.52)$$

$$\vec{J} = \vec{J}_b + \sum_{i=1}^4 \vec{I}_{w,i} + m_{w,i} (b_i^2 \vec{1} - \vec{b}_i \vec{b}_i), \quad (2.53)$$

where  $\vec{c}_b$  is the first moment of inertia of the rigid body,  $\vec{b}_i$  is the vector from  $O$  to the  $i$ 'th wheel's center of mass,  $\vec{J}_b$  is the (second) moment of inertia of the body about  $O$ .

We may now define the linear and angular momenta of the rigid body and wheel  $i$  as

$$\vec{p}_b = m_b \vec{v} + \vec{\omega}_{ib} \times \vec{c}_b \quad (2.54)$$

$$\vec{p}_{w,i} = m_w \vec{v} + m_{w,i} \vec{\omega}_{ib} \times \vec{b}_i \quad (2.55)$$

$$\vec{h}_{b/o} = \vec{c}_b \times \vec{v} + \vec{J}_b \cdot \vec{\omega}_{ib} \quad (2.56)$$

$$\vec{h}_{w,i/c} = \vec{I}_{w,i} \cdot \vec{\omega}_{w,i}, \quad (2.57)$$

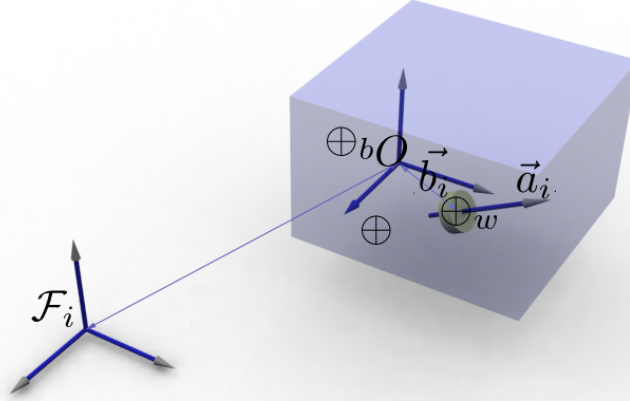


**Figure 2.1:** Gyrostat illustration

where  $\vec{h}_{b/o}$  is the angular momentum about  $O$ ,  $\vec{h}_{w,i/c}$  is the angular momentum about the  $i$ 'th wheel's center of gravity,  $\vec{v}$  is the linear velocity,  $\vec{\omega}_{ib}$  is the angular velocity of the body with respect to  $\mathcal{F}_i$  and  $\vec{\omega}_{w,i}$  is the angular velocity of the wheel frame with respect to  $\mathcal{F}_i$ .

The total angular momentum about  $O$ ,  $\vec{h}/o$ , can now be written as

$$\vec{h}/o = \vec{h}_{b/o} + \sum_{i=1}^4 (\vec{h}_{w,i/c} + \vec{b}_i \times \vec{p}_{w,i}), \quad (2.58)$$

where we have used that the the angular momentum about a point  $O$  is equal to the angular momentum about the center of gravity plus the vector between  $O$  and  $\oplus_{w,i}$  crossed with the linear momentum. Using the assumption of axial symmetry of the wheels and some algebraic manipulations, the expression may be written as

$$\vec{h}/o = \vec{c} \times \vec{v} + \vec{J} \cdot \vec{\omega}_{ib} + \sum_{i=1}^4 \vec{a}_i I_{s,i} \omega_{s,i}, \quad (2.59)$$

where  $\vec{a}_i$  is the axial vector of the  $i$ 'th wheel,  $I_{s,i}$  is the axial moment of inertia and  $\omega_{s,i}$  is the angular velocity about the axis.

If we now apply that the change of total angular momentum is due to an external force on the gyrostat, and the time derivative of a vector in a rotating frame (2.6) we obtain the expression for the

change of angular momentum as

$$\frac{d}{dt}\vec{h} = \frac{b}{dt}\vec{h} + \vec{\omega}_{ib} \times \vec{h} \triangleq \vec{\tau}_e \quad (2.60)$$

$$= \vec{c} \times \frac{b}{dt}\vec{v} + \underbrace{\vec{J} \cdot \frac{b}{dt}\vec{\omega}_{ib} + \sum_{i=1}^4 \vec{a}_i I_{s,i} \frac{d}{dt}\omega_{s,i}}_{\frac{b}{dt}\vec{h}} + \vec{\omega}_{ib} \times \vec{h} \quad (2.61)$$

Next we derive the components of  $\vec{h}_{w,i}$  along the axial direction

$$h_{a,i} = \vec{a}_i \cdot \vec{h}_{w,i} = \vec{a}_i \cdot \vec{I}_{w,i} \cdot \vec{\omega}_{w,i} \quad (2.62)$$

$$= \vec{a}_i \cdot (I_{t,i} + (I_{s,i} - I_{t,i})\vec{a}_i\vec{a}_i) \cdot (\vec{\omega}_{ib} + \vec{a}_i\omega_{s,i}) \quad (2.63)$$

$$= I_{s,i}\vec{a}_i \cdot \vec{\omega}_{ib} + I_{s,i}\omega_{s,i}, \quad (2.64)$$

where it has been used that the wheel inertia may be written as

$$\vec{I}_{w,i} = I_{t,i} + (I_{s,i} - I_{t,i})\vec{b}_i\vec{b}_i, \quad (2.65)$$

where  $I_{t,i}$  is the total wheel inertia and  $I_{s,i}$  is the inertia about the axial direction.

We now write the expressions for the total angular momentum and axial angular momentum of the wheels in  $\mathcal{F}_b$  as

$$\mathbf{h}^b = \mathbf{J}\omega_{ib}^b + \mathbf{A}\mathbf{I}_s\omega_s \quad (2.66a)$$

$$\mathbf{h}_a = \mathbf{I}_s\mathbf{A}^T\omega_{ib}^b + \mathbf{I}_s\omega_s, \quad (2.66b)$$

where  $\mathbf{A} \in \mathbb{R}^{3 \times 4}$  is a matrix of wheel axis in body coordinates,  $\mathbf{I}_s \in \mathbb{R}^{4 \times 4}$  a diagonal matrix of wheel axial inertias,  $\omega_s \in \mathbb{R}^4$  a vector of wheel velocities.

Writing (2.61) in coordinate form in  $\mathcal{F}_b$ , we obtain

$$\dot{\mathbf{h}}^b + \mathbf{S}(\omega_{ib}^b)\mathbf{h}^b + \mathbf{S}(\mathbf{c}^b)\dot{\mathbf{v}}^b = \boldsymbol{\tau}_e. \quad (2.67)$$

Through some manipulation using (2.66a),(2.66b) and (2.67) and assuming that the  $O$  coincides with the center of mass such that  $\mathbf{c}^b \equiv 0$ , we obtain the differential equation describing the rotational motion of the gyrostat as

$$\dot{\mathbf{h}}^b = \mathbf{S}(\mathbf{h}^b)\bar{\mathbf{J}}^{-1}(\mathbf{h}^b - \mathbf{A}\mathbf{h}_a) + \boldsymbol{\tau}_e^b \quad (2.68a)$$

$$\dot{\mathbf{h}}_a = \boldsymbol{\tau}_a, \quad (2.68b)$$

where  $\bar{\mathbf{J}} \in \mathbb{R}^{3 \times 3}$  is an inertia-like matrix defined as

$$\bar{\mathbf{J}} \triangleq \mathbf{J} - \mathbf{A}\mathbf{I}_s\mathbf{A}^T \quad (2.69)$$

(2.68b) may also be written in terms of the angular velocities as

$$\mathbf{J}\dot{\omega}_{ib}^b = \mathbf{S}(\mathbf{J}\omega_{ib}^b)\omega_{ib}^b + \mathbf{S}(\mathbf{A}\mathbf{I}_s\omega_s)\omega_{ib}^b - \mathbf{A}\boldsymbol{\tau}_a + \boldsymbol{\tau}_e \quad (2.70a)$$

$$\mathbf{I}_s\dot{\omega}_s = \boldsymbol{\tau}_a - \mathbf{I}_s\mathbf{A}\dot{\omega}_{ib}^b \quad (2.70b)$$

### 2.4.1 Inertial coordinate model

The model derived in the previous section, may also be given in inertial coordinates using the kinematic equation which relates angular velocity to the derivative of the attitude parameter.

Using the kinematic equation (2.35), the inverse kinematics relating the angular velocity and acceleration to the first and second derivative of the Euler angles is

$$\omega_{ib}^b = \mathbf{T}^{-1}(\boldsymbol{\Psi})\dot{\boldsymbol{\Psi}}, \quad (2.71)$$

$$\dot{\omega}_{ib}^b = \dot{\mathbf{T}}^{-1}(\boldsymbol{\Psi})\dot{\boldsymbol{\Psi}} + \mathbf{T}^{-1}(\boldsymbol{\Psi})\ddot{\boldsymbol{\Psi}}. \quad (2.72)$$

Inserting for  $\omega_{ib}^b$  and  $\dot{\omega}_{ib}^b$ , and multiplying each side with the transpose inverse kinematic matrix we obtain

$$\mathbf{M}^*(\Psi)\ddot{\Psi} + \mathbf{C}(\Psi, \dot{\Psi})\dot{\Psi} = -\mathbf{A}^*(\Psi)\tau_a + \mathbf{T}^{-T}(\Psi)\tau_e \quad (2.73)$$

where

$$\mathbf{M}^*(\Psi) = \mathbf{T}^{-T}(\Psi)\mathbf{I}_b\mathbf{T}^{-1}(\Psi) \quad (2.74)$$

$$\mathbf{C}(\Psi, \dot{\Psi}) = -\mathbf{T}^{-T}(\Psi)\mathbf{S}(\mathbf{I}_b\mathbf{T}^{-1}(\Psi)\dot{\Psi} + \mathbf{A}\mathbf{I}_s\omega_s)\mathbf{T}^{-1}(\Psi) + \mathbf{T}^{-T}(\Psi)\mathbf{I}_b\dot{\mathbf{T}}^{-T}(\Psi). \quad (2.75)$$

$$\mathbf{A}^*(\Psi) = \mathbf{T}^{-T}(\Psi)\mathbf{A} \quad (2.76)$$

It can also be shown the the matrices have the following important properties

$$\mathbf{M}^* = \mathbf{M}^{*T} > 0 \quad (2.77)$$

$$\mathbf{x}^T(\dot{\mathbf{M}}^* - 2\mathbf{C}^*)\mathbf{x} \equiv 0, \forall \mathbf{x} \in \mathbb{R}^3 \quad (2.78)$$

**Remark 2.3.** *The derivation is done using Euler angles, but it is straightforward to extend this to Euler parameters. A drawback is that  $\mathbf{M}(\mathbf{q})^*$  becomes singular for  $\eta = \pm 1$ . This is however only a problem in simulation, as it is not present in the physical system, under the condition that the control law is independent of the inverse of  $\mathbf{M}(\mathbf{q})^*$ .*

## 2.5 External forces and torques

In this section we derive expressions for the external forces and torques that affect the satellite while orbiting Earth, both environmental and the actuator generated.

### 2.5.1 Gravitational forces and torques

The gravitational force field in space, is the result of gravitational forces acting between every body in the Universe. The forces are dependent on the bodies' mass and the square of the distance between them. The field is thus non-uniform, with the result that any non-symmetrical object in space will experience a torque about its center of mass. In the most general form, the forces and torques on the body due to n celestial bodies is expressed:

$$\vec{f} = \int_B d\vec{f} = -G \sum_{n=1}^N \int_{B_n} \int_B \frac{\vec{\rho}_n dm_n dm}{\rho_n^3} \quad (2.79)$$

$$\vec{g}_o = \int_B \vec{r} \times d\vec{f} = -G \sum_{n=1}^N \int_{B_n} \int_B \frac{\vec{r} \times \vec{\rho}_n dm_n dm}{\rho_n^3} \quad (2.80)$$

These forms are too general to be of practical use, as their multiple integrations make analytical progress virtually impossible (Hughes 1986). Instead, Hughes makes four assumptions that simplifies the gravitational torque expressions.

- (1) Only one celestial primary need be considered
- (2) This primary possesses a spherical symmetrical mass distribution
- (3) The spacecraft is small compared to its distance from the mass center of the primary
- (4) The spacecraft consists of a single body

Assumption 1 means that the sums in (2.79) and (2.80) can be replaced by a single term. Assumption 2 leads to the removal of the integration over  $B_n$ , replacing it with a point mass in the mass center of  $B_n$ . Assumption 3 is equal to the statement  $\frac{r}{R_c} \ll 1$  and finally assumption 4 allows us to

choose the mass center as the reference point without loss of generality. Using these assumptions one may derive the following expression for the gravitational torque:

$$\vec{\tau}_m \triangleq 3\left(\frac{\mu}{R_c^3}\right)\vec{z}_{o3} \times \vec{I} \cdot \vec{z}_{o3}, \quad (2.81)$$

where  $\mu$  is the gravitational constant of the primary celestial body,  $R_c$  is the distance between the mass centers of the two bodies,  $\vec{z}_{o3}$  is the nadir pointing vector and  $\vec{I}$  is the inertia matrix. We note that the nadir pointing vector in body coordinates is equal to the third column in the rotation matrix between  $\mathcal{F}_b$  and  $\mathcal{F}_o$ , using that the nadir pointing vector in orbit coordinates is equal to the  $z_o$  - axis

$$\mathbf{z}_{o3}^b = \mathbf{R}_o^b \mathbf{z}_o^o = \mathbf{R}_o^b \begin{bmatrix} 0 \\ 0 \\ 1 \end{bmatrix}. \quad (2.82)$$

We may now give the gravity gradient torque in coordinate vectors in the body system as:

$$\boldsymbol{\tau}_g = 3\omega_o^2 (\mathbf{z}_{o3}^b)^\times \mathbf{I} \mathbf{z}_{o3}^b, \quad (2.83)$$

where we have also used that  $\frac{\mu}{R_c^3} = \omega_o^2$ .

A maximum bound may be found on the torque about the  $x_b$ - or  $y_b$ -axes. Due to symmetry we may consider a simple rotation about one of the axis. Rotating the body an angle  $\theta$  about the  $x_b$ -axis, results in the rotation matrix

$$\mathbf{R}_o^b = \mathbf{R}_x(\theta)^T = \begin{bmatrix} 1 & 0 & 0 \\ 0 & \cos \theta & \sin \theta \\ 0 & -\sin \theta & \cos \theta \end{bmatrix}. \quad (2.84)$$

Computing the gravitational torque from (2.81) results in the following component about the  $x_b$ -axis:

$$\tau_{g,x} = 3\omega_o^2 (i_y - i_z) \cos \theta \sin \theta \quad (2.85)$$

This function has a maximum for  $\theta = 45^\circ$ :

$$\|\tau_{g,x}\|_\infty = \frac{3}{2}\omega_o^2 (i_y - i_z) \quad (2.86)$$

**Example 2.1.** *As the satellite inertia is given as  $I_b = \text{diag}(i_x, i_y, i_z) = \text{diag}(4, 4, 3)\text{kgm}^2$  and  $\omega_o = 1.083 \times 10^{-3}\text{rad/s}$ , the bound is*

$$\|\tau_{g,x}\|_\infty = 1.7593 \times 10^{-6} \text{Nm} \quad (2.87)$$

### 2.5.2 Aerodynamical forces and torques

The aerodynamical torque on the satellite results from particles in the atmosphere colliding with a non-symmetric cross section. This effect is most severe for LEO. In the worst-case this torque is given by:

$$\boldsymbol{\tau}_a = F(c_{pa} - c_g), \quad (2.88)$$

where  $F = 0.5[\rho C_d AV^2]$  and  $\rho$  is the atmospheric density,  $C_d$  is the drag coefficient,  $A$  is the surface area and  $V$  is the spacecraft velocity.

### 2.5.3 Magnetic torques

Due to electric currents in liquid portions of the Earth's iron core, there is a magnetic field surrounding the planet as can be seen in figure 2.2 (Freedman & Kaufmann III 2002). Since the field is not generated by a permanent magnet, but instead by a liquid, the field is constantly changing and changes sign about once every 1 million years. Due to this, one needs an up to date model of the field to be able to evaluate its effect on the spacecraft. Such a model is published every five years by the

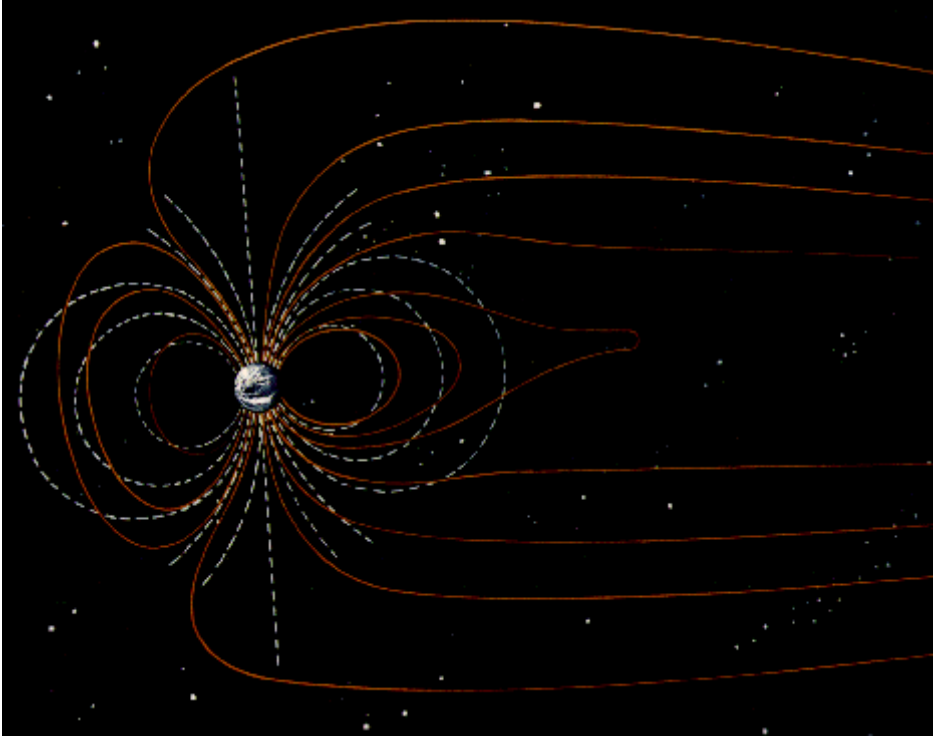


**Figure 2.2:** Illustration of the Earth's magnetic field

International Association of Geomagnetism and Astronomy (IAGA), and is called the International Geomagnetic Reference Field (IGRF). This model give the magnetic field values for a given longitude and latitude at a given decimal date between 1900-2010 (International Association of Geomagnetism and Aeronomy 2005).

As basic physics tells us, a magnet exposed to a magnetic field, will experience a torque which tries to align the magnetic field generated by the magnet with the surrounding field. The same effect is experienced by a spacecraft orbiting Earth, due to permanent magnets and current loops. This may generate unwanted disturbance torques if not balanced properly. But it may also be used as an advantage by including a controlled magnetic moment (Hughes 1986), generating a torque given by

$$\vec{\tau}_m = \vec{m} \times \vec{B}(t), \quad (2.89)$$

where  $\vec{m}$  is the generated magnetic moment and  $\vec{B}(t)$  is the local geomagnetic field.

The magnetic moment is generated by electromagnetic actuators, often referred to as magnetic torquers, and consist of two basic configurations. One is the coil based, where current is sent through a current loop which generates the magnetic moment proportional to the area of the coil and the number of windings. The other type is the magnetic rod, where a wire is wound around a rod made of high permeability material.

#### 2.5.4 Solar radiation and solar wind

Solar radiation is due to the constant bombardment of photons, and will generate a solar pressure force on the surface of the satellite, acting through a point referred to as the *the center of solar pressure,  $c_{sp}$* . The force is very small, dependent on the satellite's surface material, geometry and location, it will give only 5N to a surface of 1  $km^2$ , it may be given by (Vallado 2001)

$$F = \frac{F_s}{c} A_s (1 + q) \cos i, \quad (2.90)$$

where  $F_s$  is the solar constant  $1.367 \text{ W/m}^2$ ,  $c$  is the speed of light,  $A_s$  is the surface area,  $q$  is the reflectance factor and  $i$  is the angle of incidence of the Sun. Solar wind on the other hand consists of ionized nuclei and electrons, and is typically 100-1000 times smaller than the solar radiation forces. Dependent on the position of  $c_{sp}$  relative to the center of gravity,  $c_g$ , the force will generate a torque about  $c_g$  given by

$$\tau_{sp} = F(c_{sp} - c_g), \quad (2.91)$$

where  $F$  is given by (2.90).

These environmental forces, are usually considered disturbances, but has also been considered both for propulsion and attitude control for long term missions. On Mariner IV, launched 1969, solar vanes were used to align the probe with the sun and thereby maximize power. Experiments have also been conducted by ESA on OST-2, a geostationary communication satellite, where attitude was controlled by manipulating the solar panels. In recently control algorithms using feedback linearization and adaptive feedback have been researched in Singh & Yim (1995), Singh & Yim (2002) and Singh & Yim (1996). A review of previous literature on attitude control by means of solar pressure, is given in Venkatachalam (1993).

For propulsion, it has been proposed to use vast solar sails to generate force for interstellar exploration. And in Wallace, Ayon & Sprague (2000) it is proposed as the key enabling technology for such missions. No missions have been launched to this date, but Cosmos 1 is scheduled for launch spring 2005 and will be the first solar sail powered spacecraft.

### 2.5.5 Thruster forces and torques

Thrusters produce torque by expelling mass through a valve. The simplest and most common valve is strictly on-off and single level, but variable and dual-level thrusters are available. We divide the thrusters into cold- and hot-gas systems. In hot-gas systems the energy is produced in a chemical reaction, while in cold-gas systems it comes from the latent heat of a phase change or from the work of compression without a phase change.

Typical force capabilities of thrusters are between 0.5 to 9000 N for hot-gas systems and less than 5 N for cold-gas systems, depending on size. The torque amount from a given thruster is dependent on its distance from the center of mass (Vallado 2001).

The advantage of thrusters are that they can supply a reliable torque in any direction, anywhere in the orbit, and the possibility of large torques resulting in high slew rates. The disadvantage is of course fuel requirements, which dictates spacecraft life.

## 2.6 Internal torques

### 2.6.1 Reaction wheels

A reaction wheel is essentially a torque providing motor with a relatively high rotor inertia. It is able to load and unload angular momentum internally, and is thus often referred to as momentum exchange devices as they do not change the overall angular momentum of the satellite, but redistributes it to different parts. The amount of torque that is provided is dependent on the size of the rotor and motor, and is in the range from  $0.01 \text{ Nm}$  to  $1 \text{ Nm}$ .

A wheel complete with motor and drive electronics, is usually referred to as a reaction wheel assembly (RWA). Three wheels, one along each axis, is needed for full three-axis control. For redundancy and performance a composition of RWAs usually consists of more than three wheels. One such composition is the tetrahedron composition (Figure 2.3). A regular tetrahedron is a pyramid composed of four equilateral triangular faces, three of which meets at each vertex. Each wheel-axis is orthogonal on a face, and crosses through the center of the pyramid.

The torque from a wheel to the body equals the torque applied to the wheel from a motor attached to the body, but with opposite sign. The torque in body coordinated is equal to

$$\tau_{a,i}^b = \mathbf{a}_i^b \tau_{a,i}, \quad (2.92)$$

where  $\mathbf{a}_i^b$  is the unit wheel axis in body coordinates. The total torque may then be written as

$$\boldsymbol{\tau}_a^b = \mathbf{A}\boldsymbol{\tau}_a \quad (2.93)$$

where  $\boldsymbol{\tau}_a$  is a vector of wheel torques and  $\mathbf{A}$  is given by (Wisniewski 2000)

$$\mathbf{A} = \begin{bmatrix} \sqrt{\frac{1}{3}} & \sqrt{\frac{1}{3}} & -\sqrt{\frac{1}{3}} & -\sqrt{\frac{1}{3}} \\ \sqrt{\frac{2}{3}} & -\sqrt{\frac{2}{3}} & 0 & 0 \\ 0 & 0 & -\sqrt{\frac{2}{3}} & \sqrt{\frac{2}{3}} \end{bmatrix} \quad (2.94)$$

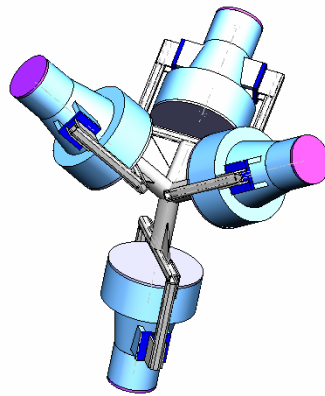


**Figure 2.3:** 4 reaction wheel assemblies in tetrahedron composition

## Chapter 3

# Stability Theory

In this chapter, a short review of the stability theory used in this thesis will be given. We will present definitions of stability, and some theorems used to establish stability of both autonomous and nonautonomous systems.

### 3.1 Introduction to nonautonomous systems

Nonautonomous or time-varying systems, are systems where the ordinary differential equations are functions of both state *and time*:

$$\dot{x} = f(t, x) \quad x(t_0) \triangleq x_0 \quad (3.1)$$

$$y = h(x), \quad (3.2)$$

where  $x \in \mathbb{R}^n$  is the state,  $y \in \mathbb{R}^l$  is the output and  $h(x) \in \mathbb{R}^n$  is function mapping the state to the output.

Though the system itself may be autonomous or time-invariant, a nonautonomous system may arise in nonlinear tracking control problems when desired states are given as functions of time. That is when the goal is to design the input  $u(t,x)$  such that the output  $y$  of the system

$$\dot{x} = f(x, u) \quad x(t_0) \triangleq x_0 \quad (3.3)$$

$$y = h(x), \quad (3.4)$$

tracks a time-varying function,  $y_d(t) = h(x_d(t))$ . Assuming the desired output is generated from some desired state  $x_d$ , satisfying  $\dot{x}_d = f(x_d, u)$ , the closed-loop system with control input  $u = u(x, x_d(t), y_d(t))$  may be written as

$$\dot{\tilde{x}} = \tilde{f}(t, \tilde{x}) \quad \tilde{x}(t_0) \triangleq \tilde{x}_0 \quad (3.5)$$

$$\tilde{y} = \tilde{h}(t, \tilde{x}) \quad (3.6)$$

where  $\tilde{x} \in \mathbb{R}^n$  is the tracking error,  $\tilde{f}$  the error dynamics,  $\tilde{y} \in \mathbb{R}^l$  the output tracking error.

A major difficulty with nonautonomous systems is in the stability analysis. As the often used invariance theorems of LaSalle no longer applies, resulting in hardships when the Lyapunov time-derivative is only negative semi-definite. Instead one must look for a new Lyapunov function which fulfills the requirements of Lyapunov's direct method or look to other stability results. Alternatively the so called Barbalat's Lemma and LaSalle-Yoshizawa can be applied, though these results can only obtain convergence results. An attractive alternative is an extension of Matrosov's theorem which allows us to conclude uniformly global asymptotic stability with a semi-definite Lyapunov function, using some auxiliary functions.

## 3.2 Stability definitions

**Definition 3.1.** A continuous function  $\alpha : \mathbb{R}_{\geq 0} \rightarrow \mathbb{R}_{\geq 0}$  is said to belong to class  $\mathcal{K}$  if it is strictly increasing and  $\alpha(s) = 0$ . Moreover, it is said to be of class  $\mathcal{K}_{\infty}$  if  $\alpha(s) \rightarrow 0$  as  $s \rightarrow \infty$ .

**Definition 3.2.** A continuous function  $\beta : \mathbb{R}_{\geq 0} \times \mathbb{R}_{\geq 0} \rightarrow \mathbb{R}_{\geq 0}$  is said to belong to class  $\mathcal{KL}$  if, for each fixed  $s$   $\beta(\cdot, s)$  is of class  $\mathcal{K}$  and for each fixed  $r$ ,  $\beta(r, \cdot)$  is strictly decreasing and  $\beta(r, s) \rightarrow \infty$  as  $s \rightarrow \infty$ .

**Definition 3.3** (Lipschitz condition). A function  $f(t, x)$  satisfies the Lipschitz condition if

$$\|f(t, x) - f(t, y)\| \leq L\|x - y\|. \quad (3.7)$$

The condition holds locally on a domain  $\mathbb{D} \subset \mathbb{R}^n$  if each point of  $\mathbb{D}$  has a neighborhood  $\mathbb{D}_0$  where  $f$  satisfies the condition for all points in  $\mathbb{D}_0$  with some Lipschitz constant  $L_0$ . It is globally Lipschitz if  $\mathbb{D} = \mathbb{R}^n$ .

## 3.3 Stability theorems and lemmas

### 3.3.1 Autonomous systems

**Theorem 3.4** (LaSalle's invariance theorem (Khalil 2000)). Given the autonomous system

$$\dot{x} = f(x), \quad (3.8)$$

with  $x = 0$  as the only equilibrium point. Given that there exists a Lyapunov function  $V$  such that:

- $V : \mathbb{R}^n \rightarrow \mathbb{R}, V > 0$ , continuously differentiable, radially unbound
- $\dot{V}(x) \leq 0 \forall x \in \mathbb{R}^n$
- Suppose no other solution than the trivial solution  $x(t) \equiv 0$  can stay identically in  $S = \{x \in \mathbb{R}^n | \dot{V}(x) = 0\}$

Then, the origin is uniformly globally asymptotically stable (UGAS).

### 3.3.2 Nonautonomous system

**Theorem 3.5** (Uniform stability (Khalil 2000)). Let  $x = 0$  be an equilibrium point for (3.1) and  $\mathbb{D} \subset \mathbb{R}^n$  be a domain containing  $x = 0$ . Let  $V : \mathbb{R}_{\geq 0} \times \mathbb{D} \rightarrow \mathbb{R}$  be a continuously differentiable function such that

$$W_1(x) \leq V(t, x) \leq W_2(x) \quad (3.9)$$

$$\frac{\partial V}{\partial t} + \frac{\partial V}{\partial t} f(t, x) \leq 0 \quad (3.10)$$

$\forall t \geq 0$  and  $\forall x \in \mathbb{D}$ , where  $W_1(x)$  and  $W_2(x)$  are continuous positive definite functions on  $\mathbb{D}$ . Then,  $x = 0$  is uniformly stable. If  $\mathbb{D} = \mathbb{R}^n$ , then  $x = 0$  is uniformly globally stable.

**Theorem 3.6** (Uniform global exponential stability (Khalil 2000)). Let  $x = 0$  be an equilibrium point of (3.1) and  $\mathbb{D} \subset \mathbb{R}^n$  be a domain containing the origin. Let  $V : \mathbb{R}_{\geq 0} \times \mathbb{D} \rightarrow \mathbb{R}$  be a continuously differentiable function such that

$$k_1 \|s\|^a \leq V(t, x) \leq k_2 \|x\|^a \quad (3.11)$$

$$\frac{\partial V}{\partial t} + \frac{\partial V}{\partial t} f(t, x) \leq -k_3 \|x\|^a \quad (3.12)$$

$\forall t \geq 0$  and  $\forall x \in \mathbb{D}$ , where  $k_1, k_2, k_3$ , and  $a$  are positive constants. Then  $x = 0$  is uniformly exponentially stable. If the assumptions hold globally, then  $x = 0$  is uniformly globally exponentially stable (UGES).

**Theorem 3.7** (Krasovskii-LaSalle (Vidyasagar 1993)). *Suppose the system (3.1) is periodic, and there exists a function  $V : \mathbb{R}_+ \times \mathbb{R}^n \rightarrow \mathbb{R}$  of class  $\mathcal{K}$ , such that:*

- $V$  is a positive definite function and radially unbounded
- $\dot{V}(t, x) \leq 0, \forall t \geq 0, \forall x \in \mathbb{R}^n$

then, if

$$R = \left\{ x \in \mathbb{R}^n : \dot{V}(t, x) = 0 \right\} \quad (3.13)$$

does not contain any trajectories other than the trivial trajectory  $x(t) \equiv 0$ , the origin is uniformly globally asymptotically stable (UGAS).

**Lemma 3.1** (Barbalat's Lemma (Khalil 2000)). *Let  $\phi : \mathbb{R} \rightarrow \mathbb{R}$  be a uniformly continuous function on  $[0, \infty)$ . Suppose that  $\lim_{t \rightarrow \infty} \int_0^t \phi(\tau) d\tau$  exists and is finite. Then,*

$$\phi(t) \rightarrow 0 \quad \text{as } t \rightarrow \infty. \quad (3.14)$$

The application of the above lemma is better described by the following result, found in Slotine & Li (1991)

**Lemma 3.2** ("Lyapunov-Like Lemma", (Slotine & Li 1991)). *If a scalar function  $V(x, t)$  satisfies the following conditions*

- $V(x, t)$  is lower bounded
- $\dot{V}(x, t)$  is negative semi-definite
- $\dot{V}(x, t)$  is uniformly continuous in time

then,  $\dot{V}(x, t) \rightarrow 0$  as  $t \rightarrow \infty$ .

A stronger result follows from an extension of the so-called Matrosov's Theorem, which were derived in Loria, Panteley, Popovic & Teel (2002). This allows us to state UGAS in the case of a semi-definite Lyapunov function derivative, with the help of some auxiliary functions.

**Theorem 3.8** (Matrosov). *Under the following assumptions, the origin of the system (3.1) is UGAS.*

**Assumption 1.** *The origin of the system (3.1) is UGS.*

**Assumption 2.** *There exist integers  $j, m > 0$  and for each  $\Delta > 0$  there exist*

- a number  $\mu > 0$
- locally Lipschitz continuous functions  $V_i : \mathbb{R} \times \mathbb{R}^n \rightarrow \mathbb{R}, i \in \{1, \dots, m\}$
- a (continuous) function  $\phi : \mathbb{R} \times \mathbb{R}^n \rightarrow \mathbb{R}^m, i \in \{1, \dots, m\}$
- continuous functions  $Y_i : \mathbb{R}^n \times \mathbb{R}^m \rightarrow \mathbb{R}, i \in \{1, \dots, j\}$

such that, for almost all  $(t, x) \in \mathbb{R} \times \mathcal{B}(\Delta)^1$ ,

$$\max\{|V_i(t, x)|, |\phi(t, x)|\} \leq \mu, \quad (3.15)$$

$$\dot{V}_i(t, x) \leq Y_i(x, \phi(t, x)). \quad (3.16)$$

**Assumption 3.** *For each integer  $k \in \{1, \dots, j\}$  we have that*

$$\{(z, \psi) \in \mathcal{B}(\Delta) \times \mathcal{B}(\mu), Y_i(z, \psi) = 0 \forall i \in \{1, \dots, k-1\}\} \Rightarrow \{Y_k(z, \psi) \leq 0\}. \quad (3.17)$$

**Assumption 4.** *We have that*

$$\{(z, \psi) \in \mathcal{B}(\Delta) \times \mathcal{B}(\mu), Y_i(z, \psi) = 0 \forall i \in \{1, \dots, j\}\} \Rightarrow \{z = 0\}. \quad (3.18)$$

*Proof.* See Loria et al. (2002). □

---

<sup>1</sup> $\mathcal{B}(\Delta) = \{x \in \mathbb{R}^n \mid \|x\| \leq \Delta\}$



## Chapter 4

# Formation Flying

In this chapter the concept of formation flying of satellites will be presented. As the main contribution of this thesis is attitude control, the focus will be on the coordinated control of attitude. We will present some possible applications and some work which have been presented in the literature.

### 4.1 Introduction

Formation flying have been successfully applied to several vehicles, from unmanned aerial vehicles (UAVs) and fighter jets to autonomous mobile robots. Lately the interest in formation flying have reached the satellite community. The reason for this increased activity, comes from a number of advantages in formation flying. The main advantage is that by successfully controlling a formation of satellites or spacecraft, one may have them cooperate in a way that enables missions that would have required an enormous single spacecraft. The ability to distribute the functionality of one large spacecraft among several much smaller, may reduce the total weight and in turn the launch costs. Since this enables one to integrate the instruments on standardized satellites, some sort of assembly line production may be possible, also reducing cost and design errors. Though formation flying has great advantages, it comes at the cost of a more complicated control system. As some application requires the relative position to be controlled with millimeter accuracy while keeping the pointing accuracy within 1/10th of a degree, the control system is required to be both robust and accurate. As will be explained in the following.

### 4.2 Application of formation flying

The formation flying concept enables several applications that would not have been possible or that are enhanced when compared to using a single large spacecraft. Two such applications are presented in the following; Earth observation and space-based interferometry.

#### 4.2.1 Earth observation

The advantage of formation flight in this application is the ability to use smaller, simpler and cheaper satellites, instead of one large and complex. The formation flying concept is especially useful in synthetic aperture radar, where either several small satellites may operate as one large virtual satellite with a much larger aperture than would be possible on a single satellite, or several satellites with SAR capabilities cooperate in formation, resulting in an enlarged field of view. Other applications include gravitational field mapping, contemporaneous spatial sampling of atmospheric data and co-observations (i.e. near-simultaneous observations of the same science target by instruments on multiple platforms.) By distributing sensors for science instrumentation, there is an enhanced fault-tolerance. If one small satellite should fail it is easier to replace this by a new satellite, than to use the space shuttle crew to repair or change the instruments on the large single satellite.

### 4.2.2 Space-based interferometry

In space-based interferometry the advantages in formation flying of spacecraft is not so much in cost and assembly line production, but rather in increased accuracy. Examples of planned missions includes ESA's Darwin mission and NASA's Terrestrial Planet Finder and MAXIM. In these missions interferometry will be applied in the search of earth-like planets. With a large aperture, it would even be possible to look for signs of life, such as ozone. (Beichman, Woolf & Lindensmith 1998).

Interferometry takes advantage of the wave properties of light. The phenomena was first reported in 1803 by Thomas Young, and is popularly known as *Young's two-slit experiment*. In this setup light is impinged upon two slits, the two resulting coherent light sources will interfere and create fringes when the light hits the surface in front of the slits (Tipler 1999).

This is also the basis for space-based interferometry. Here the two slits are replaced by two or more space-based telescopes or collector spacecraft. The observed waves are then transferred to the combiner spacecraft, where the waves interfere to make fringes. To be able to observe a planet, one has to remove the powerful light from the star it is orbiting. The idea is therefor to delay the light from the telescopes by an added phase shift,  $\pi$ , such that the light from the star interferes destructively leaving only the light received from the planet. This is referred to as nulling interferometry (Fridlund 2004). The accuracy is determined by the baseline, i.e. the distance or separation between the spacecraft. Logically with formation flying one is able to increase the separation far more than with a structurally connected craft. The drawback is of course the difficulty of keeping inter-spacecraft position and orientation.

### 4.2.3 Current projects

There are several current projects which are dealing with the formation flying and coordinated control of satellites. A list of some examples can be found in table 4.1.

Project name	Description	Affiliation
MicroSAR	Small low-cost SAR satellites, capable of land and sea observation	EADS Astrium
TanDEM-X	Close formation flight with TerraSAR-X satellites, mapping of Earth's topography with unprecedented precision	Infoterra GmbH
TechSat-21	Focus on Ground Moving Target Identification and SAR	US Air Force
EO-1	Will fly in formation with Landsat 7, SAC-C and Terra	NASA
Space Technology 3	Will use precision formation flight to perform stellar optical interferometry	NASA
Darwin	Six 2 m diameter telescopes in tight formation, to perform analyze of Earth like planets	ESA

**Table 4.1:** Current projects on formation flying

## 4.3 Literature review

In this section a review of the problems which have been addressed in the literature is given. The main focus is on the the relative attitude case.

Though most work on formation flying spacecraft, and satellites in particular, have been performed on the relative position problem, there do exist a great deal of literature on the control of relative attitude. The first work in this field, as in the relative position case, stems from the work done on automatic rendezvous and docking control of two spacecraft, as was done on the Apollo missions. Later it was utilized in the Space Shuttle, Skylab and Gemini. (Wang, Hadaegh & Mokuno 2003)

As already mentioned, in the 1990's the focus again shifted to the control of several spacecraft. From the literature one can identify three approach to formation control:

- Leader - follower
- Behavioral
- Virtual structure

#### 4.3.1 Leader-follower

In the leader-follower strategy, one typically divides the spacecraft into subgroups. Within each subgroup one craft is defined as the leader and the rest are defined as followers. While the leader will track a predefined trajectory, the followers are controlled to track the leader. This scheme is easy to understand and implement, it will allow the formation to withstand perturbations in the leader, but may fail if the follower were to be perturbed. Versions of this approach can be found in Wang, Hadaegh & Lau (1999), Pan & Kapila (2001) and Kang & Yeh (2002) and Nijmeijer & Rodriguez-Angeles (2003).

Wang et al. (1999) proposes a control technique to rotate the entire formation about a given axis and synchronize the individual spacecraft with the formation. Both position and attitude are controlled, and the error is proven to decay to zero exponentially, though under the assumption of no environmental disturbances and implementation difficulties.

In Pan & Kapila (2001) an adaptive nonlinear controller is proposed, which assumes a unknown mass and inertia, and coupled translational and attitude dynamics. Based on a Lyapunov framework they derive a controller which leads to globally asymptotic convergence of the follower spacecraft relative position and attitude.

Kang & Yeh (2002) proposes a more general way to achieve leader/follower synchronization, through the use of reference projections. The control input to each satellite is a function of its own state and the reference projection. Where the reference projection defines a desired state for the closed-loop system, as a function of the measured and desired states of the other satellites.

A general synchronization theory for mechanical systems is developed in the Nijmeijer & Rodriguez-Angeles (2003), for use on robot manipulators. The methods are applied in the synchronization of a two-satellite formation.

#### 4.3.2 Behavioral

The behavioral strategy, each spacecraft is defined as an agent and the control action for each agent is defined by a weighted average of the controls corresponding to each desired behavior for the agent. This approach eases the implementation of conflicting or competing control objectives, such tracking versus avoidance. It is however difficult to enforce group behavior, and to mathematically guarantee stability and formation convergence. Another problem is that some unforeseen behavior may occur when goals are conflicting.

A lot of results in this area have been reported in field of autonomous mobile robots, and three notable references are Mataric (1992), Balch & Arkin (1998) and Mali (2002). Mali (2002) contains a review of some work done in the field.

Lawton applies the strategy to spacecraft formations in his PhD thesis Lawton (2000). Here he treats both the relative position and the relative attitude case, and includes analytical proofs based on perfect knowledge of the states.

#### 4.3.3 Virtual structure

In the third approach, virtual structure, the spacecraft formation is viewed as a virtual rigid body. The desired states of a single spacecraft, may be specified such that the formation moves as a single structure. In this scheme it is easy to prescribe a coordinated group behavior and the formation may

be maintained well during maneuvers, given that the single spacecraft is able to follow its trajectory. The virtual structure may however limit the class of possible maneuvers.

A great deal of work have been done in this area using mobile robots Lewis & Tan (1997), and have recently been applied to spacecraft formations in Ren & Beard (2004), Beard (1998), Beard & Hadaegh (1998) and Beard, Lawton & Hadaegh (2001).

## Chapter 5

# Synchronization of mechanical systems

In this chapter the theory of synchronization of mechanical systems is introduced, and illustrated by an example from robotics.

### 5.1 Introduction

The synchronization phenomenon describes the event when dynamical systems in some sense exhibit a similar behavior, in the time domain. For instance when two pendulums are oscillating with the same frequency (Huygens 1673) or the synchronized sound in nearby organ tubes (Rayleigh 1945).

Nijmeijer, Blekman, Fradkov & Pogromsky (1997) developed some formal definitions of the synchronization phenomena. In their work they distinguish between frequency synchronization and coordinate synchronization. Frequency synchronization, also referred to as the Huygens synchronization property, may be defined for periodic motion, where the frequencies of motions coincide or are some integer multiple of a given frequency,  $\omega_s$ , referred to as the synchronization frequency. Coordinate synchronization occurs when the outputs or some state-variables of a system, coincide with the corresponding variables of some other system for all  $t \geq 0$  or asymptotically as  $t \rightarrow \infty$ .

Synchronization theory has been used for several applications in the literature. In Rodriguez-Angeles (2002) it was used in the synchronization of robot manipulators, Kyrkjebø & Pettersen (2003) proposed using the theory in the replenishment and rendezvous control of ships. In industrial application synchronization theory based feedback methods have been used in the control of servo-motors replacing the traditional mechanical interconnections in industrial machinery (Danbury & Jenkinson 1994).

### 5.2 The problem formulation

In this work we have adapted the problem formulation of Rodriguez-Angeles (2002), distinguishing between external and mutual synchronization of mechanical systems. In the following a short review of the definitions is given.

#### 5.2.1 External synchronization

In external synchronization, we define a leader system, which is the dominant system, and a bounded set of follower systems. The synchronization problem consists of creating either physical interconnections or control feedback loops, which forces the outputs of the follower systems to conform with those of the leader. In this formulation the control of the leader system is not considered, and its dynamical

model is assumed unknown. Depending on the available measurements an observer may have to be designed to estimate both the synchronization error and the states of the follower system.

### 5.2.2 Mutual synchronization

The mutual synchronization problem formulation assumes physical or control feedback interconnections between all systems, and deals with the problem of designing interconnections in such a way that all systems conforms to a predefined trajectory in a synchronized manner. All models are assumed known. As with the previous formulation, an observer may have to be designed depending on measurement availability.

## 5.3 Synchronization of robot manipulators

To help clarify the theory, some examples will be given where it is applied to the synchronization of robot manipulators as reported in Rodriguez-Angeles (2002), Bondhus, Pettersen & Nijmeijer (2004) and Sun & Mills (2002).

The system to be analyzed consists of two identical planar two-link robot manipulators. The object of the control scheme is the control the end-effectors in such a way, that the manipulators are able to cooperate in performing a task.

The dynamical model of the manipulators can be written as

$$\mathbf{M}_k(\mathbf{q}_k)\ddot{\mathbf{q}}_k + \mathbf{C}_k(\mathbf{q}_k, \dot{\mathbf{q}}_k)\dot{\mathbf{q}}_k + \mathbf{g}_k(\mathbf{q}_k) + \mathbf{F}_k(\dot{\mathbf{q}}_k) = \boldsymbol{\tau}_k, \quad k = l, f, \quad (5.1)$$

where  $\mathbf{M}_k(\mathbf{q}_k)$  is the mass matrix related to the current pose,  $\mathbf{C}_k(\mathbf{q}_k, \dot{\mathbf{q}}_k)\dot{\mathbf{q}}_k$  denotes coriolis and centrifugal forces,  $\mathbf{g}_k(\mathbf{q}_k)$  gravity forces,  $\mathbf{F}_k(\dot{\mathbf{q}}_k)$  is forces due to friction in the joints,  $\boldsymbol{\tau}_k$  is a vector of generalized torques,  $\mathbf{q}_k$  a vector of joint angles and positions,  $\dot{\mathbf{q}}_k$  gives velocities and  $\ddot{\mathbf{q}}_k$  acceleration. The indices  $l$  and  $f$  refers to leader and follower respectively.

### 5.3.1 External synchronization

In this section we assume that the dynamic model of the master is unknown, and that the generalized joint coordinates, velocities and accelerations are measured. This is an idealized situation of course, but serves well to visualize the approach.

A controller for the follower robot may then be defined similar to the feedback linearizing controller of Paden & Panja (1988) and Rodriguez-Angeles (2002, page 31):

$$\boldsymbol{\tau}_f = \mathbf{M}_f(\mathbf{q}_f)\ddot{\mathbf{q}}_l + \mathbf{C}_f(\mathbf{q}_f, \dot{\mathbf{q}}_f)\dot{\mathbf{q}}_f + \mathbf{g}_f(\mathbf{q}_f) - \mathbf{K}_{d,f}\dot{\mathbf{e}} - \mathbf{K}_{p,f}\mathbf{e}, \quad (5.2)$$

where the synchronization errors  $\dot{\mathbf{e}}$  and  $\mathbf{e}$  are defined as

$$\mathbf{e} \triangleq \mathbf{q}_f - \mathbf{q}_l \quad \dot{\mathbf{e}} \triangleq \dot{\mathbf{q}}_f - \dot{\mathbf{q}}_l \quad (5.3)$$

If only the generalized coordinates are available for measurement, an observer have to be used. Rodriguez-Angeles (2002) proposed a nonlinear model-based observer-controller structure to solve this complication, and proved stability in terms of local uniform ultimate boundedness for the closed-loop system using Lyapunov theory.

### Simulation results

To show the performance, the system with controller (5.2) is simulated. The system consists of two planar two-link robot manipulators, as described by (5.1). We are assuming that the bearings are frictionless, while the rest of the model matrices are taken as:

$$m_{11} = I_{l1} + m_{l1}l_1^2 + k_{r1}^2 I_{m1} + I_{l2} + m_{l2}(a_1^2 + l_2^2 + 2a_1l_2 \cos q_2) + I_{m2} + m_{m2}a_1^2 \quad (5.4a)$$

$$m_{12} = I_{l2} + m_{l2}(l_2^2 + a_1l_2 \cos q_2) + k_{r2} I_{m2} \quad (5.4b)$$

$$m_{21} = m_{12} \quad (5.4c)$$

$$m_{22} = I_{l2} + m_{l2}l_2^2 + k_{r2}^2 I_{m2} \quad (5.4d)$$

$$\mathbf{M}(\mathbf{q}) = \begin{bmatrix} m_{11} & m_{12} \\ m_{21} & m_{22} \end{bmatrix} \quad (5.4e)$$

$$c_{11} = -m_{l2}a_1l_2 \sin q_2 * \dot{q}_2 \quad (5.4f)$$

$$c_{12} = -m_{l2}a_1l_2 \sin q_2 (\dot{q}_1 + \dot{q}_2) \quad (5.4g)$$

$$c_{21} = m_{l2}a_1l_2 \sin q_2 \dot{q}_1 \quad (5.4h)$$

$$c_{22} = 0 \quad (5.4i)$$

$$\mathbf{C}(\mathbf{q}, \dot{\mathbf{q}}) = \begin{bmatrix} c_{11} & c_{12} \\ c_{21} & c_{22} \end{bmatrix} \quad (5.4j)$$

$$g_1 = (m_{l1}l_1 + m_{m2}a_1 + m_{l2}a_1)g \cos q_1 + m_{l2}l_2g \cos q_1 + q_2 \quad (5.4k)$$

$$g_2 = m_{l2}l_2g \cos q_1 + q_2 \quad (5.4l)$$

$$\mathbf{g}(\mathbf{q}) = \begin{bmatrix} g_1 \\ g_2 \end{bmatrix} \quad (5.4m)$$

where the parameters are defined in appendix A.1

In general the leader manipulator is assumed controlled, such that the measured angles, angular velocities and accelerations, which will be used as reference trajectories for the follower-controller, are bounded and smooth.

In this simulation the leader's reference trajectory in radians is given by

$$\mathbf{q}_d = \frac{\pi}{180} \begin{bmatrix} 45 + 5 \sin(\frac{2\pi t}{10}) + 40 \sin(\frac{2\pi t}{40}) \\ -45 + 5 \sin(\frac{2\pi t}{10}) + 40 \sin(\frac{2\pi t}{40}) \end{bmatrix} \quad (5.5)$$

and its control is given by the classical PD+gravity compensation controller

$$\boldsymbol{\tau}_l = \mathbf{g} + \mathbf{K}_{p,l}(\mathbf{q}_d - \mathbf{q}_l) - \mathbf{K}_{d,l}\dot{\mathbf{q}} \quad (5.6)$$

Where  $\mathbf{K}_{p,l} \in \mathbb{R}^{2 \times 2}$  and  $\mathbf{K}_{d,l} \in \mathbb{R}^{2 \times 2}$  are positive definite gain matrices.

From figure 5.1 we clearly see that, though the leader and follower are not able to follow the desired trajectory, the follower conform to the trajectories of the leader perfectly, such that the synchronization error converges to zero, as seen by figure 5.1(c) and 5.1(c). It should be pointed out that to achieve better tracking of the desired trajectory, a tracking controller should be applied to the leader manipulator. More results are found in Nijmeijer & Rodriguez-Angeles (2003), where cases of unavailable angular velocity and acceleration and noise contaminated measurements are considered.

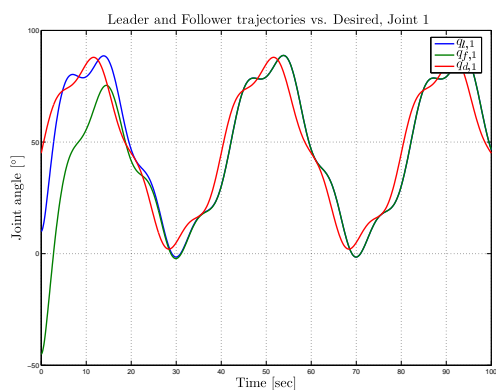
### 5.3.2 Mutual synchronization

To show the mutual synchronization scheme, we again turn to the double two-link example. Now the dynamic model of the master is assumed known, and generalized joint coordinates, velocities and accelerations are still assumed measured.

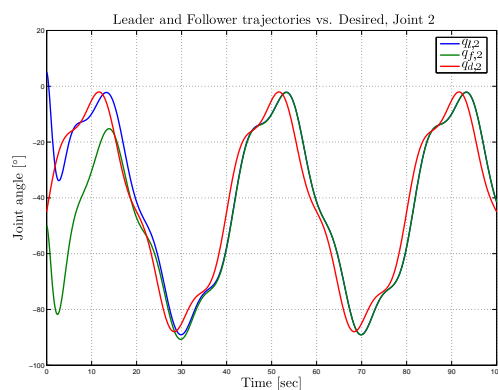
The mutual synchronization problem for the double two-manipulator case, is to design a controller for each robot which allows them to follow a common desired trajectory while still maintaining a converging relative synchronization error.

As in Nijmeijer & Rodriguez-Angeles (2003) we take the synchronizing controllers as

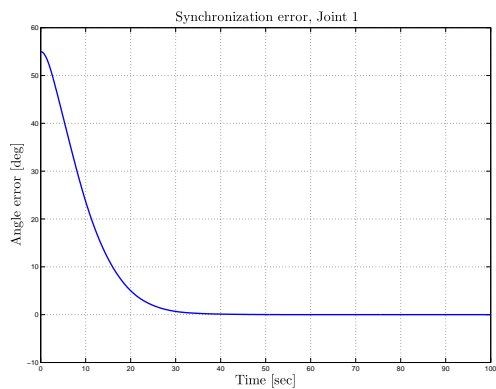
$$\boldsymbol{\tau}_i = \mathbf{M}_i(\mathbf{q}_i)\ddot{\mathbf{q}}_{ri} + \mathbf{C}_i(\mathbf{q}_i, \dot{\mathbf{q}}_i)\dot{\mathbf{q}}_{ri} + \mathbf{g}_i(\mathbf{q}_i) - \mathbf{K}_{d,i}\dot{\mathbf{s}}_i - \mathbf{K}_{p,i}\mathbf{s}_i \quad (5.7)$$



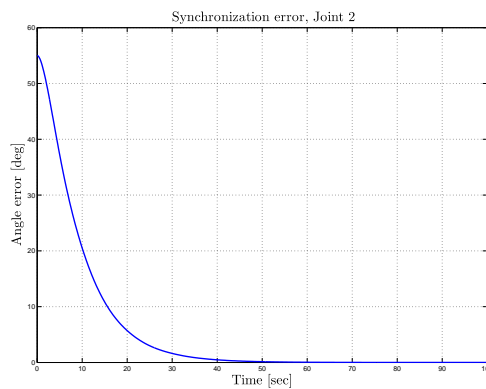
(a) Leader vs. Follower, Joint angles, Joint 1



(b) Leader vs. Follower, Joint angles, Joint 2



(c) Synchronization error, Joint angles, Joint 1



(d) Synchronization error, Joint angles, Joint 2

**Figure 5.1:** Simulation of the robot manipulator external synchronization scheme, control law (5.2)

where  $M_i(\mathbf{q}_i)$ ,  $C_i(\mathbf{q}_i, \dot{\mathbf{q}}_i)$ , and  $\mathbf{g}_i(\mathbf{q}_i)$  are defined by (5.4). And the synchronization errors are defined

$$\mathbf{s}_i \triangleq \mathbf{q}_i - \mathbf{q}_{ri} \quad \dot{\mathbf{s}}_i \triangleq \dot{\mathbf{q}}_i - \dot{\mathbf{q}}_{ri} \quad (5.8)$$

where  $\dot{\mathbf{q}}_{ri}$ ,  $\mathbf{q}_{ri}$  are reference signals given by

$$\mathbf{q}_{ri} = \mathbf{q}_d - \sum_{j=1, j \neq i}^2 \mathbf{K}_{cp_i, j} (\mathbf{q}_i - \mathbf{q}_j) \quad (5.9)$$

$$\dot{\mathbf{q}}_{ri} = \dot{\mathbf{q}}_d - \sum_{j=1, j \neq i}^2 \mathbf{K}_{cv_i, j} (\dot{\mathbf{q}}_i - \dot{\mathbf{q}}_j) \quad (5.10)$$

$$\ddot{\mathbf{q}}_{ri} = \ddot{\mathbf{q}}_d - \sum_{j=1, j \neq i}^2 \mathbf{K}_{ca_i, j} (\ddot{\mathbf{q}}_i - \ddot{\mathbf{q}}_j) \quad (5.11)$$

where  $\mathbf{K}_{cp_i, j}$ ,  $\mathbf{K}_{cv_i, j}$ ,  $\mathbf{K}_{ca_i, j}$  are positive definite gain matrices.

### Simulation results

To show how the controller (5.7) performs, the robot manipulators from the last example are simulated again, using the desired trajectory defined by (5.5), such that the desired angular velocity and acceleration are given by

$$\dot{\mathbf{q}}_d = \frac{\pi}{180} \left[ \pi \cos\left(\frac{2\pi t}{10}\right) + 4\pi \cos\left(\frac{2\pi t}{40}\right) \right] \quad (5.12)$$

$$\ddot{\mathbf{q}}_d = \frac{\pi}{180} \left[ -\frac{\pi^2}{5} \sin\left(\frac{2\pi t}{10}\right) - \frac{\pi^2}{10} \sin\left(\frac{2\pi t}{40}\right) \right] \quad (5.13)$$

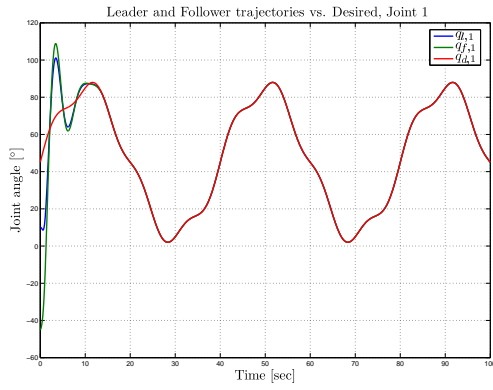
As pointed out in Nijmeijer & Rodriguez-Angeles (2003), the simulation implementation contains an algebraic loop. This is solved by rewriting the closed loop system to be implemented on the form

$$\begin{bmatrix} \ddot{\mathbf{q}}_l \\ \ddot{\mathbf{q}}_f \end{bmatrix} = M_c(K_{lf})^{-1} \begin{bmatrix} \ddot{\mathbf{q}}_d - \mathbf{M}_l(\mathbf{q}_l)^{-1} (\mathbf{C}_l(\mathbf{q}_l, \dot{\mathbf{q}}_l) \dot{\mathbf{s}}_l + \mathbf{K}_{d,l} \dot{\mathbf{s}}_l + \mathbf{K}_{p,l} \mathbf{s}_l) \\ \ddot{\mathbf{q}}_d - \mathbf{M}_f(\mathbf{q}_f)^{-1} (\mathbf{C}_f(\mathbf{q}_f, \dot{\mathbf{q}}_f) \dot{\mathbf{s}}_f + \mathbf{K}_{d,f} \dot{\mathbf{s}}_f + \mathbf{K}_{p,f} \mathbf{s}_f) \end{bmatrix} \quad (5.14)$$

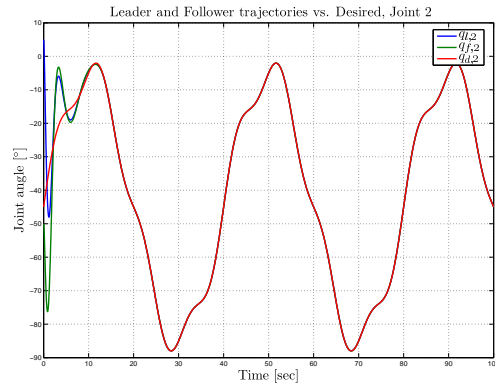
where  $M_c(K_{lf})$  is defined

$$M_c(K_{lf}) = \begin{bmatrix} \mathbf{I}_{2 \times 2} - \mathbf{K}_{l,f} & -\mathbf{K}_{l,f} \\ -\mathbf{K}_{f,l} & \mathbf{I}_{2 \times 2} + \mathbf{K}_{f,l} \end{bmatrix} \quad (5.15)$$

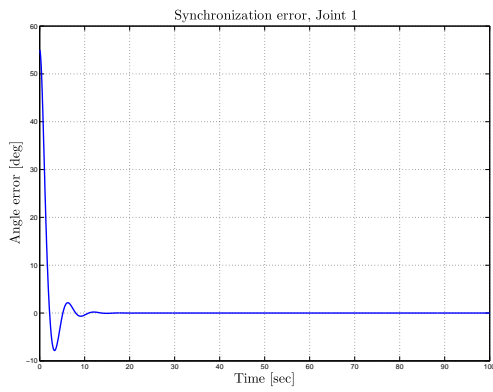
From figure 5.2, one can clearly see that the controller fulfills both the synchronization and the tracking goal. The tuning of this controller is more involved than that of the external synchronization scheme, but gives more freedom when deciding what is important; tracking or synchronization.



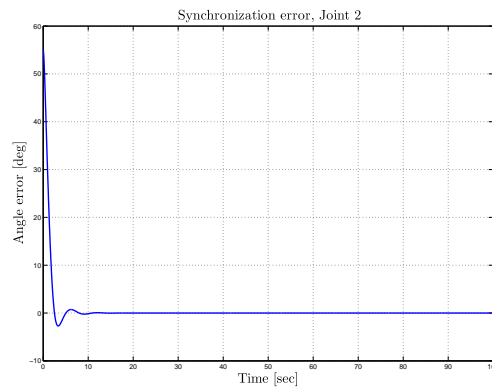
(a) Leader vs. Follower, Joint angles, Joint 1



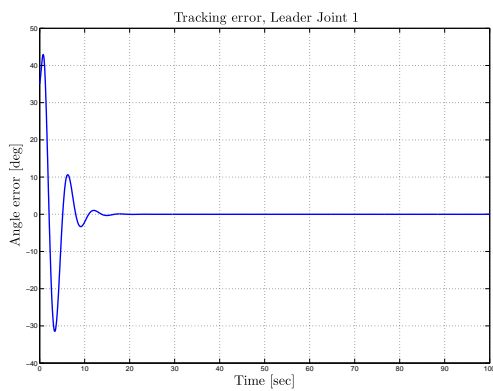
(b) Leader vs. Follower, Joint angles, Joint 2



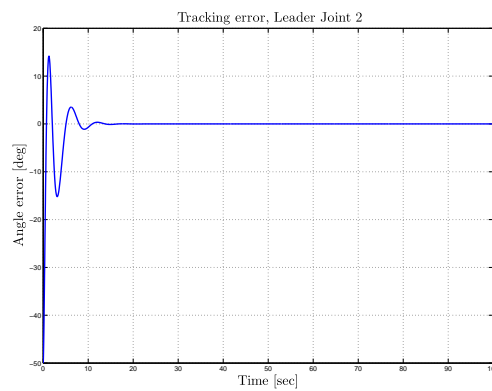
(c) Synchronization error, Joint angles, Joint 1



(d) Synchronization error, Joint angles, Joint 2



(e) Tracking error, Joint angles, Leader Joint 1



(f) Tracking error, Joint angles, Leader Joint 2

**Figure 5.2:** Simulation of the robot manipulators using the mutual synchronization scheme, control law (5.7)

## Chapter 6

# Controller Design and Analysis

The purpose of this chapter is to derive controllers for coordinated control of attitude of a two satellite formation. The control design is based on theory presented in Chapter 5; synchronization of mechanical systems. This has been successfully applied to several varieties of mechanical systems, from ships (Kyrkjebø & Pettersen 2003) and robot manipulators (Rodriguez-Angeles 2002) to satellites (Bondhus et al. 2005). In the last reference the theory was used in the synchronization of two thruster actuated satellites, the purpose of this work is however to apply the theory to a satellite actuated by means of 4 reaction wheels in a tetrahedron configuration.

As in the synchronization of robot manipulators in Rodriguez-Angeles (2002), we propose two overall control schemes; external synchronization control and mutual synchronization control.

### 6.1 Preliminaries

#### 6.1.1 System variables

$\mathbf{q}_{il}$  and  $\mathbf{q}_{if}$  denotes the quaternion between  $\mathcal{F}_i$  and  $\mathcal{F}_l$  and  $\mathcal{F}_f$  respectively. Where  $\mathcal{F}_l$  is the leader body frame and  $\mathcal{F}_f$  the follower body frame. In a similar manner angular velocities are denoted  $\boldsymbol{\omega}_{il}^l$  and  $\boldsymbol{\omega}_{if}^f$  when referring to the angular velocities of the leader (or follower) with respect to  $\mathcal{F}_i$ .

#### 6.1.2 Control deviation

The deviation variables when controlling the satellites in a coordinated manner is given as the synchronization error between the satellites. Depending on the control scheme this error variable can be selected either as an arithmetic difference or a rotational deviation. We have chosen the latter, defining the synchronization attitude error as the rotation deviation between the leader and follower body frames. That is we define the deviation rotation matrix according to

$$\tilde{\mathbf{R}} \triangleq \mathbf{R}_d^T \mathbf{R} = \mathbf{R}_i^l \mathbf{R}_f^i = \mathbf{R}_f^l. \quad (6.1)$$

As explained in section 2.3 we may parameterize the rotational deviation matrix (6.1) as a quaternion in the following manner

$$\mathbf{q}_e \triangleq \mathbf{q}_{lf} = \mathbf{q}_{li} \otimes \mathbf{q}_{if} = \mathbf{q}_{il}^{-1} \otimes \mathbf{q}_{if}. \quad (6.2)$$

The deviation in angular velocity is defined as the angular velocity between  $\mathcal{F}_l$  and  $\mathcal{F}_f$ , that is

$$\boldsymbol{\omega}_e \triangleq \boldsymbol{\omega}_{lf}^f = \boldsymbol{\omega}_{li}^f + \boldsymbol{\omega}_{if}^f = \boldsymbol{\omega}_{if}^f - \mathbf{R}_l^f \boldsymbol{\omega}_{il}^l. \quad (6.3)$$

#### 6.1.3 The attitude reference

Depending on the application, the reference is either a constant or time-varying orientation in inertial frame  $\mathcal{F}_i$ , or a constant orientation in the orbit frame  $\mathcal{F}_o$ . In the case of a time-varying attitude

reference with respect to  $\mathcal{F}_i$ ,  $\mathbf{q}_{id}(t)$  we may define the desired angular velocity and acceleration as

$$\boldsymbol{\omega}_{id}^d(t) = 2\mathbf{J}^T(\mathbf{q}_{id}(t))\dot{\mathbf{q}}_{id}(t) \quad (6.4)$$

$$\dot{\boldsymbol{\omega}}_{id}^d(t) = 2\mathbf{J}^T(\mathbf{q}_{id}(t))\ddot{\mathbf{q}}_{id}(t) \quad (6.5)$$

where we have used (2.48), (2.49) and (2.50).

## 6.2 External synchronization

In this synchronization scheme the leader satellite is controlled separately, either by a tracking or a stabilizing controller. The goal is to design feedback interconnections from the leader to the follower, in such a way that the follower synchronizes its orientation with that of the leader. The design is done by first designing controllers for the leader, then designing a synchronizing controller for the follower.

### 6.2.1 Leader controller

Three different controllers are proposed for the control of the leader; set-point control in  $\mathcal{F}_i$ , set-point control in  $\mathcal{F}_o$  and finally trajectory tracking in  $\mathcal{F}_i$ .

#### Set-point in $\mathcal{F}_i$

If the leader is to point in a specific direction in inertial space, a set-point stabilizing controller is sufficient. We define the desired inertial frame attitude quaternion as  $\mathbf{q}_{id}$  and the desired angular velocity as zero, resulting in the error variables:

$$\mathbf{q}_e \triangleq \mathbf{q}_{dl} = \mathbf{q}_{id}^{-1} \otimes \mathbf{q}_{il} \quad (6.6)$$

$$\boldsymbol{\omega}_e \triangleq \boldsymbol{\omega}_{dl}^l = \boldsymbol{\omega}_{il}^l - \boldsymbol{\omega}_{id}^l = \boldsymbol{\omega}_{il}^l - 0 = \boldsymbol{\omega}_{il}^l \quad (6.7)$$

If we give the dynamics in the form

$$\mathbf{I}_b \dot{\boldsymbol{\omega}}_{il}^l = \mathbf{S}(\mathbf{I}_b \boldsymbol{\omega}_{il}^l + \mathbf{A} \mathbf{I}_s \boldsymbol{\omega}_{s,l}) \boldsymbol{\omega}_{il}^l - \mathbf{A} \boldsymbol{\tau}_{a,l} + \boldsymbol{\tau}_{g,l} \quad (6.8)$$

$$\dot{\mathbf{q}}_{il} = \frac{1}{2} \mathbf{J}(\mathbf{q}_{il}) \boldsymbol{\omega}_{il}^l, \quad (6.9)$$

the error dynamics may be written

$$\dot{\mathbf{q}}_e = -\frac{1}{2} \mathbf{J}(\mathbf{q}_e) \boldsymbol{\omega}_e \quad (6.10)$$

$$\mathbf{I}_b \dot{\boldsymbol{\omega}}_e = \mathbf{S}(\mathbf{I}_b \boldsymbol{\omega}_e + \mathbf{A} \mathbf{I}_s \boldsymbol{\omega}_{s,l}) \boldsymbol{\omega}_e - \mathbf{A} \boldsymbol{\tau}_{a,l} + \boldsymbol{\tau}_{g,l} \quad (6.11)$$

**Proposition 6.1.** *The leader satellite, with dynamics (6.8)-(6.9), and error-dynamics (6.10)-(6.11) where the control is given by*

$$\boldsymbol{\tau}_{a,l} = -\mathbf{A}^\dagger \left( -\boldsymbol{\tau}_{g,l} - k_d \boldsymbol{\omega}_e + k_p \frac{dH(\eta_e)}{d\eta_e} \boldsymbol{\epsilon}_e \right), \quad (6.12)$$

has a uniformly globally asymptotically stable (UGAS) origin  $(\boldsymbol{\omega}_e, \boldsymbol{\epsilon}_e, \eta_e) = (0, 0, \pm 0)$ .

*Proof.* To prove the proposition we choose the Lyapunov function candidate

$$V = \frac{1}{2} \boldsymbol{\omega}_e^T \mathbf{I}_b \boldsymbol{\omega}_e + 2k_p H(\eta_e), \quad (6.13)$$

which is positive definite, zero in the origin and radially unbounded. The time-derivative along the trajectories is given by

$$\dot{V} = \boldsymbol{\omega}_e^T \mathbf{I}_b \dot{\boldsymbol{\omega}}_e + 2k_p \frac{dH(\eta_e)}{d\eta_e} \dot{\eta}_e \quad (6.14)$$

$$= \boldsymbol{\omega}_e^T \left[ \mathbf{S}(\mathbf{I}_b \boldsymbol{\omega}_{il}^l + \mathbf{A} \mathbf{I}_s \boldsymbol{\omega}_{s,l}) \boldsymbol{\omega}_{il}^l - \mathbf{A} \boldsymbol{\tau}_{a,l} + \boldsymbol{\tau}_{g,l} \right] - k_p \frac{dH(\eta_e)}{d\eta_e} \boldsymbol{\epsilon}_e^T \boldsymbol{\omega}_e \quad (6.15)$$

$$= \boldsymbol{\omega}_e^T \left[ -\mathbf{A} \boldsymbol{\tau}_{a,l} + \boldsymbol{\tau}_{g,l} - k_p \frac{dH(\eta_e)}{d\eta_e} \boldsymbol{\epsilon}_e \right] \quad (6.16)$$

If we now select the control input

$$\boldsymbol{\tau}_{a,l} = -\mathbf{A}^\dagger \left( -\boldsymbol{\tau}_{g,l} - k_d \boldsymbol{\omega}_e + k_p \frac{dH(\eta_e)}{d\eta_e} \boldsymbol{\epsilon}_e \right), \quad (6.17)$$

we get

$$\dot{V} = -k_d \boldsymbol{\omega}_e^T \boldsymbol{\omega}_e \leq -k_d \|\boldsymbol{\omega}_e\|^2 \leq 0. \quad (6.18)$$

Since this is a time-invariant system we have fulfilled the criteria of LaSalle's theorem, and have convergence to the region

$$E = \left\{ x \in \Omega_c \mid \dot{V} = 0 \right\}, \quad (6.19)$$

where  $\Omega_s = \{x \in \mathbb{R}^n \mid v \leq 0\}$ . We can show that the largest invariant set M in E is the origin, and thus we have global asymptotic stability.  $\square$

### Set-point in $\mathcal{F}_o$

If the leader satellite is supposed to be stabilized to a fixed attitude in  $\mathcal{F}_o$  rather than  $\mathcal{F}_i$ , we have to solve the problem as a tracking problem in the inertial frame. We now define the desired attitude and angular velocities as

$$\mathbf{q}_{id} \triangleq \mathbf{q}_{io}(t) \otimes \mathbf{q}_{od} \quad (6.20)$$

$$\boldsymbol{\omega}_{id}^l \triangleq \mathbf{R}_o^l \boldsymbol{\omega}_{io}^o, \quad (6.21)$$

where  $\mathbf{q}_{od}$  is the desired offset from nadir,  $\boldsymbol{\omega}_{io}^o$  is the orbit angular velocity and  $\mathbf{q}_{io}(t)$  is the attitude between  $\mathcal{F}_i$  and  $\mathcal{F}_o$  which is periodic in time. This results in the error-variables

$$\mathbf{q}_e = \mathbf{q}_{od}^{-1} \otimes \mathbf{q}_{io}^{-1}(t) \otimes \mathbf{q}_{il} \quad (6.22)$$

$$\boldsymbol{\omega}_e = \boldsymbol{\omega}_{il}^l - \mathbf{R}_o^l \boldsymbol{\omega}_{io}^o, \quad (6.23)$$

and error-dynamics

$$\mathbf{I}_b \dot{\boldsymbol{\omega}}_e = \mathbf{S}(\mathbf{I}_b \boldsymbol{\omega}_{il}^l + \mathbf{A} \mathbf{I}_s \boldsymbol{\omega}_{s,l}) \boldsymbol{\omega}_{il}^l - \mathbf{A} \boldsymbol{\tau}_a + \boldsymbol{\tau}_{g,l} + \mathbf{I}_b \mathbf{S}(\boldsymbol{\omega}_{ol}^l) \mathbf{R}_o^l \boldsymbol{\omega}_{io}^o \quad (6.24)$$

$$\dot{\mathbf{q}}_e = \frac{1}{2} \mathbf{Q}(\mathbf{q}_e) \boldsymbol{\omega}_e \quad (6.25)$$

**Proposition 6.2.** *The satellite leader, with dynamics (6.8)-(6.8) and error-dynamics (6.30)-(6.25), where the control is given by*

$$\boldsymbol{\tau}_a = -\mathbf{A}^\dagger \left( -\boldsymbol{\tau}_{g,l} - \mathbf{S}(\mathbf{I}_b \boldsymbol{\omega}_{il}^l + \mathbf{A} \mathbf{I}_s \boldsymbol{\omega}_{s,l}) \mathbf{R}_o^l \boldsymbol{\omega}_{io}^o - \mathbf{I}_b \mathbf{S}(\boldsymbol{\omega}_{ol}^l) \mathbf{R}_o^l \boldsymbol{\omega}_{io}^o + k_p \frac{dH(\eta_e)}{d\eta_e} \boldsymbol{\epsilon}_e - k_d \boldsymbol{\omega}_e \right) \quad (6.26)$$

*is uniformly globally asymptotically stable (UGAS), under the assumption of a fixed desired attitude in the orbit frame.*

*Proof.* Using the Lyapunov function candidate (6.12), which has derivative along the trajectories given by (6.14), defining the control as (6.26), results in

$$\dot{V} = \boldsymbol{\omega}_e^T [\mathbf{S}(\mathbf{I}_b \boldsymbol{\omega}_{il}^l + \mathbf{A} \mathbf{I}_s \boldsymbol{\omega}_{s,l}) \boldsymbol{\omega}_e - k_d \boldsymbol{\omega}_e] = k_d \boldsymbol{\omega}_e^T \boldsymbol{\omega}_e \leq 0, \quad (6.27)$$

where we have used property  $\mathbf{a}^T \mathbf{S}(\mathbf{b}) \mathbf{a} = 0$ . Since the error-dynamics (6.30)-(6.25) is periodic, Krasovskii-LaSalle's theorem is applicable and the system's origin is proven to be UGAS.  $\square$

### Trajectory tracking in $\mathcal{F}_i$

We now show stability of a nonlinear state feedback controller for tracking in the inertial frame. That is given a smooth trajectory  $\mathbf{q}_{id}(t)$ , such that  $\dot{\mathbf{q}}_{id}(t)$ ,  $\ddot{\mathbf{q}}_{id}(t)$  are well defined for  $t \geq 0$ , we obtain uniform global asymptotic stability of the tracking error.

Let the desired angular velocity and acceleration be given by (6.4) and (6.5). Further we define the tracking errors

$$\boldsymbol{\omega}_e \triangleq \boldsymbol{\omega}_{dl}^l = \boldsymbol{\omega}_{il}^l - \mathbf{R}_d^l \boldsymbol{\omega}_{id}^d \quad (6.28)$$

$$\mathbf{q}_e \triangleq \mathbf{q}_{dl} = \mathbf{q}_{id}^{-1}(t) \otimes \mathbf{q}_{il}, \quad (6.29)$$

such that the error-dynamics can be written

$$\mathbf{I}_b \dot{\boldsymbol{\omega}}_e = \mathbf{S}(\mathbf{I}_b \boldsymbol{\omega}_{il}^l + \mathbf{A} \mathbf{I}_s \boldsymbol{\omega}_{s,l}) \boldsymbol{\omega}_{il}^l - \mathbf{A} \boldsymbol{\tau}_{a,l} + \boldsymbol{\tau}_{g,l} + \mathbf{I}_b \mathbf{S}(\boldsymbol{\omega}_e) \mathbf{R}_d^l \boldsymbol{\omega}_{id}^d - \mathbf{I}_b \mathbf{R}_d^l \dot{\boldsymbol{\omega}}_{id}^d \quad (6.30)$$

$$\dot{\mathbf{q}}_e = \frac{1}{2} \mathbf{J}(\mathbf{q}_e) \boldsymbol{\omega}_e. \quad (6.31)$$

We are now ready to propose the tracking controller.

**Proposition 6.3.** *Given the smooth continuous trajectory  $\mathbf{q}_d(t)$ , error-dynamics (6.31), and control input*

$$\boldsymbol{\tau}_{a,l} = -\mathbf{A}^\dagger \left\{ -\boldsymbol{\tau}_{g,l} - \mathbf{S}(\mathbf{I}_b \boldsymbol{\omega}_{il}^l + \mathbf{A} \mathbf{I}_s \boldsymbol{\omega}_{s,l}) \mathbf{R}_d^l \boldsymbol{\omega}_{id}^d - \mathbf{I}_b \mathbf{S}(\boldsymbol{\omega}_e) \mathbf{R}_d^l \boldsymbol{\omega}_{id}^d + \mathbf{I}_b \mathbf{R}_d^l \dot{\boldsymbol{\omega}}_{id}^d - k_p \text{sgn}(\eta_e) \boldsymbol{\epsilon}_e - k_d \boldsymbol{\omega}_e \right\}, \quad (6.32)$$

the origin  $(\boldsymbol{\omega}_e, \mathbf{y}) = (0, 0)$ , where  $\mathbf{y} = \text{col}(1 - |\eta_e|, \boldsymbol{\epsilon}_e)$ , is uniformly globally asymptotically stable, UGAS.

*Proof.* We prove the proposition using the generalized Matrosov theorem, given in Chapter 3, (Theorem 3.8).

*Satisfying Assumption 1*

Choosing the Lyapunov function

$$V = \frac{1}{2} \boldsymbol{\omega}_e^T \mathbf{I}_b \boldsymbol{\omega}_e + k_p \mathbf{y}^T \mathbf{y}, \quad (6.33)$$

with derivative

$$\dot{V} = \boldsymbol{\omega}_e^T \mathbf{I}_b \dot{\boldsymbol{\omega}}_e + k_p \text{sgn}(\eta_e) \boldsymbol{\epsilon}_e^T \boldsymbol{\omega}_e \quad (6.34)$$

$$= \boldsymbol{\omega}_e^T \left[ k_p \text{sgn}(\eta_e) \boldsymbol{\epsilon}_e - \mathbf{S}(\mathbf{I}_b \boldsymbol{\omega}_{il}^l + \mathbf{A} \mathbf{I}_s \boldsymbol{\omega}_{s,l}) \boldsymbol{\omega}_{il}^l + \mathbf{A} \boldsymbol{\tau}_a - \boldsymbol{\tau}_{g,l} - \mathbf{I}_b \mathbf{S}(\boldsymbol{\omega}_e) \mathbf{R}_d^l \boldsymbol{\omega}_{id}^d + \mathbf{I}_b \mathbf{R}_d^l \dot{\boldsymbol{\omega}}_{id}^d \right]. \quad (6.35)$$

Inserting for (6.32), results in

$$\dot{V} = -k_d \boldsymbol{\omega}_e^T \boldsymbol{\omega}_e \leq 0. \quad (6.36)$$

Which guarantees UGS for the error dynamics, satisfying Assumption 1.

**Remark 6.1.** *From this result it is possible to show asymptotic convergence as in Fjellstad (1994), by using Barbalat's lemma and showing that convergence of  $\boldsymbol{\omega}_e$  leads to convergence of  $\boldsymbol{\epsilon}_e$ .*

*Satisfying Assumption 2*

Since the origin is UGS,  $\boldsymbol{\omega}_e$ ,  $\boldsymbol{\omega}_e$ ,  $\mathbf{y}$  are bounded functions of time. For  $i = 1$  we choose

$$V_1 \triangleq V \quad (6.37)$$

$$\phi_1 \triangleq 0 \quad (6.38)$$

$$Y_1 \triangleq -\beta \|\boldsymbol{\omega}_e\| \leq 0 \quad (6.39)$$

$V_1$  is continuously differentiable and bounded,  $\phi_1$  is continuous and bounded, and finally  $Y_1$  is continuous and hence assumption 2 is satisfied for  $i = 1$ .

For  $i = 2$ , we choose

$$V_2 \triangleq \boldsymbol{\omega}_e^T \mathbf{I}_b \boldsymbol{\epsilon}_e \eta_e \quad (6.40)$$

$$\phi_2 \triangleq \dot{\boldsymbol{\omega}}_e \quad (6.41)$$

$$Y_2 \triangleq \eta_e \phi_2^T \mathbf{I}_b \boldsymbol{\epsilon}_e + \eta_e \boldsymbol{\omega}_e^T \mathbf{I}_b \dot{\boldsymbol{\epsilon}}_e + \eta_e \boldsymbol{\omega}_e^T \mathbf{I}_b \boldsymbol{\epsilon}_e \quad (6.42)$$

Since  $\dot{\boldsymbol{\omega}}_e$ ,  $\boldsymbol{\omega}_e$ ,  $\mathbf{y}$ ,  $\eta_e$  are bounded functions of time,  $V_2, \phi_2$  and  $Y_2$  are bounded. Moreover,  $V_2$  is continuously differentiable, and  $\phi_2$  and  $Y_2$  are continuous in their arguments. Hence, Assumption 2 is satisfied for  $i = 2$ .

*Satisfying Assumption 3*

$Y_1 \leq 0$  for all  $\boldsymbol{\omega}_e \in \mathbb{R}^3$ , satisfying Assumption 3 for  $i = 1$ . Moreover,

$$Y_1 = 0 \Rightarrow \|\boldsymbol{\omega}_e\| = 0 \Rightarrow Y_2 = \eta_e \phi_2^T \mathbf{I}_b \boldsymbol{\epsilon}_e \quad (6.43)$$

Inserting for  $\phi_2$  and  $\boldsymbol{\omega}_e = 0$ , gives

$$Y_2 = -k_p \eta_e \operatorname{sgn}(\eta_e) \boldsymbol{\epsilon}_e^T \boldsymbol{\epsilon}_e = -k_p |\eta_e| \boldsymbol{\epsilon}_e^T \boldsymbol{\epsilon}_e \leq 0. \quad (6.44)$$

Thus, Assumption 3 has been satisfied for both  $i \in \{1, 2\}$ .

*Satisfying Assumption 4*

It can now be seen that

$$\{Y_1 = 0, Y_2 = 0\} \Rightarrow \boldsymbol{\omega}_e = 0, \boldsymbol{\epsilon}_e = 0 \Rightarrow 1 - |\eta_e| = 0, \quad (6.45)$$

satisfying Assumption 4 for  $i \in \{1, 2\}$ .

**Remark 6.2.** *This hold as long as  $\eta_e$  initially is different from zero. It can be shown that under this control  $\eta_e$  will not change sign, and thus the assumption holds. And it was also shown in Fjellstad (1994), that using the definition of signum, as 1 when  $\eta_e$  is zero the state cannot get stuck in  $\eta_e = 0$ .*

The Assumptions of Theorem 3.8 are satisfied, and we may conclude *uniform global asymptotic stability*.  $\square$

## 6.2.2 Synchronizing controller

### Lyapunov controller

Given that the error-variables (6.2) and (6.3), the error-dynamics may be represented as

$$\mathbf{I}_b \dot{\boldsymbol{\omega}}_e = \mathbf{S}(\mathbf{I}_b \boldsymbol{\omega}_{if}^f + \mathbf{A} \mathbf{I}_s \boldsymbol{\omega}_{s,l}) \boldsymbol{\omega}_{if}^f - \mathbf{A} \boldsymbol{\tau}_{a,f} + \boldsymbol{\tau}_{g,l} - \mathbf{I}_b \mathbf{S}(\boldsymbol{\omega}_{if}^f) \mathbf{R}_l^f \boldsymbol{\omega}_{il}^l - \mathbf{I}_b \mathbf{R}_l^f \dot{\boldsymbol{\omega}}_{il}^l \quad (6.46)$$

$$\dot{\mathbf{q}}_e = \frac{1}{2} \mathbf{Q}(\mathbf{q}_e) \boldsymbol{\omega}_e \quad (6.47)$$

The following proposition gives a model-dependent controller for the external synchronization.

**Proposition 6.4.** *The error-dynamics (6.46) - (6.47), where the control is given by*

$$\boldsymbol{\tau}_a = -\mathbf{A}^\dagger \left\{ -\mathbf{S}(\mathbf{I}_b \boldsymbol{\omega}_{if}^f + \mathbf{A} \mathbf{I}_s \boldsymbol{\omega}_{s,l}) \mathbf{R}_l^f \boldsymbol{\omega}_{il}^l - \boldsymbol{\tau}_{g,l} + \mathbf{I}_b \mathbf{S}(\boldsymbol{\omega}_{if}^f) \mathbf{R}_l^f \boldsymbol{\omega}_{il}^l + \mathbf{I}_b \mathbf{R}_l^f \dot{\boldsymbol{\omega}}_{il}^l - k_d \boldsymbol{\omega}_e + k_p \frac{dH(\eta_e)}{d\eta_e} \boldsymbol{\epsilon}_e \right\} \quad (6.48)$$

*have uniformly globally asymptotically stable origin  $(\boldsymbol{\omega}_e, \mathbf{y}) = (0, 0)$ , where  $\mathbf{y} = \operatorname{col}(1 - |\eta_e|, \boldsymbol{\epsilon}_e)$ .*

*Proof.* Inspection of the closed loop error-dynamics, show that it is equal to the error-dynamics of the previously designed tracking controller in Proposition 6.3. The proof can be directly extended to this case.  $\square$

### Adaptive backstepping controller

In some cases the inertia matrix may be unknown or poorly known, and it may also change over time due to mass expulsion when firing the thrusters. Assuming the parameters are constant or slowly varying, we may remedy the lack of information using an adaptive controller. We first assume perfect model knowledge and design a controller for this scenario. This controller is extended with a parameter update law in the following step. The design method is based on vectorial integrator backstepping as was done in Fossen (2002) for ships and in Bondhus et al. (2005) for a satellite actuated by means of thrusters. A similar approach was also designed in Egeland & Godhavn (1994) using passivity arguments.

We first define the synchronization measure  $\mathbf{s}$  as a linear parametrization of the angular velocity synchronization error and the quaternion synchronization error,

$$\mathbf{s} \triangleq \boldsymbol{\omega}_e + \lambda \mathbf{e}, \quad (6.49)$$

where  $\boldsymbol{\omega}_e$  is defined by (6.3), and  $\mathbf{e} = \boldsymbol{\epsilon}_e$  which is defined by (6.2). Further we define  $\boldsymbol{\omega}_r$  as

$$\boldsymbol{\omega}_r \triangleq \boldsymbol{\omega}_{il}^f - \lambda \mathbf{e}, \quad (6.50)$$

such that we may write

$$\mathbf{s} = \boldsymbol{\omega}_{if}^f - \boldsymbol{\omega}_r. \quad (6.51)$$

$\boldsymbol{\omega}_r$  may be viewed as a virtual reference trajectory. Defining the parametrization

$$\mathbf{Y}(\dot{\boldsymbol{\omega}}_r, \boldsymbol{\omega}_r, \boldsymbol{\omega}_{if}^f) \boldsymbol{\theta} = \mathbf{I}_b \dot{\boldsymbol{\omega}}_r - \mathbf{S}(\mathbf{I}_b \boldsymbol{\omega}_{if}^f) \boldsymbol{\omega}_r, \quad (6.52)$$

where, if  $\mathbf{I}_b$  is diagonal,

$$\mathbf{Y}(\dot{\boldsymbol{\omega}}_r, \boldsymbol{\omega}_r, \boldsymbol{\omega}_{if}^f) = \begin{bmatrix} \dot{\omega}_{r1} & -\omega_2 \omega_{r3} & \omega_3 \omega_{r2} \\ \omega_1 \omega_{r3} & \dot{\omega}_{r2} & -\omega_3 \omega_{r1} \\ \omega_1 \omega_{r2} & -\omega_2 \omega_{r1} & \dot{\omega}_{r3} \end{bmatrix}, \quad (6.53)$$

is the so called regressor matrix, with  $\dot{\omega}_{ri}$ ,  $\omega_{ri}$  and  $\omega_i$  being the components of  $\dot{\boldsymbol{\omega}}_r$ ,  $\boldsymbol{\omega}_r$  and  $\boldsymbol{\omega}_{if}^f$  and

$$\boldsymbol{\theta} = [i_{xx}, i_{yy}, i_{zz}]^T \quad (6.54)$$

the parameter vector containing the diagonal elements of inertia matrix. A differential equation in terms of  $\mathbf{s}$  and  $\mathbf{q}_e$  may be defined as

$$\dot{\mathbf{q}}_e = \frac{1}{2} \mathbf{J}(\mathbf{q}_e) (\mathbf{s} - \lambda \boldsymbol{\epsilon}_e) \quad (6.55)$$

$$\mathbf{I}_b \dot{\mathbf{s}} - \mathbf{S}(\mathbf{I}_b \boldsymbol{\omega}_{if}^f + \mathbf{A} \mathbf{I}_s \boldsymbol{\omega}_{s,f}) \mathbf{s} = -\mathbf{A} \boldsymbol{\tau}_{a,f} + \boldsymbol{\tau}_{g,f} + \mathbf{S}(\mathbf{A} \mathbf{I}_s \boldsymbol{\omega}_{s,f}) \boldsymbol{\omega}_r - \mathbf{Y} \boldsymbol{\theta}. \quad (6.56)$$

**Proposition 6.5.** *Given the dynamics (6.55)-(6.56), if the control  $\boldsymbol{\tau}_a$  is selected as*

$$\boldsymbol{\tau}_{a,f} = \mathbf{A}^\dagger \left( -\mathbf{Y}(\dot{\boldsymbol{\omega}}_r, \boldsymbol{\omega}_r, \boldsymbol{\omega}_{if}^f) \boldsymbol{\theta} - \mathbf{S}(\mathbf{A} \mathbf{I}_s \boldsymbol{\omega}_{s,f}) \boldsymbol{\omega}_r - \boldsymbol{\tau}_{g,f} - \mathbf{K}_d \mathbf{s} - \boldsymbol{\epsilon}_e \right), \quad (6.57)$$

then, the origin  $(\mathbf{s}, \boldsymbol{\epsilon}_e) = (\mathbf{0}, \mathbf{0})$  is uniformly globally exponentially stable (UGES). Which leads to the exponential convergence of  $\boldsymbol{\omega}_e$  to 0 and to the convergence of  $\eta_e$  to 1.

*Proof.* To prove UGES of the origin we start with the subsystem (6.55). Selecting the Lyapunov function for the first subsystem

$$V_1 = \boldsymbol{\epsilon}_e^T \boldsymbol{\epsilon}_e + (1 - \eta_e)^2 \quad (6.58)$$

and calculating the time-derivative

$$\dot{V}_1 = 2\boldsymbol{\epsilon}_e^T \dot{\boldsymbol{\epsilon}}_e - 2\dot{\eta}_e + 2\eta_e \dot{\eta}_e \quad (6.59)$$

$$= \boldsymbol{\epsilon}_e^T (\eta_e \mathbf{I}_{3 \times 3} - \mathbf{S}(\boldsymbol{\epsilon}_e)) (\mathbf{s} - \lambda \boldsymbol{\epsilon}_e) - \boldsymbol{\epsilon}_e^T (\mathbf{s} - \lambda \boldsymbol{\epsilon}_e) - \eta_e \boldsymbol{\epsilon}_e^T (\mathbf{s} - \lambda \boldsymbol{\epsilon}_e) \quad (6.60)$$

$$= -\lambda \boldsymbol{\epsilon}_e^T \boldsymbol{\epsilon}_e + \mathbf{s}^T \boldsymbol{\epsilon}_e \quad (6.61)$$

In the next step a control Lyapunov function is selected as

$$V_2 = \frac{1}{2} \mathbf{s}^T \mathbf{I}_b \mathbf{s} + V_1, \quad (6.62)$$

with time derivative

$$\dot{V}_2 = \mathbf{s}^T \mathbf{I}_b \dot{\mathbf{s}} + \dot{V}_1 \quad (6.63)$$

$$= \mathbf{s}^T \left[ \mathbf{S}(\mathbf{I}_b \boldsymbol{\omega}_i^f f - \mathbf{A} \mathbf{I}_s \boldsymbol{\omega}_{s,f}) \mathbf{s} + \mathbf{S}(\mathbf{A} \mathbf{I}_s \boldsymbol{\omega}_{s,f}) \boldsymbol{\omega}_r - \mathbf{A} \boldsymbol{\tau}_{a,f} + \boldsymbol{\tau}_{g,f} - \mathbf{Y}(\dot{\boldsymbol{\omega}}_r, \boldsymbol{\omega}_r, \boldsymbol{\omega}_{if}^f, \boldsymbol{\omega}_{s,f}) \boldsymbol{\theta} \right] - \lambda \boldsymbol{\epsilon}_e^T \boldsymbol{\epsilon}_e + \mathbf{s}^T \boldsymbol{\epsilon}_e. \quad (6.64)$$

Selecting the control as

$$\boldsymbol{\tau}_{a,f} = \mathbf{A}^\dagger \left( -\mathbf{Y}(\dot{\boldsymbol{\omega}}_r, \boldsymbol{\omega}_r, \boldsymbol{\omega}_{if}^f) \boldsymbol{\theta} - \mathbf{S}(\mathbf{A} \mathbf{I}_s \boldsymbol{\omega}_{s,f}) \boldsymbol{\omega}_r - \boldsymbol{\tau}_{g,f} - \mathbf{K}_d \mathbf{s} - \boldsymbol{\epsilon}_e \right), \quad (6.65)$$

(6.64) may be rewritten as

$$\dot{V}_2 = -\mathbf{s}^T \mathbf{K}_d \mathbf{s} - \lambda \boldsymbol{\epsilon}_e^T \boldsymbol{\epsilon}_e \quad (6.66)$$

$$= -\mathbf{s}^T \mathbf{K}_d \mathbf{s} - \lambda(1-t) \boldsymbol{\epsilon}_e^T \boldsymbol{\epsilon}_e - t\lambda(1-\eta_e^2) \quad (6.67)$$

$$\leq -\mathbf{s}^T \mathbf{K}_d \mathbf{s} - \lambda(1-t) \boldsymbol{\epsilon}_e^T \boldsymbol{\epsilon}_e - t\lambda(1-|\eta_e|)^2 < 0 \quad (6.68)$$

Since  $V_2$  fulfills the requirements of Theorem 3.6, with the squared two norm,  $\mathbb{D} = \mathbb{R}^n$  and the constants defined as

$$k_1 = \lambda_{\min}(\mathbf{P}) \quad (6.69)$$

$$k_2 = \lambda_{\max}(\mathbf{P}) \quad (6.70)$$

$$k_3 = \lambda_{\min}(\mathbf{Q}), \quad (6.71)$$

where  $\mathbf{P}$  is a square block diagonal matrix  $\text{diag}(\mathbf{I}_b, \mathbf{I}_{3 \times 3}, 1)$  and  $\mathbf{Q}$  a square block diagonal matrix  $\text{diag}(\mathbf{K}_d, \mathbf{I}_{3 \times 3}, 1)$ .  $\lambda_{\min}(\cdot)$  and  $\lambda_{\max}(\cdot)$  is the minimum and maximum eigenvalue respectively.

This shows that both  $\mathbf{s}$  and  $\boldsymbol{\epsilon}_e$  converges to zero exponentially, which leads to the exponential convergence of  $\boldsymbol{\omega}_e$  to zero and of  $\eta_e$  to  $\pm 1$ .  $\square$

**Remark 6.3.** *Though the synchronizing controller was proven UGES to the origin  $(\boldsymbol{\omega}_e, \boldsymbol{\epsilon}_e) = (0, 0)$ , indicating UGES of the scalar quaternion error to either 1 or -1, inspection of the equilibrium points show that  $\eta_e = -1$  is actually an unstable equilibrium point. This is a known fact for controllers using the quaternion error feedback, and was pointed out both in Fjellstad (1994) and Egeland & Godhavn (1994). Fjellstad (1994) instead used feedback from the  $\mathbf{e} = \text{sgn}(\eta_e) \boldsymbol{\epsilon}_e$ , which resulted in two stable equilibrium points. This was also used in the tracking and stabilizing controllers derived in the previous section.*

Now the adaptive control may be defined by exchanging the real parameter vector with estimated parameters, and defining a parameter estimate update law.

**Proposition 6.6.** *Given the dynamics (6.55)-(6.56), if the control  $\boldsymbol{\tau}_a$  is selected as*

$$\boldsymbol{\tau}_{a,f} = \mathbf{A}^\dagger \left( -\mathbf{Y}(\dot{\boldsymbol{\omega}}_r, \boldsymbol{\omega}_r, \boldsymbol{\omega}_{if}^f, \boldsymbol{\omega}_{s,f}) \hat{\boldsymbol{\theta}} - \boldsymbol{\tau}_{g,f} - \mathbf{K}_d \mathbf{s} - \boldsymbol{\epsilon}_e \right), \quad (6.72)$$

where the parameter estimate update law is given by

$$\dot{\hat{\boldsymbol{\theta}}} = -\boldsymbol{\Gamma}^{-1} \mathbf{Y}^T \mathbf{s} \quad (6.73)$$

then, the origin  $(\mathbf{s}, \boldsymbol{\epsilon}_e) = (\mathbf{0}, \mathbf{0})$  is globally convergent. Which leads to the convergence of  $\boldsymbol{\omega}_e$  to 0 and to the convergence of  $\eta_e$  to 1.

*Proof.* The first part of the proof follows directly from the proof of Proposition 6.5, and is not repeated. We now select

$$V_2 = \frac{1}{2} \mathbf{s}^T \mathbf{I}_b \mathbf{s} + \frac{1}{2} \tilde{\boldsymbol{\theta}}^T \boldsymbol{\Gamma} \tilde{\boldsymbol{\theta}} + V_1. \quad (6.74)$$

If the control law and parameter update law is given by (6.72) and (6.73) respectively, the time-derivative  $\dot{V}_2$ .

$$\dot{V}_2 = -\mathbf{s}^T \mathbf{I}_b \mathbf{s} - \lambda \boldsymbol{\epsilon}_e^T \boldsymbol{\epsilon}_e \leq 0 \quad (6.75)$$

Since  $V_2$  can be lower bounded,  $\dot{V}_2$  is negative semi-definite and uniformly continuous in time, the conditions of lemma 3.2 are satisfied and we have convergence of  $(\mathbf{s}, \boldsymbol{\epsilon}_e)$  to  $(\mathbf{0}, \mathbf{0})$  globally, which as in the proof of theorem 6.5, leads to

$$\boldsymbol{\omega}_e \rightarrow 0, \eta_e \rightarrow 1, \text{ as } t \rightarrow \infty. \quad (6.76)$$

□

**Remark 6.4.** *Though we can not guarantee convergence of the parameter estimation error, we now that the error will stay bounded. To obtain true parameter estimation it is necessary for the input to the adaptive update law to be persistently exciting (PE). In this case the input is the synchronization error, thus the PE property will only be possible during transients. This is observed during simulations, as the convergence of the parameter estimate stops when the synchronization error has reached zero.*

### 6.2.3 Observer design

As it has been assumed that only the attitude is available for measurement, we need some way of constructing the angular velocities and accelerations. To avoid the noise contaminated signal from a numeric derivation, we instead employ an estimator. Several possibilities exist, but the extended Kalman-filter and the nonlinear Luenberger observer seems the most obvious choices. We will here only deal with the nonlinear Luenberger observer, but a thorough analysis of the extended Kalman filter for satellites may be found in Kyrkjebø (2000) and Sunde (2005).

The nonlinear Luenberger observer for a general nonlinear system

$$\dot{\mathbf{x}} = \mathbf{f}(\mathbf{x}, t), \mathbf{x}(t_0) = \mathbf{x}_0 \quad (6.77)$$

$$\mathbf{y} = \mathbf{h}(\mathbf{x}), \quad (6.78)$$

may be written as a copy of the dynamics and an added output injection term:

$$\dot{\hat{\mathbf{x}}} = \mathbf{f}(\hat{\mathbf{x}}, t) + \mathbf{g}(\mathbf{y}, \hat{\mathbf{x}}) \quad (6.79)$$

Following the observer design in Salcudean (1991), Nijmeijer & Rodriguez-Angeles (2003), Bondhus et al. (2005) and Fjellstad (1994) a nonlinear observer for the nonlinear satellite model is designed. In this design we include the gyroscopic effect due to the spinning reaction wheels.

We begin by reviewing the attitude dynamics of a spacecraft in the inertial frame:

$$\dot{\mathbf{h}}^i = \boldsymbol{\tau}_e^i = \mathbf{R}_b^i \boldsymbol{\tau}_e^b \quad (6.80)$$

$$\boldsymbol{\omega}_{ib}^b = (\mathbf{R}_b^i \mathbf{I}_b)^{-1} (\mathbf{h}^i - \mathbf{A} \mathbf{I}_s \boldsymbol{\omega}_s) \quad (6.81)$$

$$\dot{\mathbf{q}}_{ib} = \frac{1}{2} \mathbf{Q}(\mathbf{q}_{ib}) \boldsymbol{\omega}_{ib}^b \quad (6.82)$$

We may then define the observer as a copy of the dynamics including the input injection term:

$$\dot{\hat{\mathbf{h}}}^i = \boldsymbol{\tau}_e^i = \mathbf{R}_b^i (\boldsymbol{\tau}_e^b + \mathbf{g}_1(\mathbf{q}_{ib}, \hat{\mathbf{q}}_{ib})) \quad (6.83)$$

$$\hat{\boldsymbol{\omega}}_{ib}^b = (\mathbf{R}_b^i \mathbf{I}_b)^{-1} (\hat{\mathbf{h}}^i - \mathbf{A} \mathbf{I}_s \boldsymbol{\omega}_s) \quad (6.84)$$

$$\dot{\hat{\mathbf{q}}}_{ib} = \frac{1}{2} \mathbf{Q}(\hat{\mathbf{q}}_{ib}) (\hat{\boldsymbol{\omega}}_{ib}^b + \mathbf{g}_2(\mathbf{q}_{ib}, \hat{\mathbf{q}}_{ib})) \quad (6.85)$$

Defining the observer error variables as

$$\tilde{\mathbf{h}}^i \triangleq \mathbf{h}^i - \hat{\mathbf{h}}^i \quad (6.86)$$

$$\tilde{\mathbf{q}}_{ib} \triangleq \mathbf{q}_{ib} \otimes \hat{\mathbf{q}}_{ib}, \quad (6.87)$$

the resulting error-dynamics may be written as

$$\dot{\tilde{\mathbf{h}}}^i = -\mathbf{g}_1(\mathbf{q}_{ib}, \hat{\mathbf{q}}_{ib}) \quad (6.88)$$

$$\dot{\tilde{\eta}}_{ib} = -\frac{1}{2}\tilde{\boldsymbol{\epsilon}}(\boldsymbol{\omega}_{ib}^b - \hat{\boldsymbol{\omega}}_{ib}^b - \mathbf{g}_2(\mathbf{q}_{ib}, \hat{\mathbf{q}}_{ib})) \quad (6.89)$$

$$\dot{\tilde{\boldsymbol{\epsilon}}}_{ib} = \frac{1}{2}(\eta \mathbf{I}_{3 \times 3} + \mathbf{S}(\tilde{\boldsymbol{\epsilon}}))(\boldsymbol{\omega}_{ib}^b - \hat{\boldsymbol{\omega}}_{ib}^b - \mathbf{g}_2(\mathbf{q}_{ib}, \hat{\mathbf{q}}_{ib})) \quad (6.90)$$

**Proposition 6.7.** *The observer given by (6.86)-(6.87), with error dynamics (6.88)-(6.90), has an uniformly globally asymptotically stable origin  $(\tilde{\mathbf{h}}, \tilde{\boldsymbol{\epsilon}}, \tilde{\eta}) = (\mathbf{0}, \mathbf{0}, \pm 1)$  if the output injection terms are chosen as:*

$$\mathbf{g}_1(\mathbf{q}_{ib}, \hat{\mathbf{q}}_{ib}) = -k_p \frac{dH(\tilde{\eta})}{d\tilde{\eta}} \mathbf{R}_b^i \mathbf{I}_b \tilde{\boldsymbol{\epsilon}} \quad (6.91)$$

$$\mathbf{g}_2(\mathbf{q}_{ib}, \hat{\mathbf{q}}_{ib}) = -k_v \frac{dH(\tilde{\eta})}{d\tilde{\eta}} \tilde{\boldsymbol{\epsilon}}, \quad (6.92)$$

where  $H(\cdot)$  is scalar function satisfying

- $H(\cdot) : [-1; 1] \rightarrow \mathbb{R}_+$  (non-negative)
- $H(-1) = 0$  or/and  $H(1) = 0$
- $H(\cdot)$  is Lipschitz on  $[-1, 1]$ :

$$|H(\eta_1) - H(\eta_2)| \leq L|\eta_1 - \eta_2| \quad (6.93)$$

Several suggestions of  $H(\tilde{\eta})$  were made in Fjellstad (1994), and have been summarized here in table 6.2.3

*Proof.* To prove proposition 6.7 the generalized Matrosov theorem, given in this work as Theorem 3.8, will be applied.

*Satisfying Assumption 1*

To prove that the origin of (6.88)-(6.90) is uniformly globally stable UGS, we propose the Lyapunov function candidate

$$V_{obs} = \frac{1}{2}(\tilde{\mathbf{h}}^i)^T \tilde{\mathbf{h}}^i + 2k_p H(\tilde{\eta}) \quad (6.94)$$

as given in Fjellstad (1994). We find the derivative of (6.94) along the trajectories as

$$\dot{V}_{obs} = (\tilde{\mathbf{h}}^i)^T \dot{\tilde{\mathbf{h}}}^i + 2k_p \frac{dH(\tilde{\eta})}{d\tilde{\eta}} \dot{\tilde{\eta}} \quad (6.95)$$

$$= -(\tilde{\mathbf{h}}^i)^T \mathbf{g}_1(\mathbf{q}_{ib}, \hat{\mathbf{q}}_{ib}) - k_p \frac{dH(\tilde{\eta})}{d\tilde{\eta}} \tilde{\boldsymbol{\epsilon}}^T (\boldsymbol{\omega}_{ib}^b - \hat{\boldsymbol{\omega}}_{ib}^b - \mathbf{g}_2(\mathbf{q}_{ib}, \hat{\mathbf{q}}_{ib})) \quad (6.96)$$

$$= -(\tilde{\mathbf{h}}^i)^T \mathbf{g}_1(\mathbf{q}_{ib}, \hat{\mathbf{q}}_{ib}) - k_p \frac{dH(\tilde{\eta})}{d\tilde{\eta}} \tilde{\boldsymbol{\epsilon}}^T (\mathbf{R}_b^i \mathbf{I}_b)^{-1} \tilde{\mathbf{h}}^i + k_p \frac{dH(\tilde{\eta})}{d\tilde{\eta}} \tilde{\boldsymbol{\epsilon}}^T \mathbf{g}_2(\mathbf{q}_{ib}, \hat{\mathbf{q}}_{ib}) \quad (6.97)$$

$$= -(\tilde{\mathbf{h}}^i)^T (\mathbf{g}_1(\mathbf{q}_{ib}, \hat{\mathbf{q}}_{ib}) + k_p \frac{dH(\tilde{\eta})}{d\tilde{\eta}} (\mathbf{R}_b^i \mathbf{I}_b^{-1}) \tilde{\boldsymbol{\epsilon}}) + k_p \frac{dH(\tilde{\eta})}{d\tilde{\eta}} \tilde{\boldsymbol{\epsilon}}^T \mathbf{g}_2(\mathbf{q}_{ib}, \hat{\mathbf{q}}_{ib}). \quad (6.98)$$

Selecting the output injection terms  $\mathbf{g}_1$  and  $\mathbf{g}_2$  as

$$\mathbf{g}_1(\mathbf{q}_{ib}, \hat{\mathbf{q}}_{ib}) = -k_p \frac{dH(\tilde{\eta})}{d\tilde{\eta}} \mathbf{R}_b^i \mathbf{I}_b^{-1} \tilde{\boldsymbol{\epsilon}} \quad (6.99)$$

$$\mathbf{g}_2(\mathbf{q}_{ib}, \hat{\mathbf{q}}_{ib}) = -k_v \frac{dH(\tilde{\eta})}{d\tilde{\eta}} \tilde{\boldsymbol{\epsilon}}, \quad (6.100)$$

we obtain

$$\dot{V}_{obs} = -k_p k_v \left( \frac{dH(\tilde{\eta})}{d\tilde{\eta}} \right)^2 \tilde{\epsilon}^T \tilde{\epsilon} \leq 0. \quad (6.101)$$

Thus we have fulfilled the requirements of Theorem 3.5, and we can conclude that the origin is uniformly globally stable, UGS.

*Satisfying Assumption 2*

Since the origin is UGS,  $\tilde{\mathbf{h}}, \dot{\tilde{\mathbf{h}}}, \tilde{\epsilon}, \dot{\tilde{\epsilon}}$  and  $\tilde{\eta}$  are bounded functions of time. For  $i = 1$  we choose

$$V_1 \triangleq V_{obs} \quad (6.102)$$

$$\phi_1 \triangleq 0 \quad (6.103)$$

$$Y_1 \triangleq -\beta \|\tilde{\epsilon}\|^2 \leq 0 \quad (6.104)$$

The function  $V_1$  is continuously differentiable and bounded,  $\phi_1$  is continuous and bounded and finally  $Y_1$  is continuous and hence assumption 2 is satisfied for  $i = 1$ .

For  $i = 2$ , we choose

$$V_2 \triangleq -\tilde{\eta} \tilde{\epsilon}^T (\mathbf{R}_b^i \mathbf{I}_b) \tilde{\mathbf{h}} \quad (6.105)$$

$$\phi_2 \triangleq \dot{\tilde{\epsilon}} \quad (6.106)$$

$$Y_2 \triangleq -\dot{\tilde{\eta}} \tilde{\epsilon}^T (\mathbf{R}_b^i \mathbf{I}_b) \tilde{\mathbf{h}} - \tilde{\eta} \dot{\tilde{\epsilon}}^T (\mathbf{R}_b^i \mathbf{I}_b) \tilde{\mathbf{h}} - \tilde{\eta} \tilde{\epsilon}^T (\dot{\mathbf{R}}_b^i \mathbf{I}_b) \tilde{\mathbf{h}} - \tilde{\eta} \tilde{\epsilon}^T (\mathbf{R}_b^i \mathbf{I}_b) \dot{\tilde{\mathbf{h}}} \quad (6.107)$$

Since  $\tilde{\mathbf{h}}, \dot{\tilde{\mathbf{h}}}, \tilde{\epsilon}, \dot{\tilde{\epsilon}}$  and  $\tilde{\eta}$  are bounded functions of time,  $V_2$ ,  $\phi_2$  and  $Y_2$  are bounded. Moreover,  $V_2$  is continuously differentiable and  $\phi_2$  and  $Y_2$  are continuous in their arguments. Hence, assumption 2 is satisfied for  $i = 2$ .

*Satisfying assumption 3*

The function  $Y_1 \leq 0$  for all  $\tilde{\epsilon} \in \mathbb{R}^3$ . Hence assumption 3 is satisfied for  $i = 1$ . Moreover,

$$Y_1 = 0 \Rightarrow \|\tilde{\epsilon}\| = 0 \Rightarrow Y_2 = -\tilde{\eta} \phi_2^T (\mathbf{R}_b^i \mathbf{I}_b) \tilde{\mathbf{h}} \quad (6.108)$$

Inserting for  $\phi_2$  and  $-\tilde{\epsilon} = 0$ , gives

$$Y_2 = -\tilde{\eta} \left[ \frac{1}{2} (\tilde{\eta} (\mathbf{R}_b^i \mathbf{I}_b)^{-1} \tilde{\mathbf{h}})^T (\mathbf{R}_b^i \mathbf{I}_b) \tilde{\mathbf{h}} \right] \quad (6.109)$$

$$= -\frac{1}{2} \tilde{\eta}^2 \tilde{\mathbf{h}}^T \tilde{\mathbf{h}} \quad (6.110)$$

$$= -\frac{1}{2} \tilde{\mathbf{h}}^T \tilde{\mathbf{h}} \leq 0, \quad (6.111)$$

where we have used that  $\tilde{\epsilon} = 0 \Rightarrow \tilde{\eta} = \pm 1$ . This shows that Assumption 3 is satisfied for  $i = 2$ .

*Satisfying assumption 4*

It is clear that

$$\{Y_1 = 0, Y_2 = 0\} \Rightarrow \|\tilde{\mathbf{h}}\| = 0, \|\tilde{\epsilon}\| = 0, \tilde{\eta} = \pm 1 \quad (6.112)$$

and thus assumption 4 is satisfied for  $i \in \{1, 2\}$ .

We have verified all the assumptions of theorem 3.8, and we conclude that the origin  $(\tilde{\mathbf{h}}, \tilde{\epsilon}, \tilde{\eta}) = (0, 0, \pm 1)$  is *uniformly globally asymptotically stable*.  $\square$

To obtain the angular acceleration it is proposed to use a frequency dependent derivation of the estimated angular velocity, given by

$$\dot{\omega}_{ib}^b = \frac{s}{1 + T_f s}. \quad (6.113)$$

$H(\tilde{\eta})$	$-\frac{dH(\tilde{\eta})}{d\tilde{\eta}}$
$1 -  \tilde{\eta} $	$\text{sgn}(\tilde{\eta})$
$1 - \tilde{\eta}$	$1$
$1 + \tilde{\eta}$	$-1$
$1 -  \tilde{\eta} ^{p+1}$	$(p+1)\text{sgn}(\tilde{\eta}) \tilde{\eta} ^p$
$\cos^p(\frac{\pi\tilde{\eta}}{2})$	$\frac{\pi\tilde{\eta}}{2} \cos^{p-1}(\frac{\pi\tilde{\eta}}{2}) \sin(\frac{\pi\tilde{\eta}}{2})$
$-\ln( \tilde{\eta} )$	$\frac{1}{\tilde{\eta}}$
$(\frac{1}{ \tilde{\eta} ^p}) - 1$	$\frac{p\text{sgn}(\tilde{\eta})}{ \tilde{\eta} ^{p+1}}$
$(\frac{2}{1+\tilde{\eta}})^p - 1$	$\frac{p}{1+\tilde{\eta}} (\frac{2}{1+\tilde{\eta}})^p$
$(\frac{2}{1-\tilde{\eta}})^p - 1$	$\frac{-p}{1+\tilde{\eta}} (\frac{2}{1+\tilde{\eta}})^p$

**Table 6.1:** Suggestion for the  $H(\tilde{\eta})$ -function used in output injection, and controller feedback.

## 6.3 Mutual synchronization

In the previous section, a controller enabling the follower spacecraft to keep its relative orientation with respect to the leader, was developed. A drawback with this controller is the lack of feedback from the follower to the leader of the formation. The result is that if the follower for some reason are unable to stay in formation, the formation is broken. We here propose a control scheme which joins the goals of trajectory tracking and synchronization of relative attitude, by creating interconnections between all spacecraft. It was inspired by the control scheme presented in Nijmeijer & Rodriguez-Angeles (2003), used for the synchronization in multi robot systems.

Due to difficulties in expressing the joint tracking and synchronization goal in Euler parameters, the controller has been derived using Euler angle kinematics and the model developed in section 2.4.1.

Since the angular velocity is still assumed unavailable, we propose to use the observer derived in Nicosia & Tomei (1992), which were shown to be semi-globally uniformly asymptotically stable. Semi-globally in the sense that the area of attraction can be made arbitrarily large. In this work, it was also proved that under some mild restrictions on the control algorithm the observer-controller structure remains stable using feedback from estimated states.

### 6.3.1 Synchronizing controller

We start by defining the mutual synchronization problem in the way presented in section 5.3.2. That is, to design interconnections such that the satellites' attitude track a predefined trajectory, while at the same time maintaining formation by keeping the relative attitude constant.

It is assumed that the predefined trajectory  $\Psi_d(t)$  is sufficiently smooth and exist for all time  $t \geq 0$ , such that  $\dot{\Psi}_d(t)$  and  $\ddot{\Psi}_d(t)$  are well defined.

A virtual reference trajectory combining the two separate requirements, can be defined for each spacecraft in the formation. The  $i$ 'th virtual reference is written

$$\Psi_{ri} = \Psi_d - \sum_{j=1, j \neq i}^p \mathbf{K}_{i,j} (\Psi_i - \Psi_j) \quad (6.114)$$

$$\dot{\Psi}_{ri} = \dot{\Psi}_d - \sum_{j=1, j \neq i}^p \mathbf{K}_{i,j} (\dot{\Psi}_i - \dot{\Psi}_j) \quad (6.115)$$

$$\ddot{\Psi}_{ri} = \ddot{\Psi}_d - \sum_{j=1, j \neq i}^p \mathbf{K}_{i,j} (\ddot{\Psi}_i - \ddot{\Psi}_j), \quad (6.116)$$

where  $\Psi_i$  is the attitude of the  $i$ 'th spacecraft,  $\mathbf{K}_{i,j}$  is a positive definite gain matrix weighing the synchronization error and  $i, j \in \{1, \dots, p\}$  where  $p$  is the number of satellites in the formation.

Further a mutual synchronization error variable is defined

$$\mathbf{s}_i \triangleq \Psi_i - \Psi_{ri} \quad (6.117)$$

$$\dot{\mathbf{s}}_i \triangleq \dot{\Psi}_i - \dot{\Psi}_{ri}. \quad (6.118)$$

The mutual synchronization error dynamics may now be written

$$M_i^*(\Psi_i)\ddot{\mathbf{s}} = -C(\Psi_i, \dot{\Psi}_i)\dot{\Psi}_i - A^*(\Psi)\tau_{a,i} + T^{-T}(\Psi)\tau_{g,i} - M_i^*(\Psi_i)\ddot{\Psi}_{ri}, \quad (6.119)$$

using the model derived in Section 2.4.1.

**Proposition 6.8.** *The error dynamics (6.119), with control input*

$$-A^*(\Psi)\tau_{a,i} \triangleq C(\Psi_i, \dot{\Psi}_i)\dot{\Psi}_{ri} - T^{-T}(\Psi)\tau_{g,i} + M_i^*(\Psi_i)\ddot{\Psi}_{ri} - K_{p,i}\mathbf{s}_i - K_{d,i}\dot{\mathbf{s}}_i, \forall i \in \{1, \dots, p\}, \quad (6.120)$$

where  $K_{p,i}, K_{d,i}$  is positive definite gain matrices, has a uniformly (globally) asymptotically stable origin  $(\mathbf{s}, \dot{\mathbf{s}}) = (\mathbf{0}, \mathbf{0})$ . Which implies U(G)AS for the tracking error and the synchronization error.  $\mathbf{s} = [\mathbf{s}_1, \dots, \mathbf{s}_p]^T$  and  $\dot{\mathbf{s}} = [\dot{\mathbf{s}}_1, \dots, \dot{\mathbf{s}}_p]^T$ .

*Proof.* The closed-loop error-dynamics is

$$M_i^*(\Psi_i)\ddot{\mathbf{s}}_i + K_{d,i}\dot{\mathbf{s}}_i + K_{p,i}\mathbf{s}_i = C(\Psi_i, \dot{\Psi}_i)\dot{\mathbf{s}}_i. \quad (6.121)$$

To show UGAS of the system an extension of Matrosov's theorem, given in 3.8, is used.

*Satisfying Assumption 1*

To show UGS of the origin  $(\mathbf{s}, \dot{\mathbf{s}}) = (\mathbf{0}, \mathbf{0})$ , a Lyapunov function candidate is given

$$V = \frac{1}{2}\dot{\mathbf{s}}_i^T M_i^*(\Psi_i)\dot{\mathbf{s}}_i + \frac{1}{2}\mathbf{s}_i^T K_{p,i}\mathbf{s}_i \quad (6.122)$$

Taking the derivative along the trajectories, we obtain

$$\dot{V} = \sum_{i=1}^p \dot{\mathbf{s}}_i^T M_i^*(\Psi_i)\ddot{\mathbf{s}}_i + \dot{\mathbf{s}}_i^T \dot{M}_i^*(\Psi_i)\dot{\mathbf{s}}_i + \dot{\mathbf{s}}_i^T K_{p,i}\dot{\mathbf{s}}_i \quad (6.123)$$

$$= \sum_{i=1}^p \dot{\mathbf{s}}_i^T \left[ -K_{d,i}\dot{\mathbf{s}} + \frac{1}{2}\dot{M}_i^*(\Psi_i)\dot{\mathbf{s}}_i + C(\Psi_i, \dot{\Psi}_i)\dot{\mathbf{s}}_i \right] \quad (6.124)$$

$$= \sum_{i=1}^p -\dot{\mathbf{s}}_i^T K_{d,i}\dot{\mathbf{s}} \leq 0 \quad (6.125)$$

Since the time derivative is negative semi-definite, the origin is UGS and the first assumption is satisfied.

*Satisfying Assumption 2*

Since the origin is UGS,  $\mathbf{s}_i, \dot{\mathbf{s}}_i, \ddot{\mathbf{s}}_i$  are bounded functions of time. For  $i = 1$  we choose

$$V_1 \triangleq V \quad (6.126)$$

$$\phi_1 \triangleq 0 \quad (6.127)$$

$$Y_1 \triangleq -\beta\|\dot{\mathbf{s}}\|^2 \leq 0 \quad (6.128)$$

$V_1$  is continuously differentiable and bounded,  $\phi_1$  is continuous and bounded, and finally  $Y_1$  is continuous and hence assumption 2 is satisfied for  $i = 1$ .

For  $i = 2$ , we choose

$$V_2 \triangleq \sum_{i=1}^p \dot{\mathbf{s}}_i \mathbf{K}_{p,i} \mathbf{s}_i \quad (6.129)$$

$$\phi_2 \triangleq \sum_{i=1}^p \ddot{\mathbf{s}}_i \quad (6.130)$$

$$Y_2 \triangleq \sum_{i=1}^p \phi_2^T \mathbf{K}_{p,i} \mathbf{s}_i + \dot{\mathbf{s}}_i \mathbf{K}_{p,i} \phi_2 \quad (6.131)$$

Since  $\mathbf{s}_i, \dot{\mathbf{s}}_i, \ddot{\mathbf{s}}_i$  are bounded functions of time,  $V_2, \phi_2$  and  $Y_2$  are bounded. Moreover,  $V_2$  is continuously differentiable, and  $\phi_2$  and  $Y_2$  are continuous in their arguments. Hence, assumption 2 is satisfied for  $i = 2$ .

*Satisfying Assumption 3*

$Y_1 \leq 0$  for all  $\dot{\mathbf{s}} \in \mathbb{R}^3$ , satisfying assumption 3 for  $i=1$ . Moreover,

$$Y_1 = 0 \Rightarrow \|\dot{\mathbf{s}}\| = 0 \Rightarrow Y_2 = \sum_{i=1}^p \phi_2^T \mathbf{K}_{p,i} \mathbf{s}_i \quad (6.132)$$

Inserting for  $\phi_2$  and  $\dot{\mathbf{s}} = 0$ , gives

$$Y_2 = \sum_{i=1}^p -\mathbf{s}_i \mathbf{K}_{p,i} \mathbf{s}_i \leq 0. \quad (6.133)$$

Thus, assumption 3 have been satisfied for both  $i \in \{1, 2\}$

*Satisfying Assumption 4*

It can now be seen that

$$\{Y_1 = 0, Y_2 = 0\} \Rightarrow \dot{\mathbf{s}} = 0, \mathbf{s} = 0, \quad (6.134)$$

satisfying assumption 4 for  $i \in \{1, 2\}$ .

We have verified all the assumptions of theorem 3.8, and we conclude that the origin  $(\mathbf{s}, \dot{\mathbf{s}}) = (\mathbf{0}, \mathbf{0})$  is *uniformly globally asymptotically stable*. Our problem is however that the pseudo inverse of the input matrix  $\mathbf{A}^*(\Psi)$  is not defined for  $\theta = \pm \frac{\pi}{2}$ . Thus our final conclusion can only be one of *uniform asymptotic stability*, with a domain of attractivity  $\mathbb{D} = \{[\Psi^T, \dot{\Psi}^T]^T \in \mathbb{R}^6 | \theta \neq \pm \frac{\pi}{2}\}$ .

The next step is to show that UGAS of the origin  $(\mathbf{s}, \dot{\mathbf{s}}) = (\mathbf{0}, \mathbf{0})$  implies UGAS of the tracking and synchronization error. Following the approach in Nijmeijer & Rodriguez-Angeles (2003), we write the vector of synchronization errors when  $\mathbf{s}$  have converged to zero as

$$\begin{bmatrix} \mathbf{s}_1 \\ \vdots \\ \mathbf{s}_p \end{bmatrix} = \begin{bmatrix} \mathbf{e}_{1,1} + \sum_{j=1, j \neq 1}^p \mathbf{K}_{1,j} \mathbf{e}_{1,j} \\ \vdots \\ \mathbf{e}_{p,p} + \sum_{j=1, j \neq p}^p \mathbf{K}_{p,j} \mathbf{e}_{p,j} \end{bmatrix} = \begin{bmatrix} 0 \\ \vdots \\ 0 \end{bmatrix}. \quad (6.135)$$

which implies taking the definitions of the partial synchronization errors

$$\begin{bmatrix} (\mathbf{I}_{3 \times 3} + \sum_{j=1, j \neq 1}^p \mathbf{K}_{1,j}) & -\mathbf{K}_{1,2} & \cdots & -\mathbf{K}_{1,p} \\ -\mathbf{K}_{2,1} & (\mathbf{I}_{3 \times 3} + \sum_{j=1, j \neq 2}^p \mathbf{K}_{2,j}) & \cdots & -\mathbf{K}_{2,p} \\ \vdots & \vdots & \ddots & \vdots \\ -\mathbf{K}_{p,1} & -\mathbf{K}_{p,2} & \cdots & (\mathbf{I}_{3 \times 3} + \sum_{j=1, j \neq p}^p \mathbf{K}_{p,j}) \end{bmatrix} \begin{bmatrix} \Psi_1 \\ \Psi_2 \\ \vdots \\ \Psi_p \end{bmatrix} = \begin{bmatrix} \Psi_d \\ \Psi_d \\ \vdots \\ \Psi_d \end{bmatrix} \quad (6.136)$$

Using Lemma 5.1 in Nijmeijer & Rodriguez-Angeles (2003), it follows that (??) implies

$$\begin{bmatrix} \Psi_1 \\ \Psi_2 \\ \vdots \\ \Psi_p \end{bmatrix} = \begin{bmatrix} \Psi_d \\ \Psi_d \\ \vdots \\ \Psi_d \end{bmatrix}. \quad (6.137)$$

This results in the convergence of  $\Psi_i \rightarrow \Psi_d, \forall i \in \{1, \dots, p\}$ . Similarly, one can show the convergence  $\dot{\Psi}_i \rightarrow \dot{\Psi}_d$ . This concludes the proof.  $\square$

### 6.3.2 Observer design

As the angular velocity is not available for measurements, we propose to use an observer. In Nicosia & Tomei (1992) a nonlinear model-based observer was proposed for a reaction wheel actuated spacecraft as

$$\dot{\hat{z}}_1 = \hat{z}_2 + k_d(\mathbf{y} - \hat{z}_1) \quad (6.138a)$$

$$\dot{\hat{z}}_2 = M^{*-1}(\mathbf{y}) \left[ -C^*(\mathbf{y}, \hat{z}_1, \boldsymbol{\omega}_s) \hat{z}_1 + K_p(\mathbf{y} - \hat{z}_1) + T^{-T}(\mathbf{y})\boldsymbol{\tau}_e - T^{-T}\mathbf{A}\boldsymbol{\tau}_a \right], \quad (6.138b)$$

where  $k_d$  is a positive constant,  $K_p$  is positive definite matrix and  $\mathbf{y}$  is the measured attitude  $\Psi_i$ . The estimates  $\hat{\Psi}$  and  $\hat{\dot{\Psi}}$  are defined as

$$\hat{\Psi} = \hat{z}_1 \quad (6.139)$$

$$\hat{\dot{\Psi}} = \hat{z}_2 + k_d(\Psi - \hat{z}_1). \quad (6.140)$$

This observer was shown to be uniformly asymptotically stable with region of attraction

$$\mathcal{S} = \left\{ \tilde{\mathbf{x}} \in \mathbb{R}^6 \mid \|\tilde{\mathbf{x}}\| < \sqrt{\frac{H_m}{H_M}} \left( \frac{G_m k_d}{k_c} \right) \right\} \quad (6.141)$$

where  $H_m, H_M$  and  $G_m$  are variables dependent on the inertia and observer gain,  $k_d$  is an observer gain and  $k_c$  is a constant dependent on coriolis interconnection.

We may define the estimated synchronization variables as

$$\hat{\Psi}_{ri} = \Psi_d - \sum_{j=1, j \neq i}^p K_{i,j}(\hat{\Psi}_i - \hat{\Psi}_j)\hat{\mathbf{s}}_i = \hat{\Psi} - \hat{\Psi}_{ri}. \quad (6.142)$$

with corresponding derivatives. Like in the previous observer, we construct the acceleration through frequency dependent derivation.

### 6.3.3 Control using estimated variables

Taking the control when using estimated variables as

$$-A^*(\Psi)\boldsymbol{\tau}_{a,i} \triangleq C(\Psi_i, \hat{\Psi}_i)\hat{\Psi}_{ri} - T^{-T}(\Psi)\boldsymbol{\tau}_{g,i} + M_i^*(\Psi_i)\hat{\dot{\Psi}}_{ri} - K_{p,i}\mathbf{s}_i - K_{d,i}\hat{\mathbf{s}}_i, \forall i \in \{1, \dots, p\}, \quad (6.143)$$

the error-dynamics may be written in the form

$$\dot{\mathbf{x}} = \mathbf{F}(t, \mathbf{x}) + \mathbf{g}(t, \mathbf{x})\boldsymbol{\alpha}(t, \tilde{\mathbf{x}}) \quad (6.144)$$

where  $\boldsymbol{\alpha}(t, \tilde{\mathbf{x}})$  is linear in the estimation errors. Following Theorem 3 in Nicosia & Tomei (1992), we conclude local asymptotic stability of the closed loop.

## 6.4 Desaturation of reaction wheels

Due to disturbances on the spacecraft, angular momentum will build up in the reaction wheels. When the wheels eventually saturate, i.e. they have reached their maximum rotational velocity, they cannot provide internal torques for attitude tracking. We therefore need some way of desaturating the wheels and dump excess momentum. In order to do this external torques must be applied, to change to total angular momentum of the spacecraft. This torque may be provided either from electromagnetic torquers or from attitude control system thrusters. As reported in Section 2.5.3 electromagnetic thrusters can provide only a small amount of torque, but are independent of an expendable fuel source. Another problem is that the relation between the magnetic moment and the resulting torque vector

$$\boldsymbol{\tau}_m^b = -\mathbf{S}(\mathbf{B}^b)\mathbf{m}^b, \quad (6.145)$$

is noninvertable, since  $\mathbf{S}(\mathbf{B}^b)$  is skew-symmetric and has determinant always equal to 0. Hence, it is not possible to specify the magnetic moment which results in a desired torque. In fact the only feasible torques belongs to the space of vectors which is perpendicular to the geomagnetic field vector  $\mathbf{B}^b$ , which is a 2-dimensional manifold in  $\mathbb{R}^3$ . To find the torque vector which minimizes the difference between the ideal and the actual torque, we project the ideal torque vector onto the space of possible vectors (Arduni & Baiocco 1997). Then we get the relation

$$\boldsymbol{\tau}_m = \boldsymbol{\tau}_{m,\text{ideal}} - \Delta\boldsymbol{\tau}_m, \boldsymbol{\tau}_m \in \{\boldsymbol{\tau}_m \in \mathbb{R}^3 | \boldsymbol{\tau}_m \perp \mathbf{B}^b\} \quad (6.146)$$

where  $\Delta\boldsymbol{\tau}_m$  is given by

$$\Delta\boldsymbol{\tau}_m = \frac{\mathbf{S}(\mathbf{B}^b)\boldsymbol{\tau}_{m,\text{ideal}}}{\|\mathbf{B}^b\|^2} \quad (6.147)$$

Following the approach in Lovera & Astolfi (2004), we select the magnetic moment according to

$$\mathbf{m}^b = -\frac{1}{\|\mathbf{B}^b(t)\|_2^2} \mathbf{S}(\mathbf{B}^b(t))\boldsymbol{\tau}_{m,\text{ideal}} \quad (6.148)$$

Changing the angular momentum of the reaction wheels involves forcing the vector

$$\mathbf{h}_w = \mathbf{A}\mathbf{I}_s\boldsymbol{\omega}_s, \quad (6.149)$$

to zero. The wheels are slowed down by exerting wheel torques in the opposite of speed direction. For reaction wheel attitude control systems with more than 3 wheel, (6.149) has a null space, i.e.  $\mathbf{A}\mathbf{I}_s\boldsymbol{\omega}_s$  is zero for other solutions than the trivial  $\boldsymbol{\omega}_s = 0$ . In particular when all the wheels are have equal inertia, the null space of (6.149) is given by

$$\boldsymbol{\omega}_s = c[1 \ 1 \ 1 \ 1]^T, \quad \forall c \in \mathbb{R} \quad (6.150)$$

indicating that while we are able to render the total angular momentum of the wheel system zero, the actual wheel speeds converge to a state in  $\text{Null}(\mathbf{A}\mathbf{I}_s)$ . To remedy this, we propose a procedure where we first control one wheel to zero. When this has been achieved, we may use the usual momentum dumping control laws proposed in the literature, for example in Sidi (1997):

$$\boldsymbol{\tau}^b = -\mathbf{A}\mathbf{I}_s\boldsymbol{\omega}_s. \quad (6.151)$$

We are now ready to give our momentum dumping scheme as the following procedure.

**Step 1:** Drive the speed of wheel 1 to zero while controlling the attitude with the remaining wheels, using the control law

$$\bar{\boldsymbol{\tau}}_a = -c\mathbf{B}_1\boldsymbol{\omega}_s + \mathbf{B}_2\boldsymbol{\tau}_a, \quad (6.152)$$

where  $\mathbf{B}_1 = \text{diag}(1, 0, 0, 0)$ ,  $\mathbf{B}_2 = \text{diag}(0, 1, 1, 1)$  and  $\boldsymbol{\tau}_a$  is the normal control law.

**Step 2:** While retaining the modified control law (6.152), a torque is exerted by the magnetic torquers to dump momentum:

$$\tau_{m,\text{ideal}}^b = -\mathbf{A}\mathbf{I}_s\omega_s \quad (6.153)$$

which is implemented in magnetic moment using (6.148).

**Step 3:** When the wheel speed are sufficiently lowered, resume normal control  $\tau_a$  and turn off magnetic torquers.

**Remark 6.5.** *Due to the redundancy of the wheels, stability properties are not changed under the influence of the above control law. The three remaining wheels are able to exert the required torque for three-axis stabilization about all axes.*

## 6.5 Discussion

### 6.5.1 Robustness issues

Several controllers have been derived and analyzed in the previous sections. A common factor is that all are based on cancelation of nonlinearities as well as exploiting system properties such as skew-symmetry. Cancelation of nonlinearities can be a problem in the presence of poorly known parameters, it is therefor of outmost importance that the derived controllers are robust to these cases.

As several of the controllers derived have been proven to have *uniform* stability properties, they are expected to be robust to bounded disturbances (Lamnabhi-Lagarrigue, Loria & Panteley 2004). This origins from the fact that a system which is locally Lipschitz uniformly in  $t$ , ULAS or ULES, it is also locally Input-to-State (ISS), that is, there exist  $\beta \in \mathcal{KL}$ ,  $\gamma \in \mathcal{K}$  and a number  $\delta$  such that, for all  $t \geq t_0 \geq 0$

$$\max\{|x_0|, \|u\|_\infty\} \leq \delta \Rightarrow |x(t; t_0, x_0, u)| \leq \beta(|x_0|, t - t_0) + \gamma(\|u\|_\infty). \quad (6.154)$$

Simulations will verify this.

### 6.5.2 Control using estimated states

In the external synchronization scheme it was proposed to use an observer to estimate the unmeasured states. In the absence of a general nonlinear separation principle, there is no stability guarantee for the interconnected system using estimated variables in the controller. To show stability it was considered using the theory of cascaded systems as presented in Loria (2004) and Panteley & Loria (1998). In this approach we consider the observer-controller structure as a cascaded system. This is done by considering the measurement which interconnects the observer with the controller, as a time-varying signal. Then the observer error-dynamics is only a nonlinear nonautonomous system,  $\Sigma_2$ , with estimate error as state-variable, assuming the total system has the *forward completeness* property, defined e.g. in Loria, Fossen & Panteley (2000).

$$\Sigma_2 : \xi_2 = f_2(t, y(t), \xi_2) = f(t, \xi_2). \quad (6.155)$$

Moreover, the error-dynamics of the synchronization closed-loop, can be written as a UGAS nonlinear nonautonomous system with an added perturbation term which is linear in the synchronization error.

$$\Sigma_1 : \xi_1 = f_1(t, \xi_2) + g(t, \xi). \quad (6.156)$$

Using Theorem 2 of Panteley & Loria (1998), stability of the cascade could be shown under the assumption of integrability of the estimation error. This is not guaranteed for a UGAS system, thus no conclusion could be drawn.

A second approach is to consider the estimation error as a bounded perturbation to the system. Then, due to the uniformity of the stability properties, the solutions should at least stay uniformly bounded.

### 6.5.3 Acceleration feedback

A drawback of some of the proposed controllers, are their dependency on acceleration feedback for perfect tracking. This is the case for most trajectory tracking and synchronizing controllers. For trajectory tracking, this acceleration is the desired acceleration, but for synchronization it is the acceleration of the leader. It must therefore somehow be estimated, as remarked earlier this was done using a frequency dependent derivative of the estimated angular velocities.

### 6.5.4 Adaptive controller

The adaptive controller was proved to be globally convergent in the state-error variables. For the parameter estimate we could however only able to conclude boundedness. As remarked earlier, for true parameter convergence we need to guarantee the PE property of the driving signal, in this case the synchronization error. Since we proved convergence of the error, the parameter update will eventually stop.

### 6.5.5 Unstable equilibrium point $\eta = -1$

In the previous sections, we have seen cases where the equilibrium point of  $\eta = -1$  is unstable. This is however seldom a problem in physical implementations, as  $\eta = -1$  and  $\eta = 1$  corresponds to the same physical Euler angle. A behavior which may occur is that if the attitude error is determined to have a scalar quaternion part equal to 1, the satellite would rotate 360 degrees about some axis.



# Chapter 7

## Simulations

In this chapter the satellite cluster is simulated with the different controllers and observers. The simulations have been performed in MATLAB Simulink, using the model-files and scripts available on the included CD. All models have been simulated using the ODE45 integration technique with a maximum step-size of 10 and relative tolerance of  $10^{-3}$ .

The environmental torques included in the simulation, include the gravity gradient, the solar pressure and the aerodynamic drag. The gravity gradient is modeled using the theory in section 2.5.1, assuming a circular orbit. We have also ignored the perturbations in the gravity torque due to the oblateness of the Earth, since these are very small compared to other perturbations. The solar pressure and aerodynamic drag are difficult to model accurately, especially when the exact spacecraft design is not readily known. These forces have therefor been modeled as a constant plus a sinusoidal term which varies during the course of the orbit. In a more rigorous simulation these should be modeled as a function of orbit position, angle of incidence with the sun and the angle with respect to the direction of velocity. This is however out of the scope of this thesis. The reaction wheel assemblies used in this theses are based on the specification of the DRALLRAD wheel assembly, which can be found in Sidi (1997). The relevant data have been summarized in table A.2 and table A.3.

**Remark 7.1.** *Most simulation plots of attitude have been given using Euler angles for easier interpretation.*

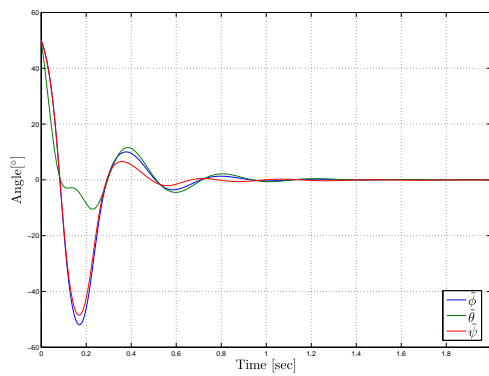
### 7.1 Observer simulation

To show asymptotic convergence and performance of the nonlinear observer, it has been simulated during feedback control, with and without measurement noise and environmental disturbances.

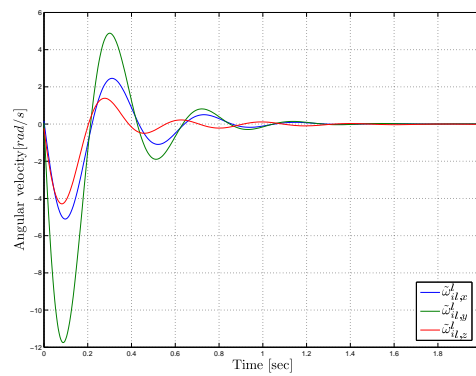
Parameter	Value
Initial satellite attitude	$\Psi_{ib} = [50, 50, 50]^T [^\circ]$
Initial satellite angular velocity	$\omega_{ib}^b = [0.0001, 0.0003, 0.0001]^T [rad/s]$
Initial observer attitude	$\hat{\Psi}_{ib} = [0, 0, 0]^T [^\circ]$
Initial observer angular velocity	$\hat{\omega}_{ib}^b = [0, 0, 0]^T [rad/s]$

**Table 7.1:**

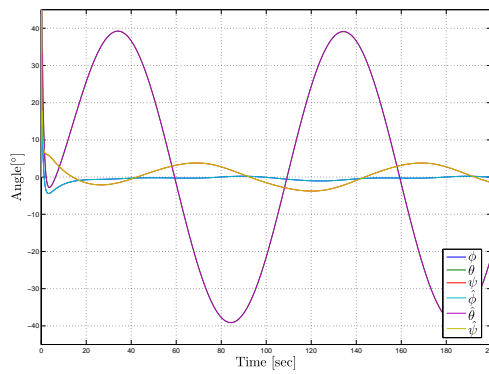
In figure 7.1(a) and 7.1(b) the asymptotic stability which was proved in section 6.2.3 is clearly seen, both in the angular velocity and in the Euler angles. And 7.1(c) and 7.1(d) show how the estimated variables clearly follow the actual. The asymptotic convergence is also seen when introducing measurement noise and environmental force, in figure 7.2. But as seen from figure 7.2(d), the error-is only bounded at steady-state, indicating asymptotic convergence to a ball about the origin.



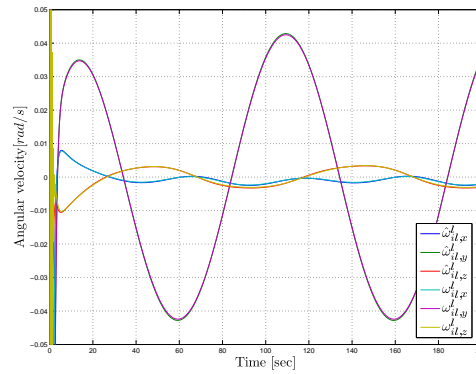
(a) Transient estimation errors in euler angles



(b) Transient estimation errors in angular velocity

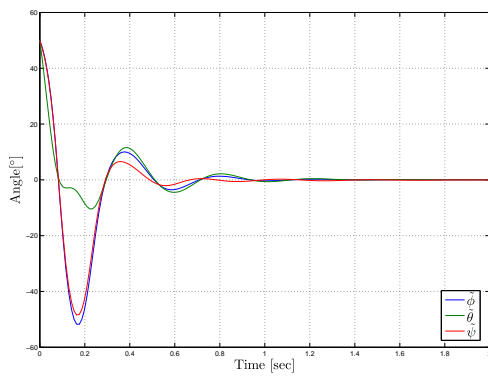


(c) Estimated vs. actual euler angles

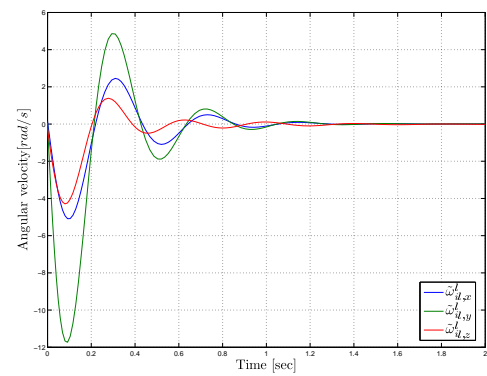


(d) Estimated vs. actual angular velocity

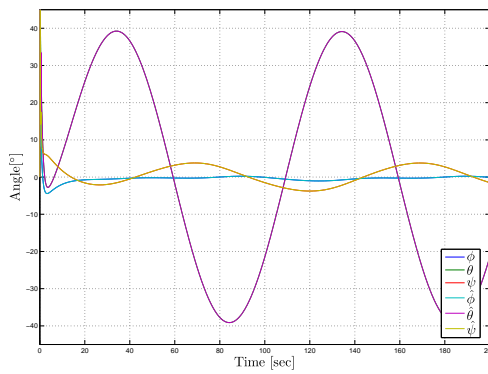
**Figure 7.1:** Observer simulation, no measurement noise



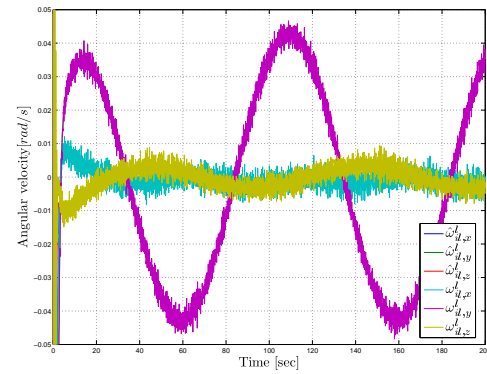
(a) Transient estimation errors in euler angles



(b) Transient estimation errors in angular velocity



(c) Estimated vs. actual euler angles



(d) Estimated vs. actual angular velocity

**Figure 7.2:** Observer simulation, measurement noise and environmental forces

## 7.2 Leader controller simulation

In this section the leader satellite is simulated in closed loop with the different leader controllers, to show transient, steady-state and tracking performance. Initial conditions for the simulations are given in tables 7.2, 7.3 and 7.4.

Figure 7.3 show the asymptotic convergence proved in the previous chapter for all controllers. The actual performance is governed by the selected controller gains and of course the maximum allowable wheel torque. High gains will cause the actuators to saturate, then the stability proofs no-longer holds. Thus, to ensure stability, controller gains must be chosen with care. Simulations were done while choosing the proportional gain too high, resulting in constant chattering between maximum and minimum torque, eventually leading to instability.

Parameter	Value
Initial satellite attitude	$\Psi_{ib} = [50, 50, 50]^T [^\circ]$
Initial satellite angular velocity	$\omega_{ib}^b = [0.0001, 0.0003, 0.0001] [rad/s]$
Initial observer attitude	$\hat{\Psi}_{ib} = [0, 0, 0]^T [^\circ]$
Initial observer angular velocity	$\hat{\omega}_{ib}^b = [0, 0, 0] [rad/s]$
Set point 1	$\Psi_{d1} = [0, 50, 0]^T [^\circ]$ at t = 0s
Set point 2	$\Psi_{d2} = [-60, 50, 0]^T [^\circ]$ at t = 50s

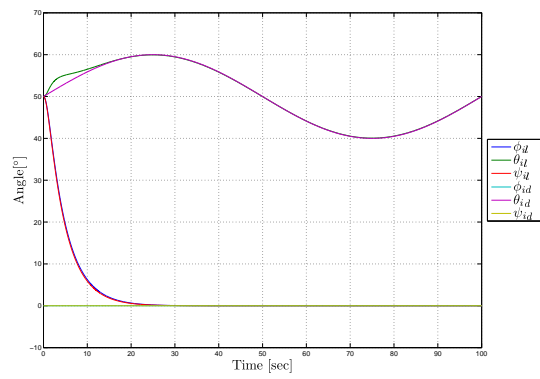
**Table 7.2:** Simulation initial conditions and desired state for the  $\mathcal{F}_i$  set-point controller

Parameter	Value
Initial satellite attitude	$\Psi_{ib} = [50, 50, 50]^T [^\circ]$
Initial satellite angular velocity	$\omega_{ib}^b = [0.0001, 0.0003, 0.0001] [rad/s]$
Initial observer attitude	$\hat{\Psi}_{ib} = [0, 0, 0]^T [^\circ]$
Initial observer angular velocity	$\hat{\omega}_{ib}^b = [0, 0, 0] [rad/s]$
Set point 1	$\Psi_{d1} = [0, 50, 0]^T [^\circ]$ at t = 0s
Set point 2	$\Psi_{d2} = [-60, 50, 0]^T [^\circ]$ at t = 50s

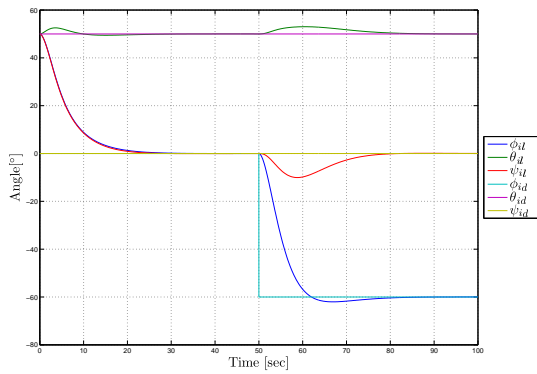
**Table 7.3:** Simulation initial conditions and desired state for the  $\mathcal{F}_o$  set-point controller

Parameter	Value
Initial satellite attitude	$\Psi_{ib} = [50, 50, 50]^T [^\circ]$
Initial satellite angular velocity	$\omega_{ib}^b = [0.0001, 0.0003, 0.0001] [rad/s]$
Initial observer attitude	$\hat{\Psi}_{ib} = [0, 0, 0]^T [^\circ]$
Initial observer angular velocity	$\hat{\omega}_{ib}^b = [0, 0, 0] [rad/s]$
Desired Euler angles	$\Psi_d = \begin{bmatrix} 0 \\ 50^\circ + 10^\circ \sin(\frac{2\pi}{100}) \\ 0 \end{bmatrix}$

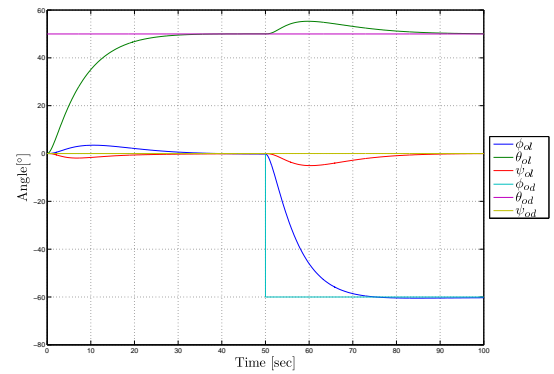
**Table 7.4:** Simulation initial conditions and desired state for tracking controller in  $\mathcal{F}_i$



(a) Leader vs. desired states: Tracking controller in  $\mathcal{F}_i$



(b) Leader vs. desired states: Set-point controller in  $\mathcal{F}_i$



(c) Leader vs. desired states: Set-point controller in  $\mathcal{F}_o$

**Figure 7.3:** Simulation of leader controllers, no measurement noise, no process noise

### 7.3 Lyapunov-based external synchronization controller

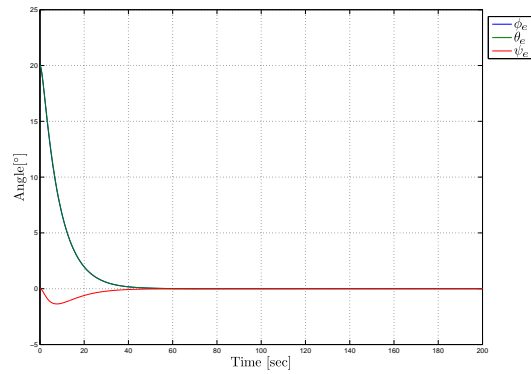
In this section the Lyapunov-based external synchronizing controller is simulated. The system was first simulated with perfect state-variable knowledge and neither measurement noise or environmental disturbances. Then, estimated variables were introduced instead of the actual, and finally the system was simulated with feedback from estimated states, including disturbances.

Parameter	Value
Initial leader satellite attitude	$\Psi_{ib} = [0, 0, 0]^T [^\circ]$
Initial leader satellite angular velocity	$\omega_{ib}^b = [0.0001, 0.0003, 0.0001] [rad/s]$
Initial follower attitude	$\hat{\Psi}_{ib} = [20, 20, 0]^T [^\circ]$
Initial follower angular velocity	$\hat{\omega}_{ib}^b = [0.0001, 0.0003, 0.0001] [rad/s]$
Set point 1	$\Psi_{d1} = [0, 70, 0]^T [^\circ]$ at $t = 0s$
Set point 2	$\Psi_{d2} = [-60, 70, 0]^T [^\circ]$ at $t = 50s$

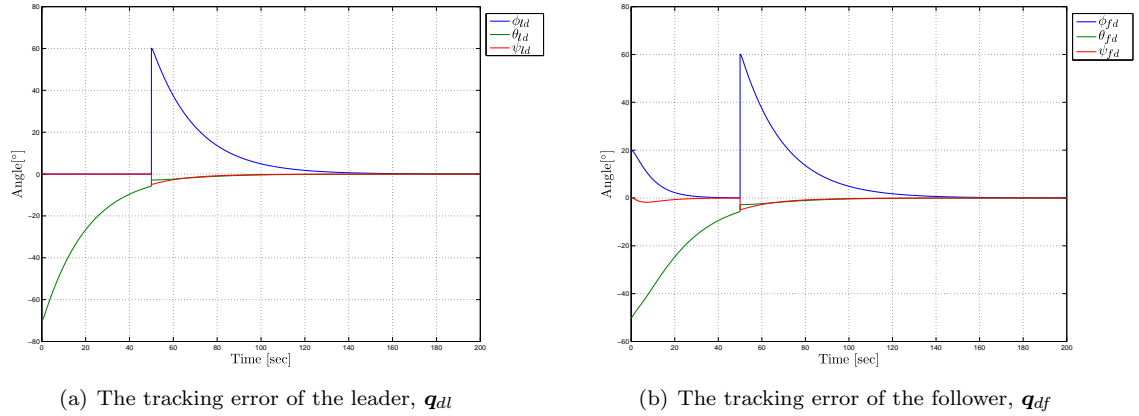
**Table 7.5:** Simulation initial conditions and desired states, Lyapunov-based synchronizing controller.

Figures 7.4, 7.8 and 7.12 show fast convergence of the synchronization errors, also when using feedback from estimated states and with noise contaminated measurements. With only small transients when using estimated states. From 7.6, 7.9 and 7.13, we clearly see that the attitude of the follower tracks that of the leader, also during large transients with deviation  $< 1^\circ$ .

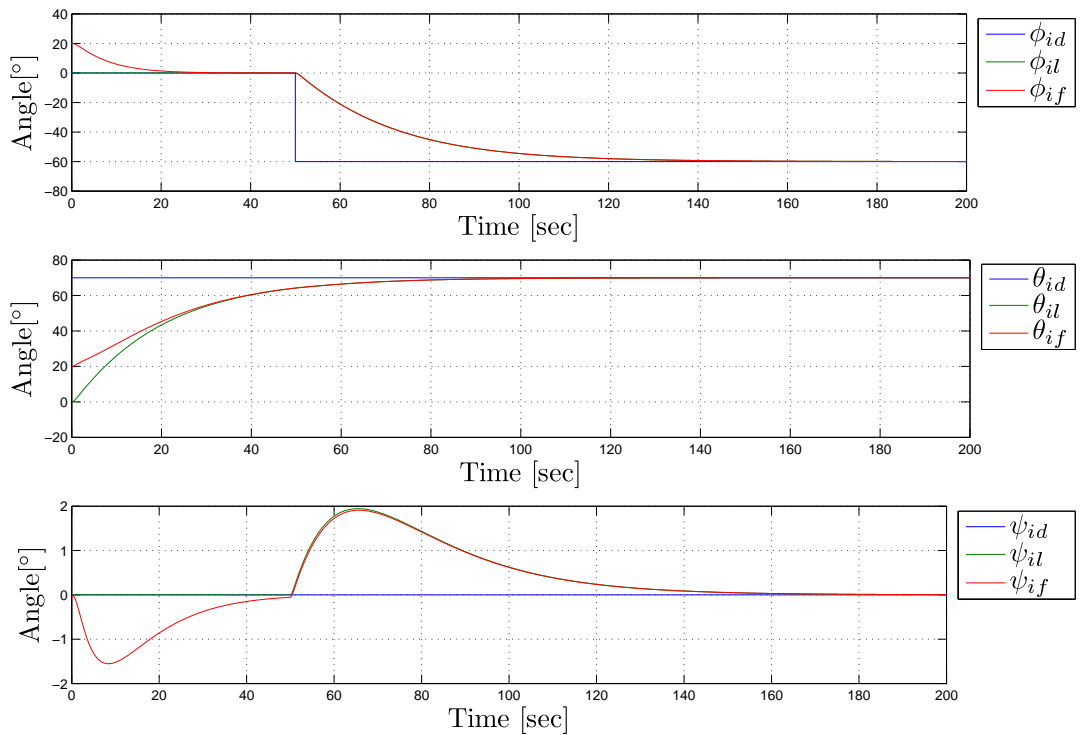
#### 7.3.1 With actual variables and no noise



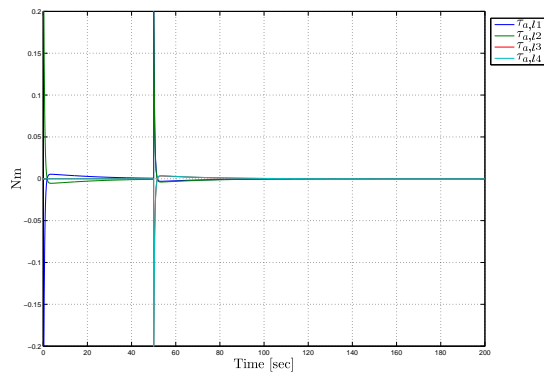
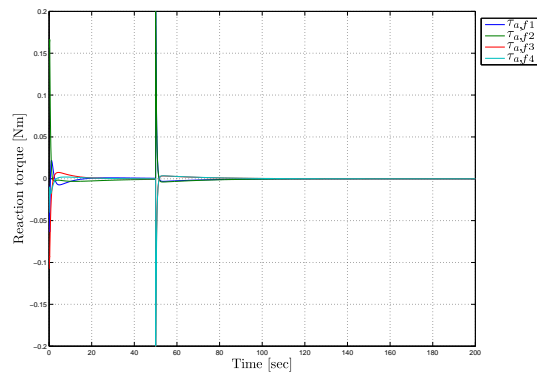
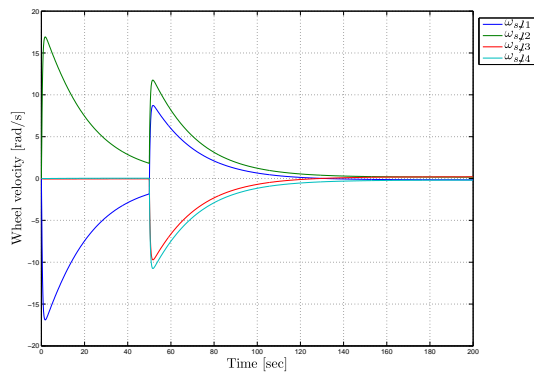
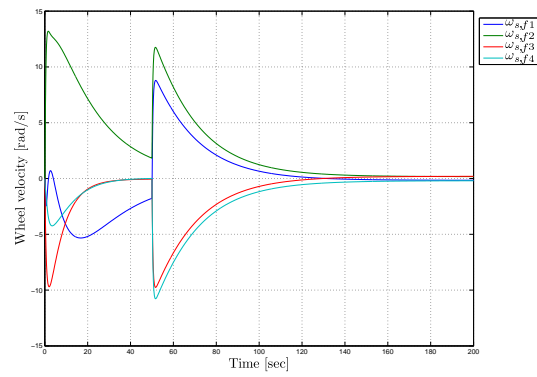
**Figure 7.4:** Simulation of external synchronization control law (6.48), with feedback from actual states. The plots show the synchronization error  $q_{lf}$ .



**Figure 7.5:** Simulation of external synchronization control law (6.48), with feedback from actual states. The plots show the tracking errors.



**Figure 7.6:** Simulation of external synchronization control law (6.48), with feedback from actual states. The plots show the trajectories of the leader and follower vs. the desired.

(a) Reaction wheel torque,  $\tau_{a,l}$ (b) Reaction wheel torque,  $\tau_{a,f}$ (c) Wheel velocity,  $\omega_{a,l}$ (d) Wheel velocity,  $\omega_{a,f}$ 

**Figure 7.7:** Simulation of external synchronization control law (6.48), with feedback from actual states. The plots show input torque and wheel velocity of both satellites.

## 7.3.2 With estimated state variables, no noise

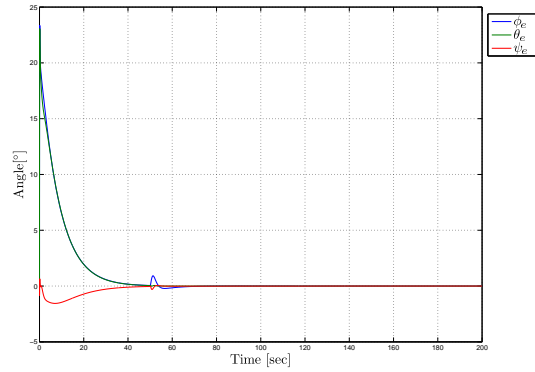


**Figure 7.8:** Simulation of external synchronization control law (6.48), with feedback from estimated states. The plots show the synchronization error  $q_{lf}$ .

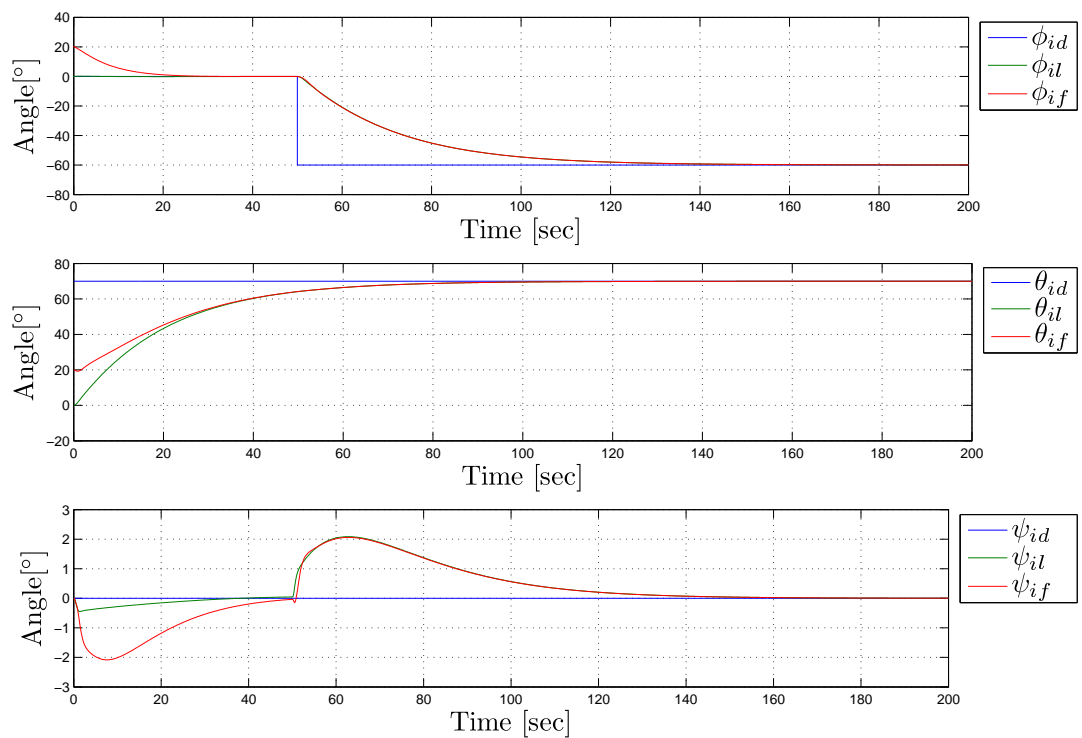


**Figure 7.9:** Simulation of external synchronization control law (6.48), with feedback from estimated states. The plots show the trajectories of the leader and follower vs. the desired.

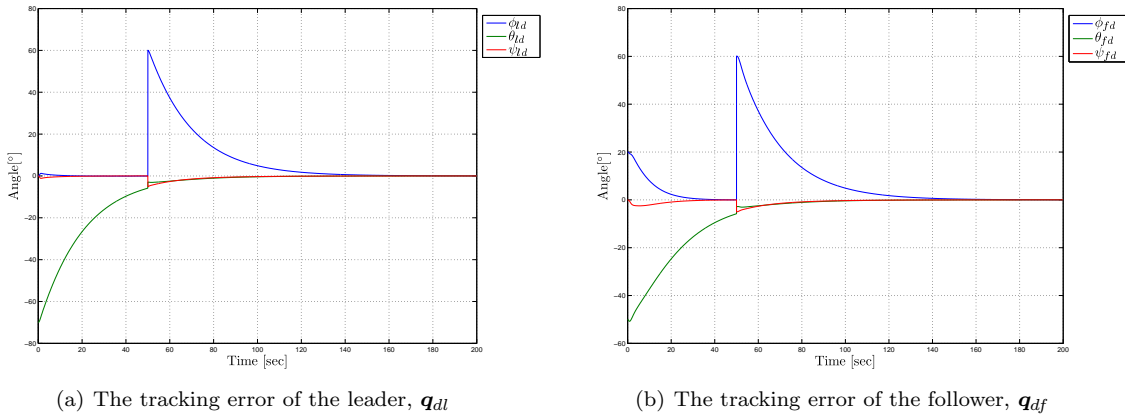


**Figure 7.10:** Simulation of external synchronization control law (6.48), with feedback from estimated states. The plots show the tracking errors.

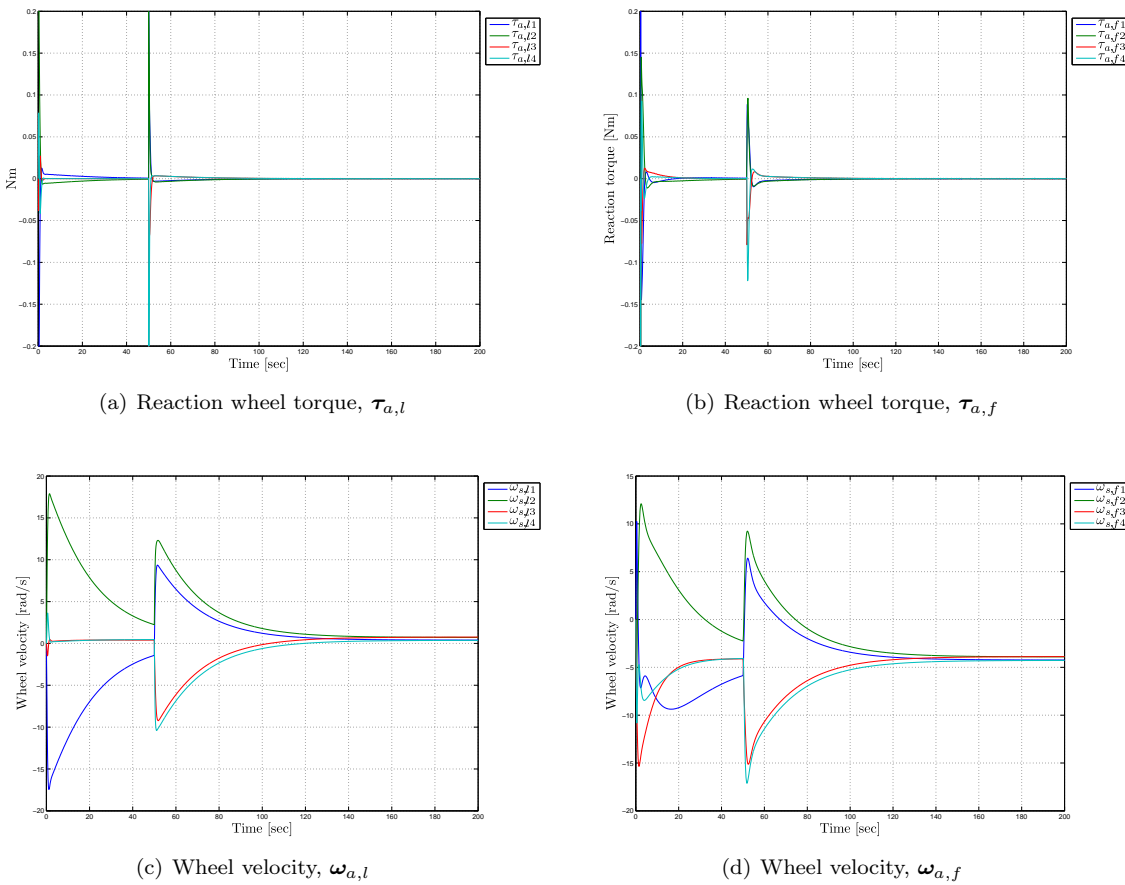


**Figure 7.11:** Simulation of external synchronization control law (6.48), with feedback from estimated states. The plots show input torque and wheel velocity of both satellites.

## 7.3.3 With estimated state variables, measurement noise

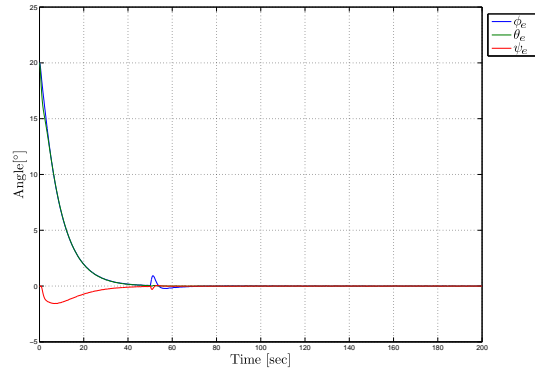


**Figure 7.12:** Simulation of external synchronization control law (6.48), with feedback from estimated states, noise contaminated measurements. The plots show the synchronization error  $q_{lf}$ .

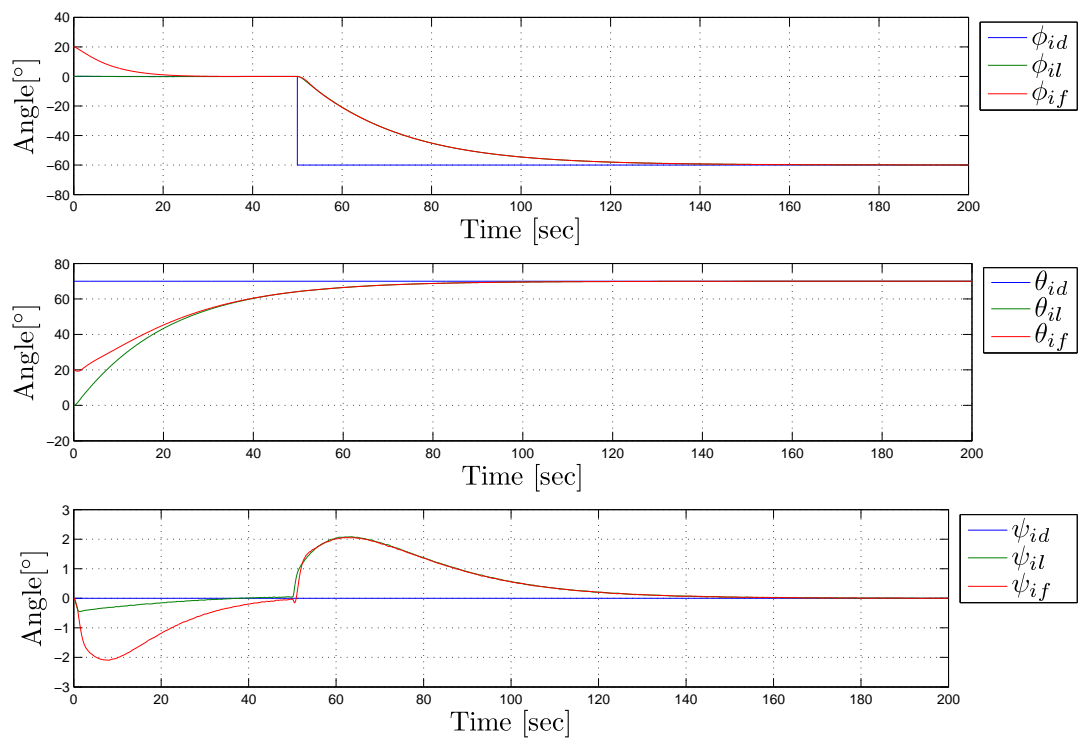


**Figure 7.13:** Simulation of external synchronization control law (6.48), with feedback from estimated states, noise contaminated measurements. The plots show the trajectories of the leader and follower vs. the desired.

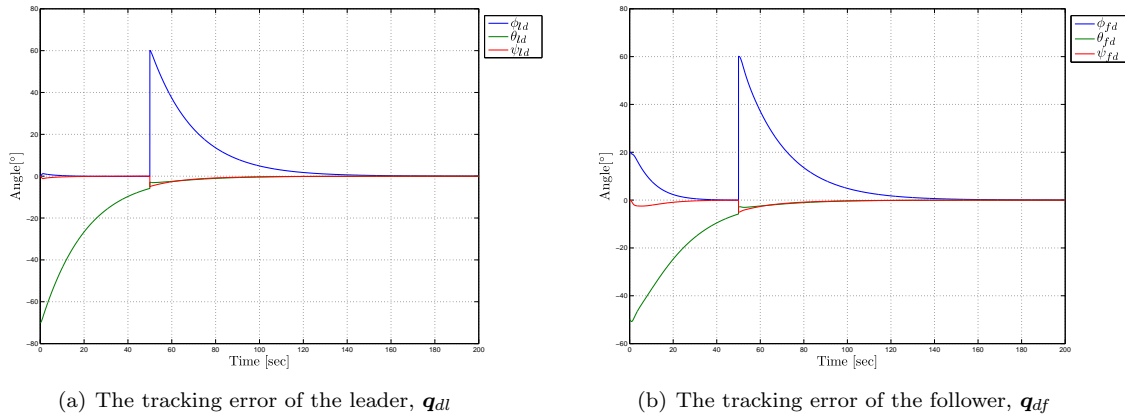


**Figure 7.14:** Simulation of external synchronization control law (6.48), with feedback from estimated states, noise contaminated measurements. The plots show the synchronization error and tracking errors.

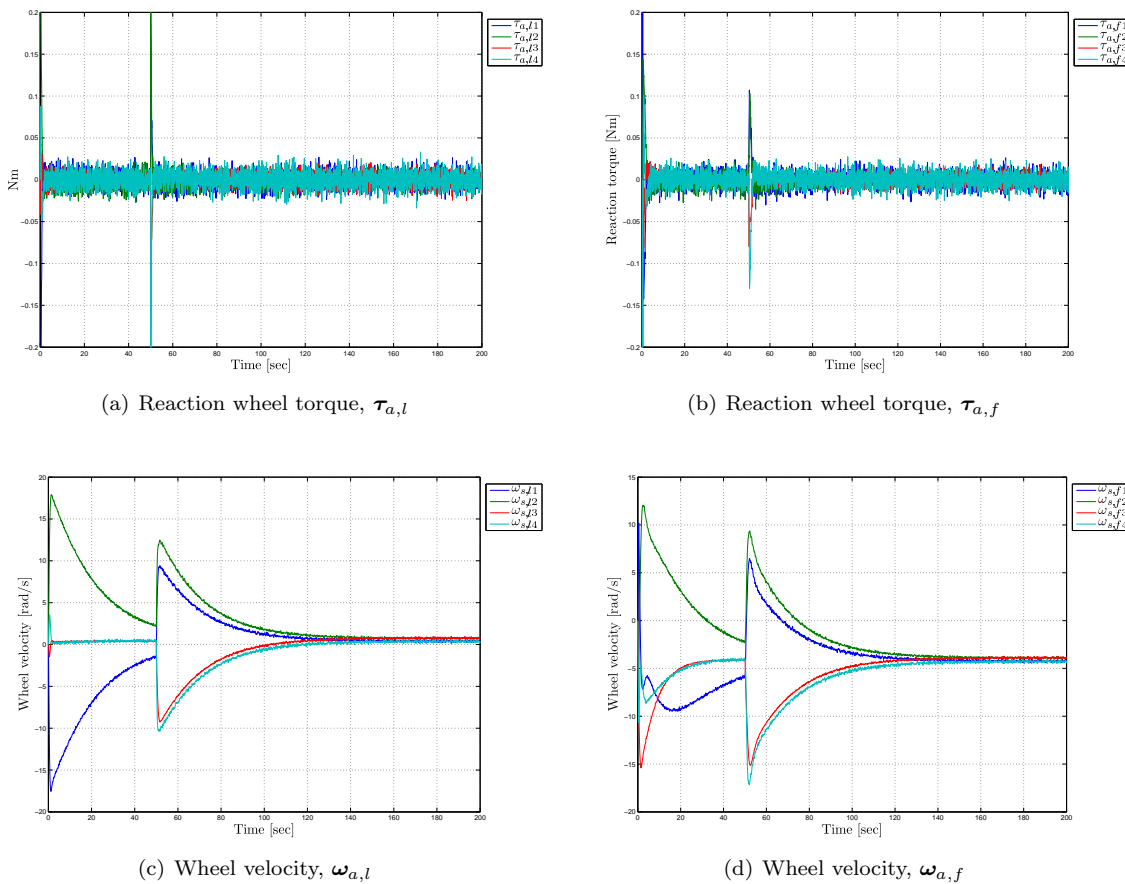


**Figure 7.15:** Simulation of external synchronization control law (6.48), with feedback from estimated states, noise contaminated measurements. The plots show input torque and wheel velocity of both satellites.

## 7.4 Adaptive synchronizing controller

The adaptive synchronizing controller is simulated as the Lypunov-based in the previous section, but with different desired states. Now we want the leader to track a time-varying trajectory. We have used the set-point controller, to visualize the fact that the satellites stay synchronized when tracking is not obtained. We also see that though parameter convergence is not obtained, the synchronization error converges to zero as predicted.

Parameter	Value
Initial leader satellite attitude	$\Psi_{ib} = [0, 0, 0]^T [^\circ]$
Initial leader satellite angular velocity	$\omega_{ib}^b = [0.0001, 0.0003, 0.0001] [rad/s]$
Initial follower attitude	$\hat{\Psi}_{ib} = [20, 20, 0]^T [^\circ]$
Initial follower angular velocity	$\hat{\omega}_{ib}^b = [0.0001, 0.0003, 0.0001] [rad/s]$
Set point 1	$\Psi_{d1} = \begin{bmatrix} 50 \\ 10 \sin(\frac{2\pi}{100}) \\ 0 \end{bmatrix} [^\circ] \text{ at } t = 0s$
Set point 2	$\Psi_{d2} = \begin{bmatrix} 50 \\ 10 \sin(\frac{2\pi}{100}) \\ 80 \end{bmatrix} [^\circ] \text{ at } t = 50s$

**Table 7.6:** Simulation initial conditions and desired states, adaptive synchronizing controller.

### 7.4.1 With actual state variables, no measurement noise

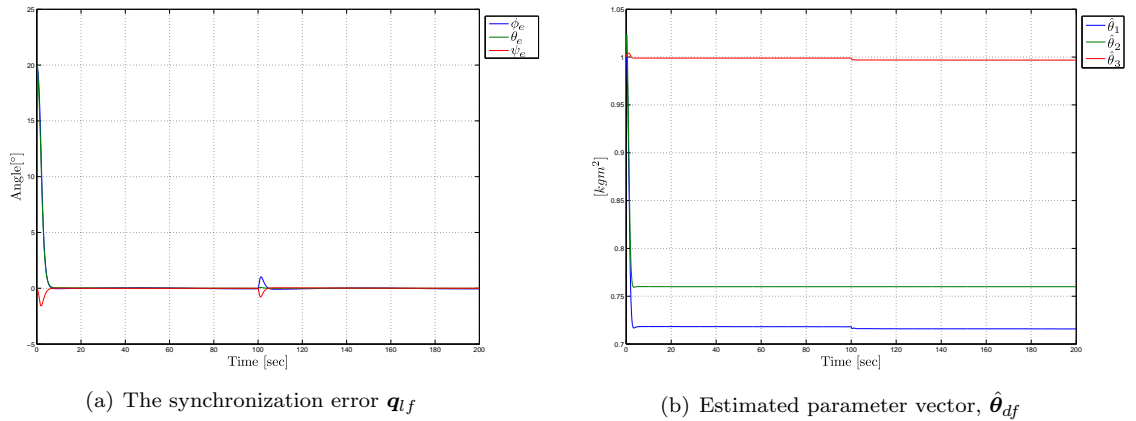


**Figure 7.16:** Simulation of external synchronization control law (6.48), with feedback from estimated states. The plots show the synchronization error and the estimated parameter vector.

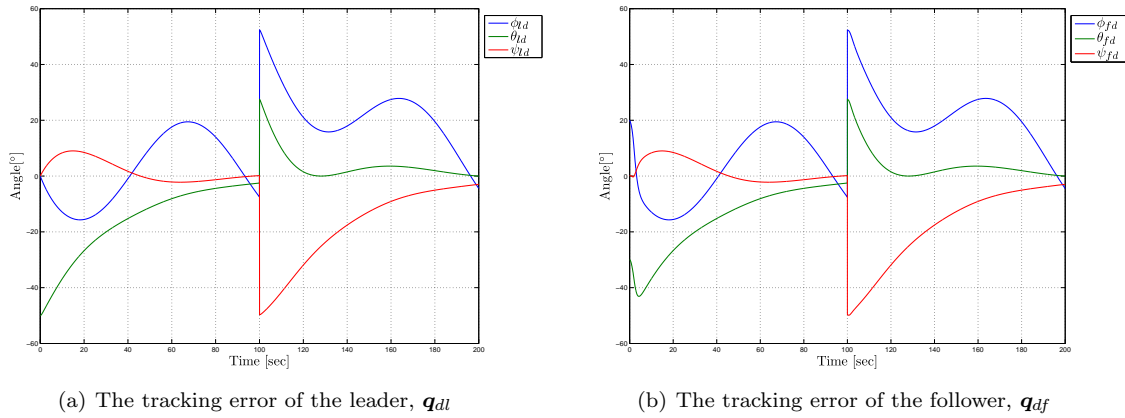


**Figure 7.17:** Simulation of external synchronization control law (6.48), with feedback from estimated states. The plots show the tracking errors.

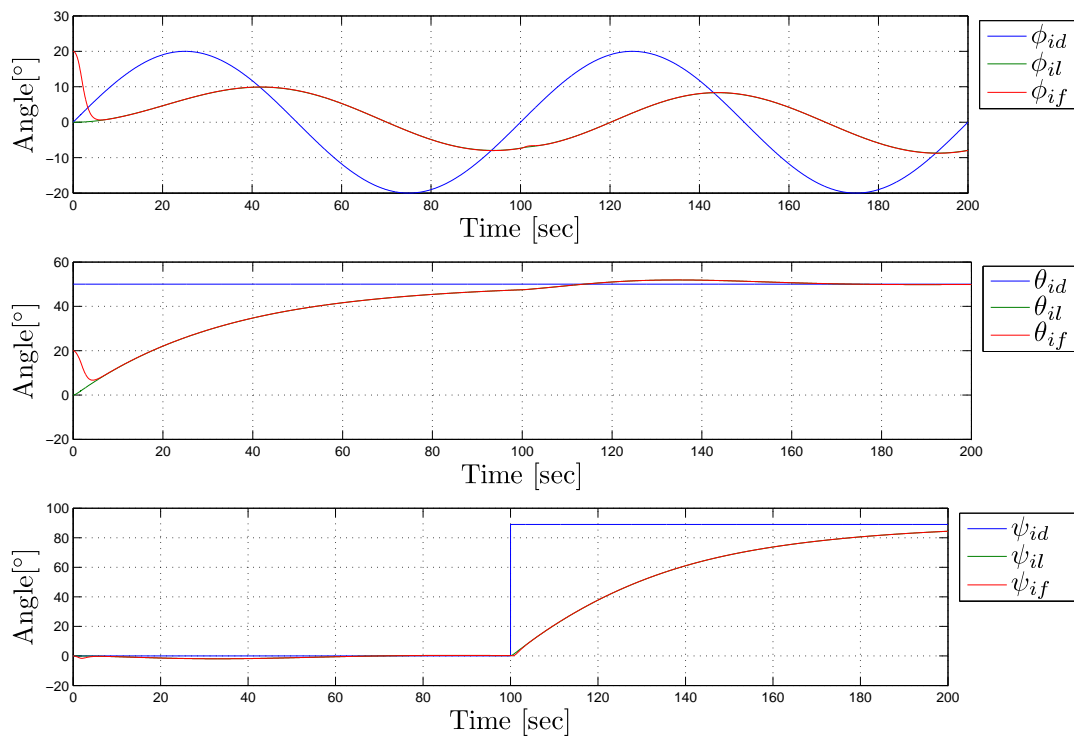
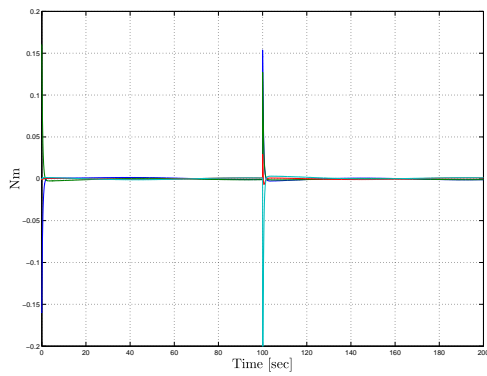
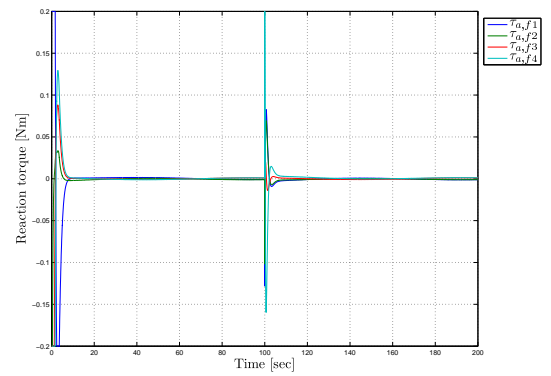


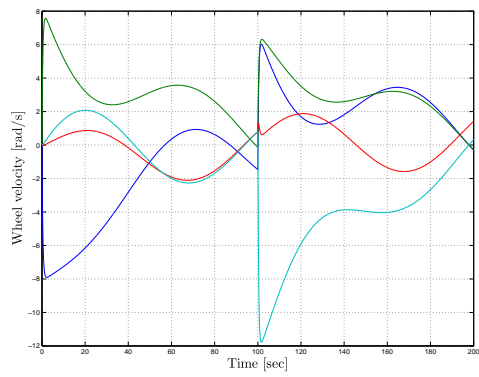
**Figure 7.18:** Simulation of external synchronization control law (6.48), with feedback from estimated states. The plots show the trajectories of the leader and follower vs. the desired.



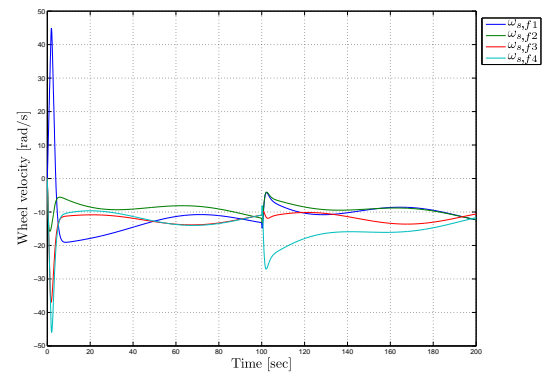
(a) Reaction wheel torque,  $\tau_{a,l}$



(b) Reaction wheel torque,  $\tau_{a,f}$



(c) Wheel velocity,  $\omega_{a,l}$



(d) Wheel velocity,  $\omega_{a,f}$

**Figure 7.19:** Simulation of external synchronization control law (6.48), with feedback from estimated states. The plots show input torque and wheel velocity of both satellites.

### 7.4.2 With estimated state variables, measurement noise and environmental noise

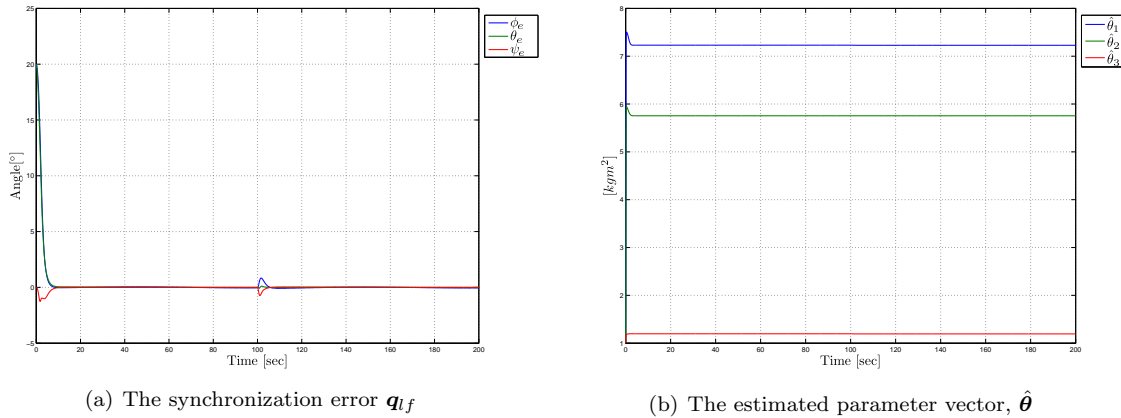


**Figure 7.20:** Simulation of external synchronization control law (6.48), with feedback from estimated states. The plots show the synchronization error and estimated parameter vector.

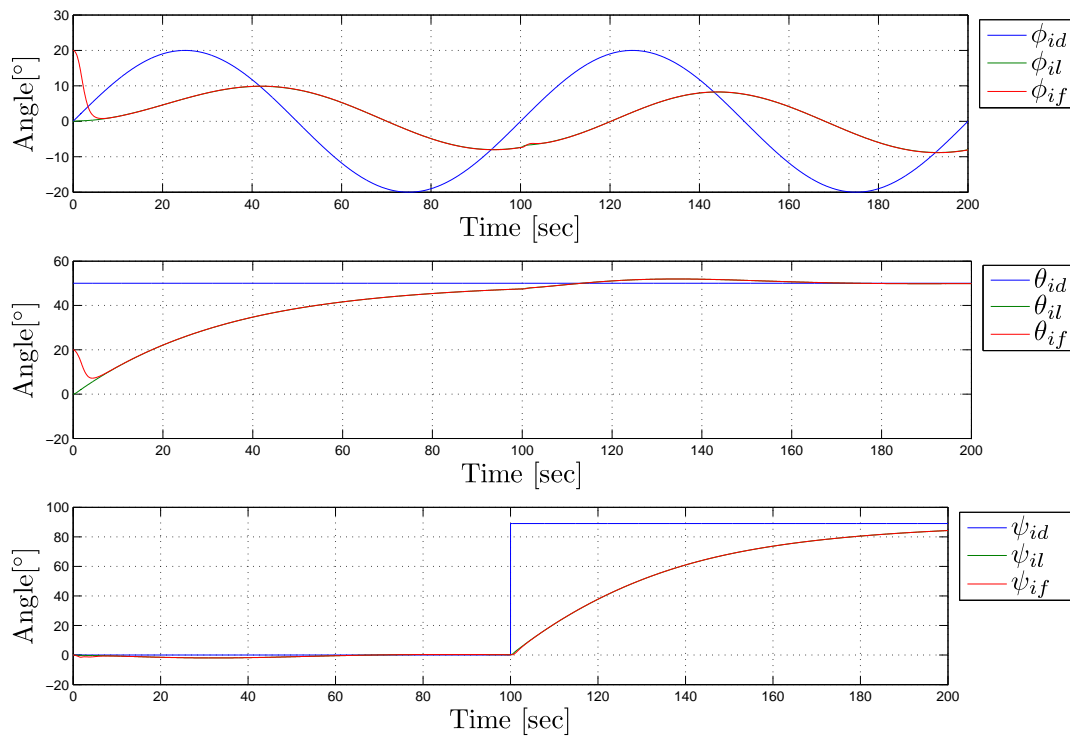


**Figure 7.21:** Simulation of external synchronization control law (6.48), with feedback from estimated states. The plots show the trajectories of the leader and follower vs. the desired.

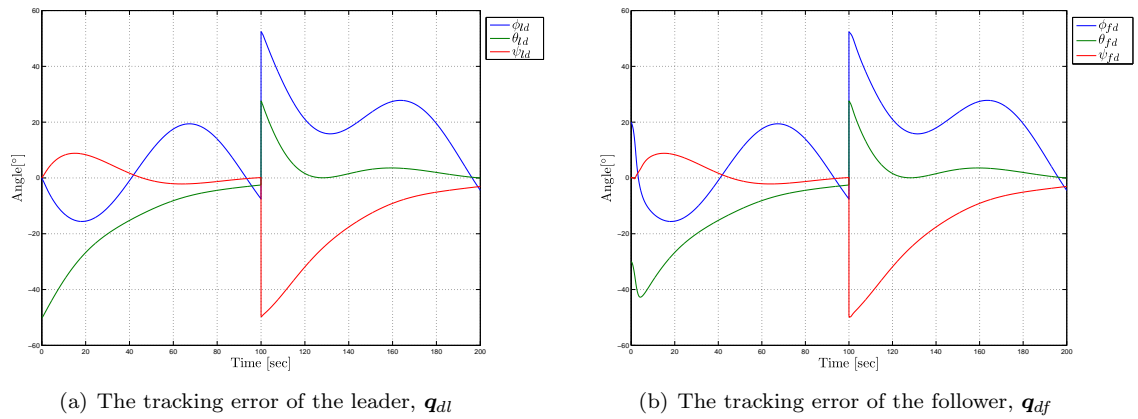


**Figure 7.22:** Simulation of external synchronization control law (6.48), with feedback from estimated states. The plots show the tracking errors.

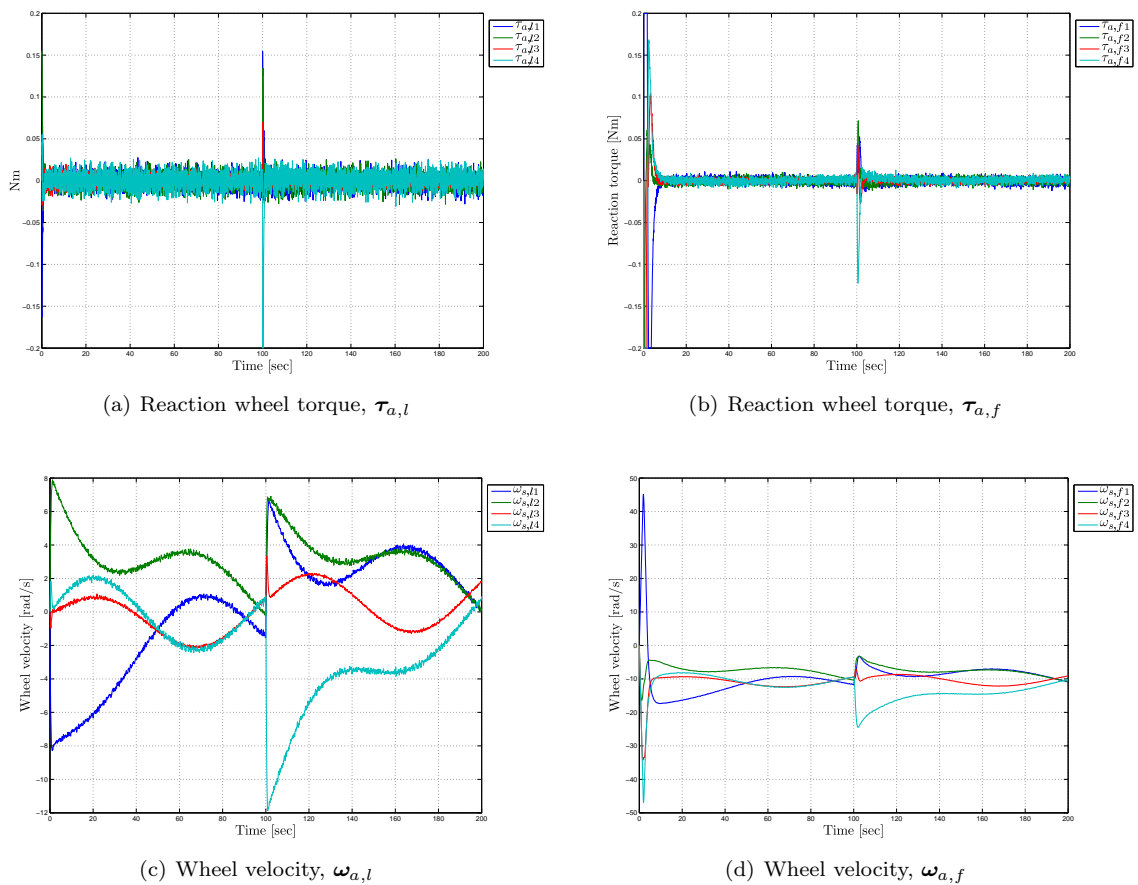


**Figure 7.23:** Simulation of external synchronization control law (6.48), with feedback from estimated states. The plots show input torque and wheel velocity of both satellites.

## 7.5 Mutual synchronization

The mutual synchronization scheme, (6.120), is simulated with feedback from actual variables. Figure 7.24, visualize how the satellites synchronize with each other mutually, while they at the same time converge to the desired trajectory. When implementing the controller (6.120), we create an algebraic loop, since the controller which governs the acceleration of the leader is a function of the acceleration. This was solved in the same way as in Rodriguez-Angeles (2002), by instead simulating the system

$$\begin{bmatrix} \ddot{\Psi}_l \\ \ddot{\Psi}_f \end{bmatrix} = M_c(K_{lf})^{-1} \begin{bmatrix} \ddot{\Psi}_d - M_l^*(\Psi_l)^{-1}(C(\Psi_l, \dot{\Psi}_l)\dot{s}_l + K_{d,l}\dot{s}_l + K_{p,l}s_l) \\ \ddot{\Psi}_d - M_f^*(\Psi_f)^{-1}(C(\Psi_f, \dot{\Psi}_f)\dot{s}_f + K_{d,f}\dot{s}_f + K_{p,f}s_f) \end{bmatrix}. \quad (7.1)$$

where  $M_c(K_{lf})$  is defined in (6.136).

Parameter	Value
Initial leader satellite attitude	$\Psi_{ib} = [10, 0, 21]^T [^\circ]$
Initial leader satellite angular velocity	$\omega_{ib}^b = [0, 0, 0] [rad/s]$
Initial follower attitude	$\hat{\Psi}_{ib} = [-20, 10, 35]^T [^\circ]$
Initial follower angular velocity	$\hat{\omega}_{ib}^b = [0, 0, 0] [rad/s]$
Desired trajectory	$\Psi_d = \begin{bmatrix} 20 \sin(\frac{2\pi}{200}) \\ 20 \sin(\frac{2\pi}{200}) \\ 20 \sin(\frac{2\pi}{200}) \end{bmatrix} [^\circ] \text{ at } t = 0s$

**Table 7.7:** Simulation initial conditions and desired states, adaptive synchronizing controller.

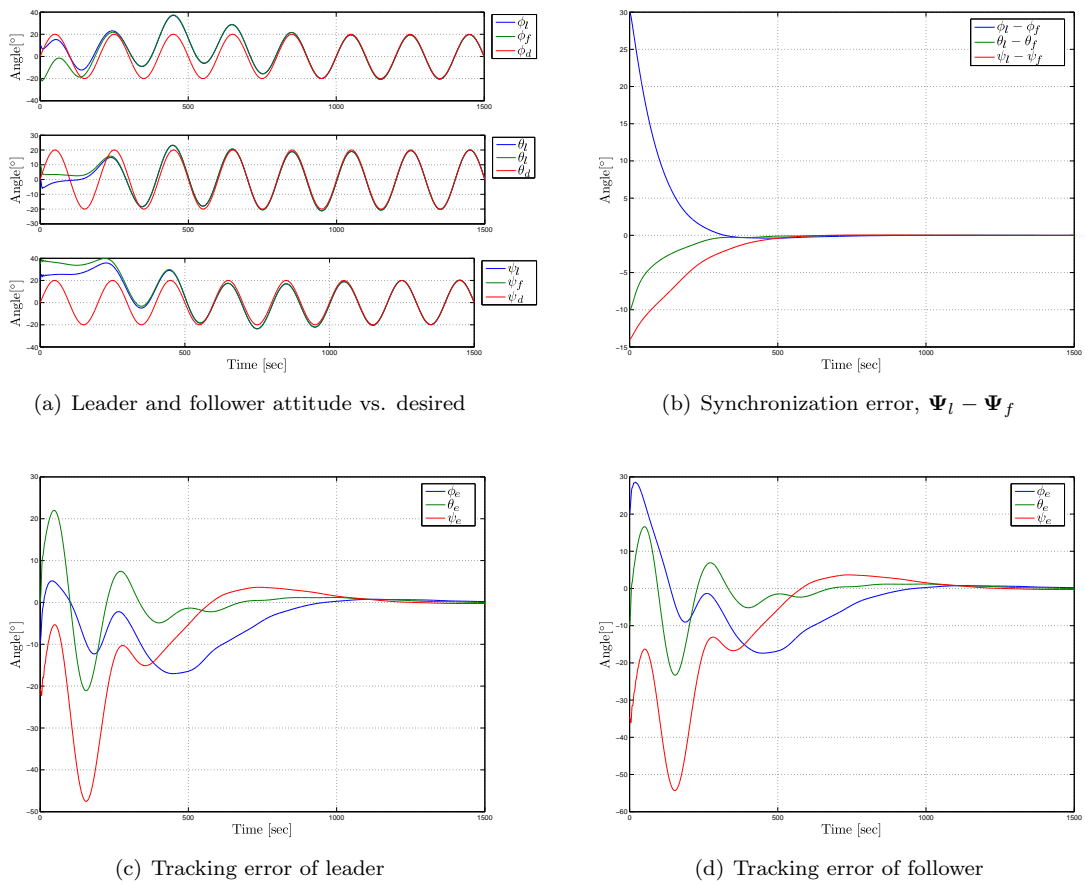


**Figure 7.24:** Simulation of external synchronization control law (6.48), with feedback from actual states. The plots show tracking capabilities and synchronization capabilities.

## 7.6 Momentum dumping scheme

The momentum dumping scheme is simulated during momentum dumping using the procedure given in section 6.4. In the simulation the satellite is first stabilized to a desired constant attitude  $\Psi_{od} = [30, 0, 0]^T$  in  $\mathcal{F}_o$ , then the wheel momentum is dumped. It is clear from figure 7.25(c), that the satellite keeps its attitude throughout the dumping apart from a minor transient of less than  $0.1^\circ$ . From the figures 7.25(a) and 7.25(b), it is clear that the both the total wheel momentum *and* the wheel speeds are reduced.

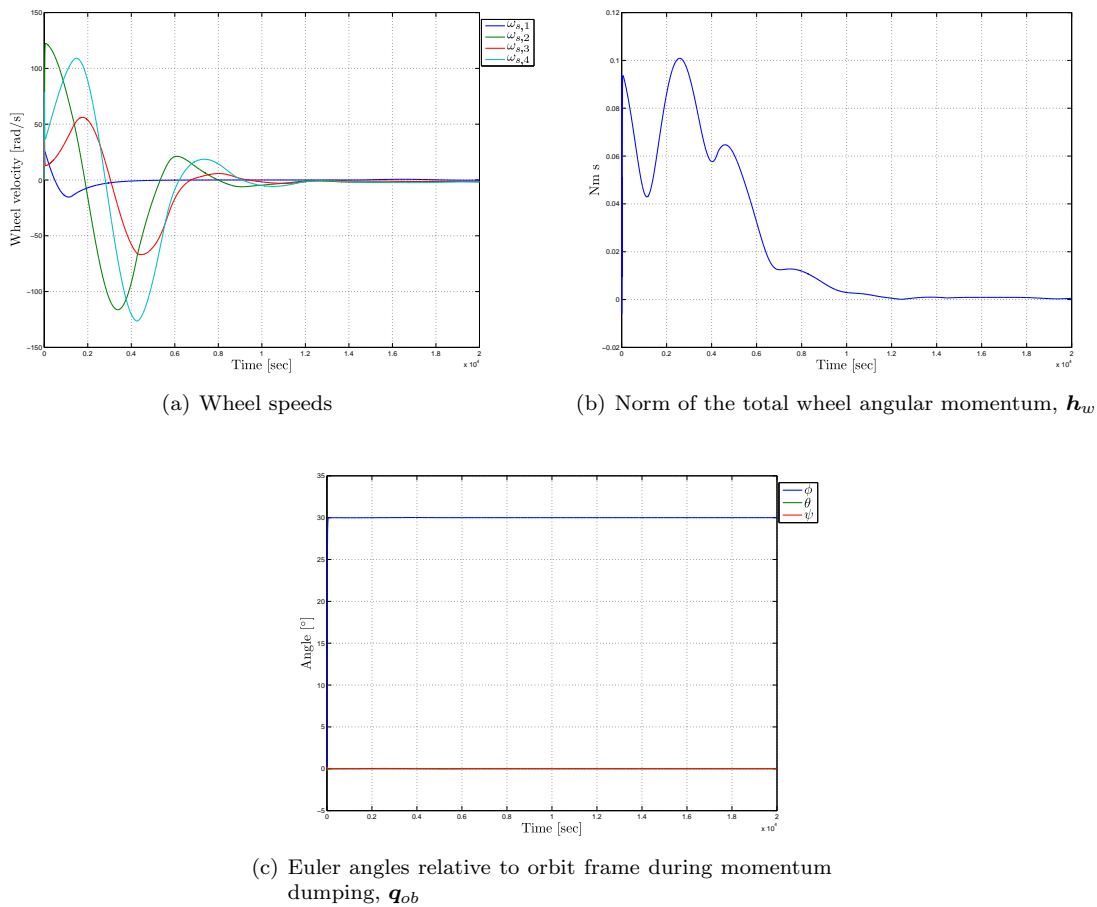


**Figure 7.25:** Simulation of momentum dumping scheme

## 7.7 Summary

In this chapter we have simulated the controllers to substantiate the proofs presented earlier, and to evaluate their robustness properties. It was observed that all controllers gave asymptotical convergence of the synchronization error-variables, such that the leader and follower satellite were able to keep a constant relative attitude. They seemed also to be robust to bounded disturbances, which was suggested based on the uniform stability.

The two synchronizing controllers, both ensured synchronization of the attitude. The difference is that in the mutual case we have more freedom when tuning performance either for tracking or synchronization. This freedom, comes at the price of a more involved tuning procedure.

---

It was also seen that when using the momentum dumping scheme, we were able to keep a desired set-point with very small transients. This indicates that the satellites are able to stay synchronized, when applying the presented momentum dumping procedure.



# Chapter 8

## Concluding Remarks

### 8.1 Conclusions

In this thesis the coordinated attitude control of satellites in clusters has been studied. Using methods from nonlinear systems theory, several control schemes have been explored both theoretically and in simulations. We have also proposed observers and have suggested means which should show uniform global asymptotic stability of the overall system. In addition a literature study on coordinated attitude control of satellites during formation flying have been presented, along with the theory of synchronization of mechanical systems.

Two control schemes for coordinating the attitude of the satellites were proposed, both originating from the synchronization of mechanical systems, referred to as external and mutual synchronization. In these schemes satellites in a formation are defined as leaders and followers. In the external synchronization control scheme, the leader is controlled independently by some stable control law. Three such control laws were proposed, and proved stable using Lyapunov analysis. Taking the states of the leader as the desired states of the follower, two external synchronizing control laws were proposed and analyzed. A nonlinear observer was also proposed, and proved UGAS of the estimation error.

The second synchronization scheme, mutual synchronization, was derived using Euler angles and was proved to be ULAS. The local result is due to a singularity when using Euler angles.

A momentum dumping scheme, enabling the satellite to keep its attitude while desaturating the wheels, was proposed and demonstrated in simulations while performing set-point control.

The closed-loop systems were simulated to evaluate performance. The results were satisfying showing asymptotic convergence also when introducing feedback from estimated states. When including measurement noise and environmental disturbances, the satellite still showed asymptotic convergence, but now to a ball about the origin, indicating robustness to bounded disturbances.

### 8.2 Recommendations

- It is recommended that further work is performed in developing a mutual synchronization scheme based on quaternion feedback. This would enhance robustness and it would be possible to obtain global results.
- It would be interesting to get a more accurate model for the environmental disturbances, especially as a function of spacecraft states. Such that, in example, the drag torque is larger when the solar panel are facing in the speed direction and so on.
- More work could be put into researching how to optimize the simulation models for speed, as the simulation models obtained through this work are quite slow when simulating the full formation.
- Extending the controllers derived in this thesis to the relative position case, would be useful for the sake of completeness.

- A model test of the controllers, either on submerged models or gyroscopic models to verify simulations and theory should prove useful.
- Further investigations should be put into stability of the interconnected observer-controller structure.

# Bibliography

- Arduni, C. & Baiocco, P. (1997), 'Active magnetic damping attitude control for gravity gradient stabilized spacecraft', *Journal of Guidance, Control and Dynamics* **20**(1), pp. 117–122.
- Balch, T. & Arkin, R. (1998), 'Behavior-based formation control for multirobot teams', *IEEE Transactions on Robotics and Automation* **14**(6).
- Beard, R. (1998), Architecture and algorithms for constellation control, Technical report, Jet Propulsion Laboratory, California Institute of Technology, 4800 Oak Grove Dr., Pasadena, CA 91109. Available online [[http://www.ee.byu.edu/grad1/users/beard/www\\_docs/research\\_formation.html](http://www.ee.byu.edu/grad1/users/beard/www_docs/research_formation.html)].
- Beard, R. & Hadaegh, F. Y. (1998), Constellation templates: An approach to autonomous formation flight, in 'World Automation Congress', ISIAC, Anchorage, Alaska, pp. pp. 177.1 – 177.6.
- Beard, R., Lawton, J. & Hadaegh, F. (2001), 'A coordination architecture for formation control', *IEEE Transactions on Control Systems Technology* **9**, pp. 777–790.
- Beichman, C., Woolf, N. & Lindensmith, C. (1998), *Terrestrial Planet Finder - Origins of Stars, Planets and Life*, National Aeronautics and Space Administration.
- Bondhus, A. K., Pettersen, K. & Gravdahl, J. (2005), Leader/follower synchronization of satellite attitude without angular velocity measurements, in 'Proceedings of the 44th IEEE Conf. on Decision and Control'. Submitted.
- Bondhus, A., Pettersen, K. & Nijmeijer, H. (2004), Master-slave synchronization of robot manipulators, in 'Proc. 2004 IFAC Symposium on Nonlinear Control Systems Design', Stuttgart, Germany.
- Bryson, A. E. (1994), *Control of Spacecraft and Aircraft*, Princeton University Press.
- Chobotov, V. (1991), *Spacecraft Attitude Dynamics and Control*, Krieger Publishing Company.
- Danbury, R. & Jenkinson, M. (1994), 'Synchronized servomechanisms - the scalar-field approach', *IEE Proceedings Control Theory and Applications* **141**(4), 261–273.
- Egeland, O. & Godhavn, J.-M. (1994), 'Passivity-based adaptive attitude control of a rigid spacecraft', *IEEE Transactions of Automatic Control* **39**(4), pp. 842 – 846.
- Egeland, O. & Gravdahl, J. T. (2001), *Modeling and Simulation for Automatic Control*, Marine Cybernetics.
- Fjellstad, O.-E. (1994), Control of unmanned underwater vehicles in six degrees of freedom, PhD thesis, Norwegian University of Science and Technology.
- Fossen, T. (2002), *Marine Control Systems: Guidance, Navigation, and Control of Ships, Rigs and Underwater Vehicles*, Marine Cybernetics.
- Freedman, R. & Kaufmann III, W. (2002), *Universe*, sixth edition edn, Freeman.

- Fridlund, C. (2004), 'The darwin mission', *Advances in Space Research* **34**, 613–617.
- Hegrenæs, O. (2004), Attitude control by means of explicit model predictive control, via multi-parametric quadratic programming, Master's thesis, Norwegian University of Science and Technology.
- Hughes, P. C. (1986), *Spacecraft attitude dynamics*, John Wiley & Sons.
- Huygens, C. (1673), *Horologium Oscilatorium*, Paris, France.
- International Association of Geomagnetism and Aeronomy (2005), 'International geomagnetic reference field, 10th generation', ONLINE [<http://www.ngdc.noaa.gov/IAGA/vmod/igrf.html>]. [last accessed 02.05.2005].
- Kang, W. & Yeh, H. (2002), 'Co-ordinated attitude control of multi-satellite systems', *International Journal of Robust and Nonlinear Control* **12**, 185–205.
- Khalil, H. (2000), *Nonlinear Systems*, 3 edn, Prentice Hall.
- Krogstad, T. (2004), 'Stability analysis of satellites in earth and moon orbits'. MSc. Project work.
- Krogstad, T., Gravdahl, J. & Tøndel, P. (2005), Explicit model predictive control of a satellite with magnetic torquers, in 'proceedings of the 13th Mediterranean Conference on Control and Automation, Limassol, Cyprus'.
- Kyrkjebø, E. (2000), Satellite attitude determination, Master's thesis, Department of Engineering Cybernetics, Norwegian University of Science and Technology.
- Kyrkjebø, E. & Pettersen, K. (2003), Ship replenishment using synchronization control, in 'Proc. 6th Conference on Manoeuvring and Control of Marine Crafts'.
- Lamnabhi-Lagarrigue, F., Loria, A. & Panteley, E. (2004), Advanced topics in control systems theory: Lecture notes from fap 2004. [Unpublished lecture notes].
- Lawton, J. (2000), A Behavior-Based Approach to Multiple Spacecraft Formation Flying, PhD thesis, Brigham Young University, Dept. of El. and Comp. Engineering.
- Lewis, M. & Tan, K. (1997), 'High precision formation control of mobile robots using virtual structures', *Autonomous Robots* **4**, pp. 387–403.
- Loria, A. (2004), Cascaded nonlinear time-varying systems: analysis and design. [Unpublished lecture notes, Available online:<http://www.lss.supelec.fr/perso/loria/Teaching/lecture-notes-cascades.pdf>]. [Last accessed: May 27th 2005].
- Loria, A., Fossen, T. & Panteley, E. (2000), 'A separation principle for dynamic positioning of ships: Theoretical and experimental results', *IEEE Transactions on Control System Technology* **8**(2), pp. 332–343.
- Loria, A., Panteley, E., Popovic, D. & Teel, A. (2002), An extension of matrosov's theorem with application to stabilization of nonholonomic control systems, in 'Proceedings of the 41st IEEE Conference on Decision and Control', Vol. 2, pp. pp. 1528–1533.
- Lovera, M. & Astolfi, A. (2004), 'Spacecraft attitude control using magnetic actuators', *Automatica* **20**, pp. 1405–1414.
- Mali, A. D. (2002), 'On the behavior-based architectures of autonomous agency', *IEEE Transactions on Systems, Man and Cybernetics, Part C: Applications and Reviews* **32**(3).
- Mataric, M. (1992), Minimizing complexity in controlling a mobile robot population, in '1992 IEEE Int. Conf. on Robotics and Automation Proceedings', Vol. 1, pp. 830–835.

- Nicosia, S. & Tomei, P. (1992), 'Nonlinear observer and output feedback attitude control of spacecraft', *IEEE Transactions on Aerospace and Electronic Systems* **28**, pp. 973–977.
- Nijmeijer, H., Blekhman, I., Fradkov, A. & Pogromsky, A. (1997), 'Self-synchronization and controlled synchronization', *Proceedings of 1st International Conference on Control of Oscillations and Chaos* **1**, 36–41.
- Nijmeijer, H. & Fossen, T., eds (1999), *New Directions in Nonlinear Observer Design*, Springer Verlag.
- Nijmeijer, H. & Rodriguez-Angeles, A. (2003), *Synchronization of Mechanical Systems*, World Scientific.
- Paden, B. & Panja, R. (1988), 'Globally asymptotically stable 'pd+' controller for robot manipulators', *International Journal of Control* pp. 1697–1712.
- Pan, H. & Kapila, V. (2001), Adaptive nonlinear control for spacecraft formation flying with coupled translational and attitude dynamics, in 'Proceedings of the 40th IEEE Conference on Decision and Control'.
- Panteley, E. & Loria, A. (1998), 'On global uniform asymptotic stability of nonlinear time-varying systems in cascade', *Systems & Control Letters* **33**, pp. 131–138.
- Rayleigh, J. (1945), *Theory of Sound*, Dover, New York.
- Ren, W. & Beard, R. (2004), Formation feedback control for multiple spacecraft via virtual structures, in '2004 IEEE Proceedings of Control Theory Application'.
- Robertsson, A. (1999), On Observer-Based Control of Nonlinear Systems, PhD thesis, Lund Institute of Technology.
- Rodriguez-Angeles, A. (2002), Synchronization of Mechanical Systems, PhD thesis, Technische Universiteit Eindhoven.
- Salcudean, S. (1991), 'A globally convergent angular velocity observer for rigid body motion', *IEEE Transactions on Automatic Control* **36**(12), pp. 1493–1497.
- Sciavicchio, L. & Siciliano, B. (2000), *Modelling and Control of Robot Manipulators*, second edition edn, Springer-Verlag.
- Sidi, M. J. (1997), *Spacecraft Dynamics & Control: A Practical Engineering Approach*, Cambridge.
- Singh, S. & Yim, W. (1995), Dynamic feedback linearization and large pitch attitude control of satellite using solar radiation pressure, in 'Proceedings of the 1995 American Control Conference', Vol. 5, American Control Conference 1995, pp. 3131–3135.
- Singh, S. & Yim, W. (1996), 'Feedback linearization and solar pressure satellite attitude control', *IEEE Transactions on Aerospace and Electronic Systems* **32**(2), 732–742.
- Singh, S. & Yim, W. (2002), Nonlinear adaptive backstepping design for spacecraft attitude control using solar radiation pressure, in 'Proceedings of the 41st IEEE Conference on Decision and Control', Vol. 2, pp. 1239–1244.
- Slotine, J.-J. E. & Li, W. (1991), *Applied Nonlinear Control*, Prentice Hall.
- Sun, D. & Mills, J. (2002), Adaptive synchronized control for coordination of two robot manipulators, in 'Proceedings of the 2002 IEEE Int. Conference on Robotics & Automation', Washington, DC, USA.
- Sunde, B. O. (2005), Satellite attitude determination, Master's thesis, Department of Engineering Cybernetics, Norwegian University of Science and Technology.

- Tipler, P. (1999), *Physics for Scientists and Engineers*, W.H. Freeman and company and Worth Publishers.
- Vallado, D. A. (2001), *Fundamentals of Astrodynamics and Applications*, Kluwer Academic Publishers.
- Venkatachalam, R. (1993), 'Large angle pitch attitude maneuver of a satellite using solar radiation power', *IEEE Transactions on Aerospace and Electronic Systems* (4), 1164–1169.
- Vidyasagar, M. (1993), *Nonlinear Systems Analysis*, Prentice Hall.
- Wallace, R., Ayon, J. & Sprague, G. (2000), Interstellar probe mission/system concept, in '2000 IEEE Aerospace Conference Proceedings', Vol. 7.
- Wang, P., Hadaegh, F. & Lau, K. (1999), 'Synchronized formation rotation and attitude control of multiple free-flying spacecraft', *Journal of Guidance, Control and Dynamics* pp. 28–35.
- Wang, P., Hadaegh, F. & Mokuno, M. (2003), Formation flying of multiple spacecraft with automatic rendezvous and docking capability, in '2003 AIAA Guidance, Navigation and Control Conference and Exhibit Proceedings'.
- Wen, T.-Y. J. & Kreutz-Delgado, K. (1991), 'The attitude control problem', *IEEE Transactions on Automatic Control* **36**(10), pp. 1148–1162.
- Wisniewski, R. (2000), Lecture notes on modeling of a spacecraft. [Available on-line: [www.control.auc.dk/raf/ModellingOfMech/Rep8sem.ps](http://www.control.auc.dk/raf/ModellingOfMech/Rep8sem.ps), Last accessed: 05.06.2005].

# Appendix A

## Model Parameters

### A.1 Robot manipulator parameters

Parameter	Value
$a_1$	1
$a_2$	1
$l_1$	0.5
$l_2$	0.5
$m_{l1}$	50
$m_{l2}$	50
$I_{l1}$	10
$I_{l2}$	10
$k_{r1}$	100
$k_{r2}$	100
$m_{m1}$	5
$m_{m2}$	5
$I_{m1}$	0.01
$I_{m2}$	0.01
$g$	9.81

Table A.1: Parameters for the robot manipulators

### A.2 Satellite data

Data type	Value
Wheel diameter	20 cm
Max reaction torque	0.2 Nm
Axial moment of inertia	$6.5 \times 10^{-3} \text{ kgm}^2$

Table A.2: Relevant data for the reaction wheel assembly DRALLRAD by TELDIX-Bosch Telecom

---

Data type	Value
Inertia matrix	$\text{diag}(4,4,3) \text{ kgm}^2$
Max magnetic moment	$20 \text{ Am}^2$

**Table A.3:** Relevant data for the simulated satellite

# Appendix B

## CD contents

### B.1 Other

- PDF version of this report
- Powerpoint presentation for STEC 2005

### B.2 Matlab source files and Simulink diagrams

In this appendix an index of the different matlab source files are given with a short description and their location on the included CD.

#### B.2.1 Robotic-manipulator example files

Filename	Description	Location
<code>main_robman.m</code>	The main file for running the simulation of the two-link manipulator using external synchronization scheme	<code>\Matlab\robot\main_robman.m</code>
<code>robman.m</code>	The model file used in the ode45 integration command	<code>\Matlab\robot\robman.m</code>
<code>main_robman_mut.m</code>	The main file for running the simulation of the two-link manipulator using mutual synchronization scheme	<code>\Matlab\robot\main_robman_mut.m</code>
<code>robman_mut.m</code>	The model file used in the ode45 integration command	<code>\Matlab\robot\robman_mut.m</code>

**Table B.1:** Matlab files for the robotic-manipulator example

## B.2.2 Mutual matlab files

Matlab scripts used in most simulations.

Filename	Description	Location
euler2q.m	Converts Euler angles to unit quaternions	\Matlab\euler2q.m
q2euler.m	Converts unit quaternions to Euler angles	\Matlab\q2euler.m
sgn.m	Return the sign of the variable	\Matlab\sgn.m
Rquat.m	Return the rotation matrix corresponding to the given unit quaternion	\Matlab\Rquat.m
skew.m	Returns the skew symmetric operator	\Matlab\skew.m

## B.2.3 Simulink simulation files

The following Simulink diagrams are used for closed-loop simulations of the controllers, observers and momentum dumping scheme.

Filename	Description	Location
leaderctrl_setfi.mdl	Simulate the leader set-point controller in $\mathcal{F}_i$	Matlab\lctrl\set point fi
leaderctrl_setfo.mdl	Simulate the leader set-point controller in $\mathcal{F}_o$	Matlab\lctrl\Set point Fo
leaderctrl.mdl	Simulate the leader tracking controller in $\mathcal{F}_i$	Matlab\lctrl\Tracking i frame
observer.mdl	Observer simulation	Matlab\Observer
synchron_lyap.mdl	Simulation of the Lyapunov-based synchronizing controller	Matlab\Synchronizing Lyap
synchron_adap.mdl	Simulation of the adaptive synchronizing controller	Matlab\Synchadap

## B.2.4 Mutual synchronization files

The following files were used to simulate the mutual synchronization scheme.

Filename	Description	Location
mutualsynch_main.m	Sets initial conditions, runs integration and plot the result	Matlab\Mutual synch
mutualsynch.m	Contains dynamic equations	Matlab\Mutual synch

## Appendix C

# Accepted Papers, Posters and Presentation

- C.1 Paper accepted for the proceedings of 13th Mediterranean Conference on Control and Automation

# Explicit Model Predictive Control of a Satellite with Magnetic Torquers

Thomas R. Krogstad   Jan Tommy Gravdahl   Petter Tøndel

Department of Engineering Cybernetics,  
Norwegian University of Science and Technology  
7491 Trondheim, Norway  
{thomakro, tommy.gravdahl, petter.tondel} @itk.ntnu.no

**Abstract**—In this paper we present the design of a linear constrained MPC controller for magnetic actuated small satellites. The controller may be derived by formulating a linear constrained MPC problem as a multi-parametric quadratic program (mpQP). The solution will be a piecewise affine (PWA) function, which may be evaluated at each sample to obtain the optimal control law. We apply this approach to the design of an explicit model predictive controller (eMPC) for the Norwegian student satellite nCube.

## I. INTRODUCTION

The purpose of this paper is to derive an attitude controller for a small satellite actuated by means of magnetic coils. This is an area of research that has attracted much attention internationally. Noticeable contributions are [2] and [11], where nonlinear controllers have been proposed, a recent survey can be found in [16].

In order to handle the constraints on the available current and power, and limited computational power, we propose in this paper to solve the problem using an explicit model predictive control scheme. In [16] a MPC was proposed for magnetically controlled spacecraft, but to the best knowledge of the authors, the eMPC approach has not previously been applied to this problem. However, it has recently been used in [1] for a satellite actuated by means of thrusters and a reaction wheel. The eMPC approach retains MPC's ability to handle constraints, and in addition requires a small amount of online computational power. This property is obtained as the controller computation is solved off-line, requiring only fixed-point arithmetics online, making it possible to realize the controller i embedded hardware.

For comparison in the simulations, we have implemented two nonlinear controllers [2] based on feedback from the angular velocity and attitude measurements, along with a measurement of the local magnetic field.

An outline of a stability proof using piecewise quadratic Lyapunov functions is proposed. This will however only show stability for each linearized model.

The results in this paper are based on the work in [3], where further details may be found.

### A. Explicit Model Predictive Control

Model Predictive Control or MPC, involves solving a finite horizon optimal control problem at every time step.

The solution of this optimization problem is a series of control inputs for the whole horizon, giving an open loop controller. The control action computed for the first time-step is then applied to the plant, the horizon is shifted forward one time-step and the process is repeated, with the current state as initial values. In this manner MPC becomes a closed loop approach. Due to the shifting of the horizon this is also referred to as *Receding Horizon Control* or RHC. In this paper we will consider the linearized system

$$\begin{aligned}\mathbf{x}_{k+1} &= \mathbf{A}\mathbf{x}_k + \mathbf{B}\mathbf{u}_k \\ \mathbf{y}_k &= \mathbf{C}\mathbf{x}_k,\end{aligned}\tag{1}$$

when designing the controller. Where  $\mathbf{x}_k \in \mathbb{R}^n$  are the state variables,  $\mathbf{u}_k \in \mathbb{R}^m$  are the input variables,  $\mathbf{A} \in \mathbb{R}^{n \times n}$ ,  $\mathbf{B} \in \mathbb{R}^{n \times m}$ , and  $(\mathbf{A}, \mathbf{B})$  is a stabilizable pair. In addition we may have hard constraints on both the states and inputs

$$\mathbf{x}_k \in \mathbb{X}\tag{2}$$

$$\mathbf{u}_k \in \mathbb{U},\tag{3}$$

where  $\mathbb{X}$  is a convex closed subset of  $\mathbb{R}^n$  and  $\mathbb{U}$  is a convex compact subset of  $\mathbb{R}^m$ , both containing the origin in the interior. A terminal constraint may also be imposed for stability reasons,

$$\mathbf{x}_{k+N} \in X_f \subset \mathbb{X},\tag{4}$$

where  $N$  is the prediction horizon.

If we now consider the regulator problem, that is, the problem of driving the state vector to the origin, the traditional MPC solves the following convex optimization problem for the current  $\mathbf{x}_k$

$$\min_{\mathbf{U}, \mathbf{s}} [J(\mathbf{U}, \mathbf{x}(t)) + \rho \|\mathbf{s}\|_{\mathcal{L}_2}^2]\tag{5a}$$

$$\text{s.t. } \mathbf{y}_{\min} - \mathbf{s} \leq \mathbf{y}_{t+k|t} \leq \mathbf{y}_{\max} + \mathbf{s}, k = 1, \dots, N\tag{5b}$$

$$\mathbf{u}_{\min} \leq \mathbf{u}_{t+k} \leq \mathbf{u}_{\max}, k = 0, \dots, M-1\tag{5c}$$

$$\mathbf{u}_{t+k} = \mathbf{K}\mathbf{x}_{t+k|t}, M \leq k \leq N-1\tag{5d}$$

$$\mathbf{x}_{t|t} = \mathbf{x}(t)\tag{5e}$$

$$\mathbf{x}_{t+k+1|t} = \mathbf{A}\mathbf{x}_{t+k|t} + \mathbf{B}\mathbf{u}_{t+k}, k \geq 0\tag{5f}$$

$$\mathbf{y}_{t+k|t} = \mathbf{C}\mathbf{x}_{t+k|t}, k \geq 0,\tag{5g}$$

where  $J(\mathbf{U}, \mathbf{x}(t))$  is the quadratic cost function

$$J(\mathbf{U}, \mathbf{x}(t)) = \mathbf{x}_{t+N|t}^T \mathbf{P} \mathbf{x}_{t+N|t} + \sum_{k=0}^{N-1} \mathbf{x}_{t+k|t}^T \mathbf{Q} \mathbf{x}_{t+k|t} + \mathbf{u}_{t+k}^T \mathbf{R} \mathbf{u}_{t+k}, \quad (6)$$

$\|\mathbf{s}\|_{\mathcal{L}_2}$  is the  $\mathcal{L}_2$ -norm of the slack variables  $\mathbf{s}$ ,  $\rho$  is the penalty weight of the slack variables,  $\mathbf{U} \triangleq [\mathbf{u}(k)^T, \mathbf{u}(k+1)^T, \dots, \mathbf{u}(k+N-1)^T]^T$  is the vector of inputs at each sample time,  $\mathbf{s} \triangleq [\mathbf{s}^T(k), \dots, \mathbf{s}^T(k+N-1)]^T$  is the vector of slack variables,  $\mathbf{K}$  is the control gain matrix when the input is unconstrained,  $\mathbf{x}_{t+k|t}$  is the prediction of  $\mathbf{x}_{t+k}$  at time  $t$ , and  $N$  and  $M$  are the output and input constraint horizons respectively.  $\mathbf{P} \in \mathbb{R}^{n \times n}$ ,  $\mathbf{P} = \mathbf{P}^T \geq 0$ ,  $\mathbf{R} \in \mathbb{R}^{m \times m}$ ,  $\mathbf{R} = \mathbf{R}^T \geq 0$ ,  $\mathbf{Q} \in \mathbb{R}^{n \times n}$ ,  $\mathbf{Q} = \mathbf{Q}^T \geq 0$ . The final-state weight matrix  $\mathbf{P}$  is typically computed using the algebraic Riccati equation. The solution to (5) is now given as:  $\mathbf{U}^* = [\mathbf{u}^*(k)^T, \mathbf{u}^*(k+1)^T, \dots, \mathbf{u}^*(k+N-1)^T]^T$ ,  $\mathbf{s}^* = [\mathbf{s}^*(k)^T, \dots, \mathbf{s}^*(k+N-1)^T]^T$

In order to compute the explicit MPC controller, we need to formulate the linear MPC problem as an mpQP problem. The details of the derivation are given in [5], [6]. By some algebraic manipulation the problem may be reformulated as

$$V_z(\mathbf{x}) = \min_z \frac{1}{2} \mathbf{z}^T \mathbf{H} \mathbf{z} \quad (7)$$

$$\text{s.t. } \mathbf{G} \mathbf{z} \leq \mathbf{W} + \mathbf{S} \mathbf{x}(t), \quad (8)$$

where  $\mathbf{z} \triangleq \mathbf{U} + \mathbf{H}^{-1} \mathbf{F}^T \mathbf{x}(t)$ ,  $\mathbf{x}(t)$  is the current state, which can be treated as a vector of parameters to the optimization problem. Note that  $\mathbf{H} \succ 0$  since  $\mathbf{R} \succ 0$ . The number of inequalities is denoted by  $q$  and the number of free variables is  $n_z = m \cdot N$ . Then  $\mathbf{z} \in \mathbb{R}^{n_z}$ ,  $\mathbf{H} \in \mathbb{R}^{n_z \times n_z}$ ,  $\mathbf{G} \in \mathbb{R}^{q \times n_z}$ ,  $\mathbf{W} \in \mathbb{R}^{q \times 1}$ ,  $\mathbf{S} \in \mathbb{R}^{q \times n}$ ,  $\mathbf{F} \in \mathbb{R}^{n \times q}$ . The optimization problem (7)-(8) is now considered to be an mpQP, meaning that we seek a solution on explicit form, as a function of the parameter  $\mathbf{x}(t)$ .

The task is now to find the explicit solution of this mpQP problem,  $\mathbf{z}^* = \mathbf{z}^*(\mathbf{x}(t))$ , so that we may use the definition of  $\mathbf{z}$  to find the explicit controller  $\mathbf{U}^*$  as a function of the state vector. As shown in [6], this can be solved by applying the Karush-Kuhn-Tucker (KKT) conditions. Where the KKT-conditions are necessary and sufficient for an optimal solution for a convex quadratic problem [10].

The solution will then be a continuous PWA function, defined over a polyhedral partition of the parameter space. Which may be evaluated at each sample to obtain the control input

$$\mathbf{u}_k = \mathbf{K}_i \mathbf{x}_k + \mathbf{k}_i, \forall \mathbf{x}_k \in \mathcal{X}_i, \quad (9)$$

where  $\mathbf{K}_i$  is the gain-matrix for region  $i$ ,  $\mathbf{k}_i$  is a constant vector,  $\mathbf{x}_k$  the current state and  $\mathcal{X}_i$  is the  $i$ 'th region.

### B. Electromagnetic Actuators

Electromagnetic actuators are often chosen due to the independence of a limited fuel source, depending instead on power from solar arrays and batteries and thereby

prolonging the lifespan of the satellite. Electromagnetic actuators, often referred to as magnetic torquers, are based on two basic configurations. One is the coil based, where current is sent through a current loop which generates the magnetic moment proportional to the area of the coil and the number of windings. The other type is the magnetic rod, where wire is wound around a rod made of a high permeability material. Both variations interact with the local geomagnetic field, generating a torque vector in the direction perpendicular to the magnetic moment vector and the local field direction.

## II. MODELLING

In this section, the model of a satellite actuated by means of electromagnetic torquers will be derived. The notation is based on [7] and [8].

### A. Kinematics

We will describe the attitude kinematics in the form of Euler parameters, which may be defined from the angle-axis parameters  $\theta$  and  $\mathbf{k}$

$$\eta = \cos \frac{\theta}{2}, \quad \boldsymbol{\epsilon} = \mathbf{k} \sin \frac{\theta}{2}, \quad (10)$$

which gives the corresponding rotation matrix

$$\mathbf{R}(\eta, \boldsymbol{\epsilon}) = \mathbf{1} + 2\eta \boldsymbol{\epsilon}^\times + 2\boldsymbol{\epsilon}^\times \boldsymbol{\epsilon}^\times, \quad (11)$$

where  $\times$  denotes the vector cross product operator, and  $\boldsymbol{\epsilon}^\times$  is skew-symmetric. The choice of Euler parameters is motivated by their properties as a nonsingular representation.

From the properties of the rotation matrix, it can be shown that

$$\dot{\mathbf{R}}_o^b = (\boldsymbol{\omega}_{bo}^b)^\times \mathbf{R}_o^b = -(\boldsymbol{\omega}_{ob}^b)^\times \mathbf{R}_o^b, \quad (12)$$

where  $\boldsymbol{\omega}_{bo}^b$  is the angular velocity of the body frame  $\mathcal{F}_b$  with respect to the orbit frame  $\mathcal{F}_o$ , and  $\mathbf{R}_o^b$  is the rotation matrix between frames.  $\mathcal{F}_o$  has its origin in the satellites center of mass, its z-axis always pointing towards Earth (nadir direction), its y-axis is chosen in the direction of the negative orbit normal and finally the x-axis is chosen in order to complete a right-handed system.

Using (11) and (12) the kinematic differential equations

$$\dot{\eta} = -\frac{1}{2} \boldsymbol{\epsilon}^T \boldsymbol{\omega}_{ob}^b \quad (13a)$$

$$\dot{\boldsymbol{\epsilon}} = \frac{1}{2} [\eta \mathbf{I} + \boldsymbol{\epsilon}^\times] \boldsymbol{\omega}_{ob}^b, \quad (13b)$$

can be derived.

### B. Dynamics

Assuming that the satellite is a rigid body, with the body coordinate frame coinciding with the principal axes, we may write the attitude dynamics as [9]

$$\mathbf{I} \dot{\boldsymbol{\omega}}_{ib}^b + (\boldsymbol{\omega}_{ib}^b)^\times \mathbf{I} \boldsymbol{\omega}_{ib}^b = \boldsymbol{\tau}_e^b, \quad (14)$$

where  $\mathbf{I} = \text{diag}(i_{xx}, i_{yy}, i_{zz})$  is the inertia matrix,  $\boldsymbol{\omega}_{ib}^b$  is the body frame's angular velocity relative to the inertial frame  $\mathcal{F}_i$ , and  $\boldsymbol{\tau}_e^b$  is the external torque given in  $\mathcal{F}_b$ .



obtain the scaled model we first define the scaled variables and inputs  $\bar{\mathbf{x}} \triangleq \mathbf{N}_x^{-1}\mathbf{x}$  and  $\bar{\mathbf{u}} \triangleq \mathbf{N}_u^{-1}\mathbf{u}$ , where the scaling matrices are defined as

$$\mathbf{N}_x = \text{diag}([1 \ 1 \ 1 \ 10^{-3} \ 10^{-3} \ 10^{-3}]) \quad (21a)$$

$$\mathbf{N}_u = \text{diag}([0.1 \ 0.1 \ 0.1]). \quad (21b)$$

A scaled model may then be written

$$\begin{aligned} \dot{\bar{\mathbf{x}}} &= \mathbf{N}_x^{-1}\mathbf{A}\mathbf{N}_x\bar{\mathbf{x}} + \mathbf{N}_x^{-1}\mathbf{B}\mathbf{N}_u\bar{\mathbf{u}} \\ &= \bar{\mathbf{A}}\bar{\mathbf{x}} + \bar{\mathbf{B}}\bar{\mathbf{u}}. \end{aligned} \quad (22)$$

Using the scaled model, we discretize the system with a time-step  $T_s$  of 0.5 seconds, using the first order hold method.

TABLE I  
ALGORITHM PARAMETERS

Parameter	Value
$\mathbf{Q}$	$\text{diag}\{10, 100, 100, 10, 10, 10\}$
$\mathbf{R}$	$\text{diag}\{100000, 100000, 100000\}$
$N$ (Horizon)	10
$\rho$	1
Parameter space	$-[10, 10, 10, 1, 1, 1]^T \leq \mathbf{x} \leq [10, 10, 10, 1, 1, 1]^T$
Actuator constraints	$-1 \leq u_i \leq 1 \forall i \in \{1, 2, 3\}$

Using the parameters in Table I, we employ the mpQP algorithm. The solution is a polyhedral partitioning of the parameter space  $\mathbb{X}$ , into 21 regions, where for each region the optimal linear state-feedback control law is given by (9). The solution is thus 8 PWA controllers which are scheduled according to the measured sign of the magnetic field.

### B. Nonlinear controllers

To assess the performance of the eMPC controller, we have implemented two nonlinear controllers (23) and (24), which based on feedback from the angular velocity and attitude [2]:

$$\mathbf{m}^b = h\boldsymbol{\omega}_{ob}^b \times \mathbf{B}^b \quad (23)$$

$$\mathbf{m}^b = h\boldsymbol{\omega}_{ob}^b \times \mathbf{B}^b - \alpha\boldsymbol{\epsilon} \times \mathbf{B}^b, \quad (24)$$

where  $h > 0$  and  $\alpha > 0$  are constants.

### IV. STABILITY

Stability of the linearized system with eMPC control can be derived using a piecewise quadratic Lyapunov function, as suggested by [14], by defining the closed-loop system as a PWA system:

$$\mathbf{x}_{k+1} = \mathbf{A}_i\mathbf{x}_k + \mathbf{a}_i, \forall \mathbf{x}_k \in \mathcal{X}_i \quad (25)$$

where  $\mathbf{A}_i \in \mathbb{R}^{n \times n}$ ,  $\mathbf{a}_i \in \mathbb{R}^n$  and the state belongs to the set of states  $\mathbf{X} \subset \mathbb{R}^n$ . The set of cells  $\{\mathcal{X}_i\}_{i=1}^s$  represent a polyhedral partition of  $\mathbf{X}$ , i.e. each set  $\mathcal{X}_i$  is a (not necessarily closed) convex polyhedron such that the origin belongs to  $\mathbf{X}$ .

In [14]  $\mathcal{S}$ -PWQ stable with relaxations, is presented as the least conservative criterion:

$$\mathbf{P}_i - \bar{\mathbf{E}}_i^T \bar{\mathbf{U}}_i \bar{\mathbf{E}}_i > 0, \forall i \in \mathcal{I} \quad (26)$$

$$\bar{\mathbf{A}}_j^T \mathbf{P}_i \bar{\mathbf{A}}_j - \gamma \mathbf{P}_j + \bar{\mathbf{E}}_i^T \bar{\mathbf{Z}}_{ij} \bar{\mathbf{E}}_i < 0, \forall (i, j) \in \mathcal{S}, \quad (27)$$

where  $\mathcal{I}$  is the set of indices denoting the regions of the state-space, and  $\mathcal{S}$  denotes the set of ordered pairs  $(i, j)$  of possible transitions between regions. If we can find a feasible solution  $\mathbf{P}_i = \mathbf{P}_i^T, \bar{\mathbf{U}}_i$  and  $\bar{\mathbf{Z}}_{ij}$  for this LMI, the origin is *exponentially stable on  $\mathbb{X}_0$*  with a degree  $\gamma$ . We may now refer to the system as  *$\mathcal{S}$ -PWQ stable with relaxations*.

The stability of the satellite system is currently being investigated.

### V. SIMULATIONS

In this section we present simulations of the different controllers. The Norwegian student satellite is used as a case. Further information on this project can be found in [12] and [13]. The simulation parameters are summarized in Table II.

In the remainder the controller parameters for the nonlinear controllers are

$$\begin{aligned} h &= 2.25 \times 10^5 \\ \alpha &= 450. \end{aligned}$$

The controllers were tuned for best possible performance. The eMPC controller is derived using the parameters of Table I.

TABLE II  
SIMULATION PARAMETERS

Parameter	Value
Inertia matrix	$\text{diag}\{0.1043, 0.1020, 0.0031\}$ [kgm <sup>2</sup> ]
Maximal magnetic moment	0.1 [Am <sup>2</sup> ]
Desired Euler angles	[0 0 0] <sup>T</sup> [deg]
Desired angular velocity	[0 0 0] <sup>T</sup> [rad/s]
Pointing accuracy required	$\pm 10^\circ$ on roll and pitch
Orbit angular velocity - $\omega_o$	$1.083 \times 10^{-3}$ [rad/s]
Orbit period	5801.6 [sec]
Initial attitude	$\Phi = [20, 40, 60]^T$ [Deg]
Initial angular velocity	$\boldsymbol{\omega}_{ob}^b = [5, -3, 3]^T \times 10^{-3}$ [rad/s]

The model is simulated with the presence of noise on the inputs to simulate disturbance torques and on the measurements of the magnetic field. The magnetic field values is generated using an orbit propagator and the IGRF 2000 model of the Earth's magnetic field [15].

As can be seen from fig. 1 and 2, both the eMPC controller and the nonlinear controller 2, manages to steer the state to the required accuracy. However, the nonlinear controller 1 points the satellite in the negative nadir direction.

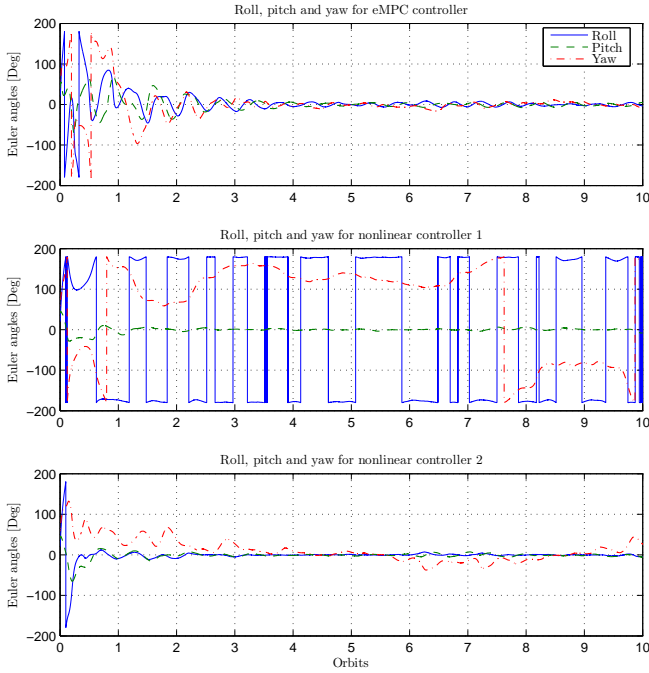


Fig. 1. The Euler angles

Fig. 4 and 3 shows that the energy consumption is clearly decreased in the case of the eMPC controller, and shows a lower peak in the power drawn from the power supply. An attempt was made to tune the nonlinear controller 2, through the variables  $h$  and  $\alpha$ , in order to minimize the energy consumption while keeping the desired accuracy. The consumption was decreased to about 8 J for 10 orbits, thus still higher than with eMPC control. On the other hand, the control law (24) results in the fastest convergence of the three controllers.

## VI. DISCUSSION

It is clear that although the proposed controller achieves the required accuracy in roll and pitch, the nonlinear controller with attitude feedback does outperform it, at the cost of higher energy consumption. In particular the transient response is faster, and a greater accuracy is maintained at steady-state.

Nonlinear model predictive control (NMPC) would probably outperform the proposed controller, but the computational requirements for NMPC makes this an infeasible solution for satellite control.

## VII. CONCLUSIONS

We have in this paper presented the design of an explicit model predictive controller and compared it to other possible control schemes. The results show a decrease in total energy consumption while still maintaining the desired accuracy. Hence it has been shown to be a highly attractive solution for satellite control, where energy consumption is of the greatest importance.

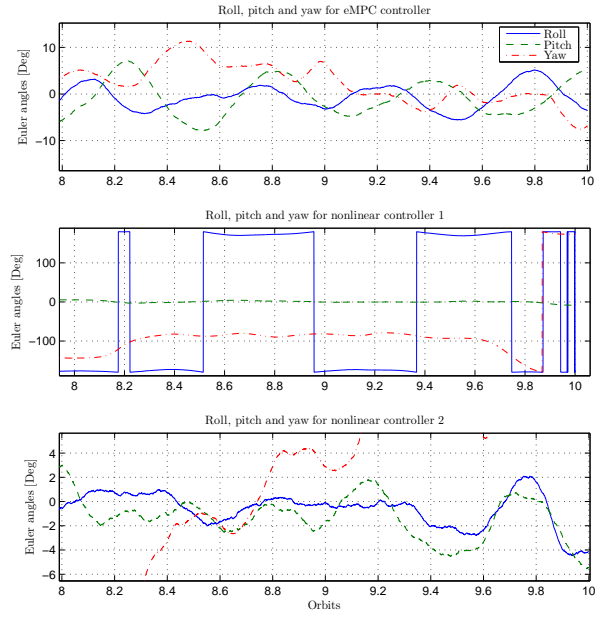


Fig. 2. The Euler angles, zoomed in on the 2 last orbits

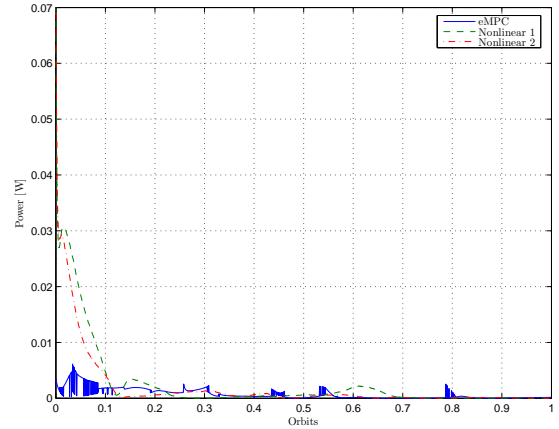


Fig. 3. Power usage in coils, zoomed in on the first orbit

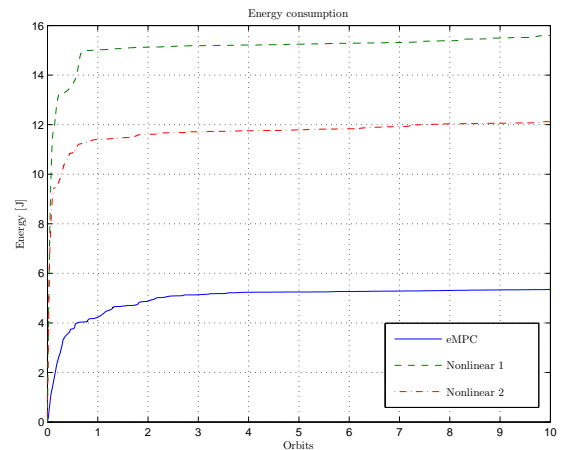


Fig. 4. Energy consumption

## REFERENCES

- [1] Hegrenæs, Ø., "Attitude Control by means of Explicit Model Predictive Control, via Multi-parametric Quadratic Programming", *MSc. thesis*, Norwegian University of Science and Technology, (2004).
- [2] Wiśniewski, R. and Blanke, M., "Fully magnetic attitude control for spacecraft subject to gravity gradient", *Automatica*, Vol. 35, pp. 1201-1214, (1999).
- [3] Krogstad, T. R., "Attitude Control and Stability Analysis of Satellites in Earth and Moon Orbits", *Msc. Project work*, Norwegian University of Science and Technology, (2004)
- [4] Tøndel, P., T. A. Johansen and A. Bemporad, "An algorithm for multiparametric quadratic programming and explicit MPC solutions", *Automatica*, Vol. 39, pp. 489-497, (2003).
- [5] Tøndel, P., "Constrained Optimal Control via Multiparametric Quadratic Programming", *Ph.D. Thesis*, Norwegian University of Science and Technology, (2003).
- [6] Bemporad, A., M. Morari, V. Dua and E. N. Pistikopoulos, "The explicit linear quadratic regulator for constrained systems", *Automatica*, Vol. 38, pp. 3-20, (2002).
- [7] Hughes, P. C., "Spacecraft attitude dynamics", *John Wiley & Sons*, (1986).
- [8] Egeland, O. and J. T. Gravdahl, "Modeling and Simulation for Automatic Control", *Marine Cybernetics, Trondheim, Norway*, (2002).
- [9] Fossen, T.I., "Matematiske modeller for styring av fly og satelitter", *Technical report*, Norwegian University of Science and Technology, (1998).
- [10] Nocedal, J. and Wright, S.J., "Numerical Optimization", *Springer-Verlag*, (1999).
- [11] Lovera, M. and Astolfi, A., "Spacecraft Attitude Control Using Magnetic Actuators", *Automatica*, Vol. 40, pp. 1405-1414, (2004).
- [12] Riise, Å.-R., Samuelsen, B., Sokolova, N., Cederblad, H., Fasseland, J., Nordin, C., Otterstad, J., Fauske, K., Eriksen, O., Indergaard, F., Svartveit, K., Furebotten, P., Sæther, E., and Eide, E., "Ncube: The First Norwegian Student Satellite", *In Proceedings of The 17th AIAA/USU Conference on Small Satellites*, Logan, Utah, August, (2003)
- [13] Gravdahl, J.T, E. Eide, A.Skavhaug, K. Svartveit, K. M. Fauske and F. M. Indergaard, "Three axis Attitude Determination and Control System for a picosatellite: Design and implementation", *Proceedings of the 54th International Astronautical Congress*, Bremen, Germany, 2003
- [14] Ferrari-Trecate, G., Cuzzola, F. A., Mignone, D. and Morari, M., "Analysis of discrete-time piecewise affine and hybrid systems", *Automatica*, Vol. 38, pp. 2139-2146, (2002)
- [15] Vallado, D. A., "Fundamentals of Astrodynamics and Applications", *Kluwer Academic Publishers*, (2001)
- [16] Silani, E., M. Lovera "Magnetic spacecraft attitude control: a survey and some new results", *Control Engineering Practice*, Vol. 13, pp. 357-371, (2005)

## **C.2 Abstract of 2 papers accepted for IAC 2005, and ESA Outreach sponsorship**

Astrodynamics (C1.)

Attitude Control (3.)

Exclude Poster: No

Student (student: yes - sponsor: ESA Student participation programme)

Author Mr. Thomas Krogstad

Norwegian University of Science and Technology, Norway, thomakro@stud.ntnu.no

Associate Professor Jan Tommy Gravdahl

Norwegian University of Science and Technology, Norway, Tommy.Gravdahl@itk.ntnu.no

Post doc Petter Tøndel

Norwegian University of Science and Technology, Norway, Petter.Tondel@itk.ntnu.no

## ATTITUDE CONTROL OF SATELLITES IN EARTH AND MOON ORBITS

### Abstract

This project presents a way of controlling the attitude of a pico satellite, actuated by means of magnetic torquers, using a technique called explicit model predictive control. This is an optimal control algorithm, designed to reduce the energy needed to control the satellite.

The work was done using the mathematical model of the Norwegian student satellite nCube. This is a pico-satellite based on the cubesat design, developed by Professor Bob Twiggs at Stanford University, limiting the size and weight of the satellite to a box measuring 10cm×10cm×10cm of less than 1 kg. Due to the small size, the space available to solar arrays are limited, this in turn reduces the available power, requiring high energy efficiency of the control system.

In order to reduce the power requirements, the satellite will use a combination of active and passive control. The passive control method consists of a gravity boom stabilizing the satellite along the positive or negative nadir vector. The active control performed by 3 magnetic torquers, along the three body axes, to provide full 3-axis control. The magnetic torquers are copper coils which produce a variable magnetic moment, which interacts with the Earth's magnetic field generating a torque vector.

In this work a new way of controlling the magnetic torquers based on the theory of optimal control, is proposed. This controller is analyzed for stability and performance, and compared to a nonlinear controller using feedback from euler parameters and angular velocities.

The control method proposed, is based on the theory of explicit model predictive control, eMPC. This theory originates in traditional model predictive control, but instead of computing the control actions online at every sample, the state-space is divided into regions and a optimal linear controller is computed off-line for each region. This reduces the online computational effort, while retaining the optimal qualities of the control law. This is especially useful in a spacecraft, where power and computational resources are scarce.

The mathematical model of the satellite was simulated, using a model of the magnetic and gravitational field, with both the nonlinear controller and the eMPC controller. The results showed that while the nonlinear controller managed to regulate the satellite along the nadir vector in 2-3 orbits, the eMPC controller achieved almost the same accuracy after about 5

Astrodynamics (C1.)  
Attitude Control (3.)  
Exclude Poster: No  
Student (student: yes - sponsor: )

Author Mr. Thomas Krogstad  
Norwegian University of Science and Technology, Norway, thomakro@stud.ntnu.no

Associate Professor Jan Tommy Gravdahl  
Norwegian University of Science and Technology, Norway, Tommy.Gravdahl@itk.ntnu.no  
Raymond Kristiansen  
Narvik University College, Norway, rayk@hin.no

## COORDINATED CONTROL OF SATELLITES: THE ATTITUDE CASE

### Abstract

In this work coordinated attitude control of satellites in formations, applying methods from mechanical synchronization is studied. Using these techniques, a nonlinear observer and controller is developed for a satellite actuated by means of reaction wheels and thrusters.

The work is part of a study on formation flying of satellites, where the satellite cluster is to perform optical and radar measurements. The individual satellite is actuated by four reaction wheels in a tetrahedron arrangement, providing attitude control thrust about all three axes. For position control, two gas or ion thrusters are positioned along the y axis of the body. Each satellite weighs approximately 150 kg, and has the dimensions  $70 \times 70 \times 70 \text{ cm}^3$ .

The satellites are required to point at the object or position which is to be observed, and this puts strict requirements on the attitude determination and control system. The euler angles should be estimated with  $\pm 0.001^\circ$  accuracy about all axes and a pointing requirement of  $\pm 0.1^\circ$ .

The approach to solving this problem is inspired by the synchronization of mechanical system, especially the synchronization of robot manipulators. In the synchronization problem, there is the leader system which typically either is controlled manually or follows a predefined reference trajectory, and one or more followers which tries to follow the leader system and synchronize its movement. This may be directly transferred to problem of coordinated control of several satellites. The approach presented here is to define one satellite as the leader and the remaining as follower systems. The follower satellite will then follow the attitude of the leader satellite.

To implement this, a nonlinear observer-controller structure is designed, since measurements of the angular velocities are unavailable. The controller is designed using observer-backstepping, and the asymptotic stability of the total system is proven using Lyapunov analysis.

The satellite cluster is simulated in Matlab/Simulink, including the relevant disturbances like J2-perturbations, atmospheric drag, solar pressure, off-diagonal elements in the inertia matrix, measurement noise and so on. The simulations indicate good robustness and performance.

## **C.3 Powerpoint presentation**

The following presentation was held at Space Technology Education Conference 2005. A modified version is to be held at the ISIC-MED05 in Limassol, Cyprus and during the IAC 2005 in Fukuoka, Japan.

# Attitude Control and Stability Analysis of Satellites in Earth and Moon Orbits

Thomas R. Krogstad

Department of Engineering Cybernetics  
Norwegian University of Science and Technology  
N-7491 Trondheim  
Norway

## Outline of the talk

- Introduction
- Modeling
- Attitude controller design
  - eMPC
  - Nonlinear
- Stability analysis
- Simulations of attitude control
- Conclusions

## Introduction

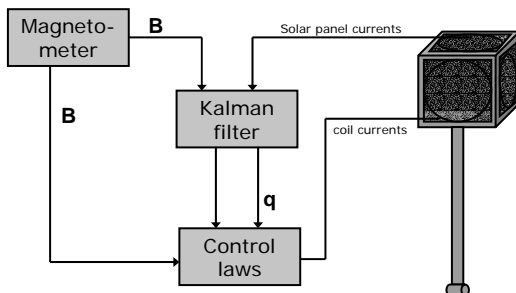
- Initiative from The Norwegian Space Center and Andøya Rocket Range: Develop a pico-satellite based on the cubesat concept
- Work started in 2001
- Design an attitude controller for a magnetically actuated satellite, based on optimal control
- Proposed a controller based on explicit model predictive control

## nCube

- $V=1$  liter,  $m=1$  kg
- Low earth sun synchronous orbit
- Altitude 600 km
- Inclination  $98^\circ$
- Actuators
  - Magnetic torquers
  - Gravity boom



## nCube ADCS



## Modeling: Reference frames

- We will operate with 3 different reference frames
  - ECI – inertial earth centered frame, x-axis in the direction of vernal equinox, y-axis points  $90^\circ$  east
  - Orbit frame – centered in the satellite, z-axis in the nadir direction, y-axis along the negative orbit normal.
  - Body frame – coincides with the principal axis, with the z-axis pointing along the gravity boom

## Modeling: Kinematic equations

The kinematic equations are expressed using quaternions, which can be derived from the angle-axis parameters.

$$\eta = \cos \frac{\theta}{2}$$

$$\epsilon = k \sin \frac{\theta}{2}$$

Further we define the rotational matrix and the time derivative of a general rotation matrix

$$\mathbf{R}_o(\eta, \epsilon) = \mathbf{I} + 2\eta\epsilon^\times + 2\epsilon^\times\epsilon^\times$$

$$\dot{\mathbf{R}}_o^b = (\dot{\omega}_{ob}^\times)^\times \mathbf{R}_o^b = \mathbf{R}_o^b (\omega_{ob}^b)^\times$$

## Modeling: Kinematic equations

The kinematic differential equations may then be expressed as

$$\dot{\eta} = -\frac{1}{2}\epsilon^T \omega_{ob}^b$$

$$\dot{\epsilon} = \frac{1}{2}[\eta \mathbf{I} + \epsilon^\times] \omega_{ob}^b$$

Giving the attitude of the body frame relative to the orbit frame.

## Modeling: Dynamic equations

Attitude dynamics:  $\mathbf{I}\dot{\omega}_{ob}^b + (\omega_{ob}^b)^\times \mathbf{I}\omega_{ob}^b = \tau_o^b$

Torque on the body:  $\tau_o^b = \tau_g^b + \tau_m^b + \tau_j^b$   
 $\tau_g^b = 3\omega_o^2 (\mathbf{z}_{ob}^b)^\times \mathbf{I}(\mathbf{z}_{ob}^b)$   
 $\tau_m^b = (\mathbf{m}^b)^\times \mathbf{B}^b(t)$

- $\mathbf{m}^b$  The magnetic moment generated by the coils
- $\mathbf{B}^b$  The local geomagnetic field
- $\mathbf{z}_{ob}^b$  Is the components of the nadir vector in the body system

The disturbance forces are modelled as zero mean white noise

## Modeling: Dynamic equations

Inserting the torque expressions and giving the angular velocity with respect to the orbit frame

$$\dot{\omega}_{ob}^b = -\mathbf{I}^{-1}(\omega_{ob}^b + \mathbf{R}_o^o \omega_{io}^o)^\times \mathbf{I}(\omega_{ob}^b + \mathbf{R}_o^o \omega_{io}^o)$$

$$+ 3\omega_o^2 \mathbf{I}^{-1}(\mathbf{z}_{ob}^b)^\times \mathbf{I}(\mathbf{z}_{ob}^b) + (\omega_{ob}^b)^\times \mathbf{R}_o^b \omega_{io}^o$$

$$+ \mathbf{I}^{-1}(\mathbf{m}^b)^\times \mathbf{B}^b(t)$$

## Explicit Model Predictive Control

eMPC is a variation of MPC control where the state-space is divided into a number of regions, an optimal controller is computed for each region, by solving a multi-parametric quadratic program (mpQP)

By using eMPC the computational effort is moved offline, the online computation is reduced to fixed-point arithmetic.

## Explicit Model Predictive Control

To derive the eMPC controller we linearize the system about the operating point:

$$\mathbf{x}_p = [0, 0, 0, 1, 0, 0, 0]^T$$

$$\mathbf{u}_p = [0, 0, 0]^T$$

Using Taylor expansion we derive the linear equations

$$\Delta \dot{\mathbf{x}} = \mathbf{A}_c \Delta \mathbf{x} + \mathbf{B}_c \Delta \mathbf{u}$$

## Explicit Model Predictive Control

Applying the mpQP matlab toolbox, developed at NTNU, we solve the problem. The resulting controller is a piecewise affine function

$$\mathbf{u}_k = \mathbf{K}_i \mathbf{x}_k + \mathbf{k}_i, \forall \mathbf{x}_k \in \mathcal{X}_i$$

Examining the controller, it is clear that it is in the form of a MIMO PD-controller. With a variable gain.

## Nonlinear Control

Two nonlinear controllers (Wisniewski 1996) were used to evaluate the result

$$\mathbf{m}^b = h\omega_{ob}^b \times \mathbf{B}^b$$

$$\mathbf{m}^b = h\omega_{ob}^b \times \mathbf{B}^b - \alpha \epsilon \times \mathbf{B}^b$$

## Stability analysis

To show stability of the closed loop system we are exploring the possibility of using piecewise quadratic Lyapunov functions (PWQ-LF), since the system may be interpreted as PWA.

The idea is to find a PWQ-LF which fulfills the following condition, by solving linear matrix inequalities

$$\mathbf{P}_i - \mathbf{E}_i^T \mathbf{U}_i \mathbf{E}_i > 0, \forall i \in \mathcal{I}$$

$$\mathbf{A}_j^T \mathbf{P}_j \mathbf{A}_j - \gamma \mathbf{P}_j + \mathbf{E}_j^T \mathbf{Z}_{ij} \mathbf{E}_i < 0, \forall (i, j) \in \mathcal{S}$$

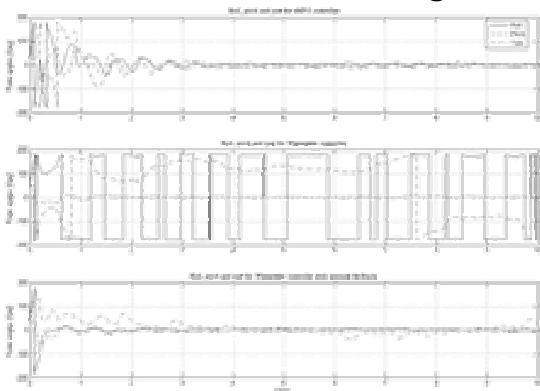
## Simulation

The simulation was done in Matlab Simulink, using the presented model and the following parameters

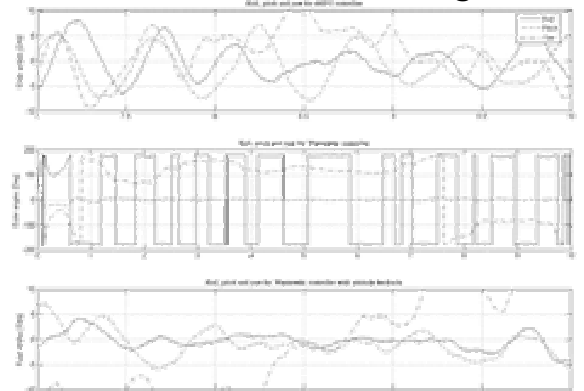
SIMULATION PARAMETERS

Parameter	Value
Inertia matrix	$\text{diag}\{0.1041, 0.1020, 0.0011\}$ [kgm <sup>2</sup> ]
Maximal magnetic moment	0.1 [Am <sup>2</sup> ]
Desired Euler angles	$[0 \ 0 \ 0]^T$ [Deg]
Desired angular velocity	$[0 \ 0 \ 0]^T$ [rad/s]
Pointing accuracy required	$\pm 10^\circ$ on roll and pitch
Orbit angular velocity $\omega_{ob}$	$1.083 \times 10^{-3}$ [rad/s]
Orbit period	5801.6 [sec]
Initial attitude	$\Phi = [20 \ 40 \ 60]^T$ [Deg]
Initial angular velocity	$\omega_{ob}^b = [3 \ -3 \ 3]^T \times 10^{-3}$ [rad/s]

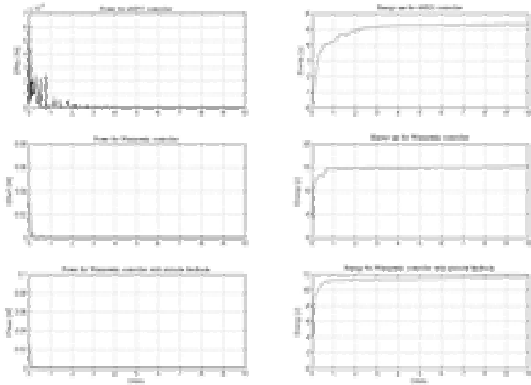
## Simulation – Euler angles



## Simulation – Euler angles



## Simulation – Energy and Power



## Conclusions

- Have designed a controller which reduces the energy consumption
- Able to fulfill the accuracy demands of the payload

## Ongoing work

- Stability proof using piecewise quadratic Lyapunov function